CAPITAL UNIVERSITY OF SCIENCE AND TECHNOLOGY, ISLAMABAD

Implementation and Analysis of Maximum Power Point Tracking in Photo-Voltaic System under Dynamic Environmental Conditions using Machine Learning

by

Noman Mujeeb Khan

A thesis submitted in partial fulfillment for the degree of Master of Science

in the

Faculty of Engineering
Department of Electrical Engineering

2022

I dedicate this work to my dearest parents and my wife

CERTIFICATE OF APPROVAL

Implementation and Analysis of Maximum Power Point Tracking in Photo-Voltaic System under Dynamic Environmental Conditions using Machine Learning

by

Noman Mujeeb Khan

(MEE193004)

THESIS EXAMINING COMMITTEE

S. No.	Examiner	Name	Organization
(a)	External Examiner	Dr. Muhammad Jafar	FAST, Islamabad
(b)	Internal Examiner	Dr. Muhammad Tahir	CUST, Islamabad
(c)	Supervisor	Dr. Umer Amir Khan	CUST, Islamabad

Dr. Umer Amir Khan
Thesis Supervisor
March 2022

Dr. Noor Muhammad Khan
Head
Dept. of Electrical Engineering
March 2022

Dr. Imtiaz Ahmad Taj
Dean
Faculty of Engineering
March 2022

Author's Declaration

I, **Noman Mujeeb Khan** hereby state that my MS thesis titled "**Implementation and Analysis of Maximum Power Point Tracking in Photo-Voltaic System under Dynamic Environmental Conditions using Machine Learning**" is my own work and has not been submitted previously by me for taking any degree from Capital University of Science and Technology, Islamabad or anywhere else in the country/abroad.

At any time if my statement is found to be incorrect even after my graduation, the University has the right to withdraw my MS Degree.

(Noman Mujeeb Khan)
Registration No: MEE193004

Plagiarism Undertaking

I solemnly declare that research work presented in this thesis titled "**Implementation and Analysis of Maximum Power Point Tracking in Photo-Voltaic System under Dynamic Environmental Conditions using Machine Learning**" is solely my research work with no significant contribution from any other person. Small contribution/help wherever taken has been dully acknowledged and that complete thesis has been written by me.

I understand the zero tolerance policy of the HEC and Capital University of Science and Technology towards plagiarism. Therefore, I as an author of the above titled thesis declare that no portion of my thesis has been plagiarized and any material used as reference is properly referred/cited.

I undertake that if I am found guilty of any formal plagiarism in the above titled thesis even after award of MS Degree, the University reserves the right to withdraw/revoke my MS degree and that HEC and the University have the right to publish my name on the HEC/University website on which names of students are placed who submitted plagiarized work.

(Noman Mujeeb Khan)
Registration No: MEE193004

List of Publications

It is certified that following publication(s) have been made out of the research work that has been carried out for this thesis:-

1. **N. M. Khan**, U. A. Khan, and M. H. Zafar, "Maximum Power Point Tracking of PV System under Uniform Irradiance and Partial Shading Conditions using Machine Learning Algorithm Trained by Sailfish Optimizer," *2021 4th International Conference on Energy Conservation and Efficiency (ICECE)*, 2021.

2. **N. M. Khan**, U. A. Khan, and M. H. Zafar, "Radial Basis Function trained with Dynamic Differential Annealed Optimization algorithm based Maximum Power Point Tracking Control of PV system under Uniform and Non-Uniform irradiance," *2021 International Conference on Emerging Power Technologies (ICEPT)*, 2021.

3. **N. M. Khan**, U. A. Khan, and M. H. Zafar, "Short Term Power Forecasting of Wind Energy System using Deep Neural Network (DNN) Trained by a Novel Meta-Heuristic Optimization Algorithm," *2021 16th International Conference on Emerging Technologies (ICET)*, 2021.

(Noman Mujeeb Khan)
Registration No: MEE193004

Acknowledgement

After being utmost grateful to **Almighty Allah** who gave me help and courage to complete my M.S research work, I would like to express huge gratitude towards the person who is not only my supervisor but also my mentor **Dr. Umer Amir Khan** whose constant support, guidance and true motivation kept me steering in the right direction during my entire research work to get through this demanding and tiresome task.

I pay my deep regards to my friend **Muhammad Hamza Zafar** who has helped me a lot in the final formatting of my work.

I would like to show my deepest gratitude and respect to my parents, the ones to whom I owe all the success in my life. No words can express my gratitude to them, but I pray Almighty Allah to bless them and reward them.

A final word to my wife; without you I could have never been able to achieve this work. Your patience and encouragement were always a source of strength for me. You are the shining moon that lightens my life.

(Noman Mujeeb Khan)

Abstract

The rapid depletion of conventional energy sources such as fossil fuel, oil, and coal has shifted researchers' focus towards more green sustainable energy sources. The conventional energy sources leave carbon footprints, sulphur and other harmful contents which are not only harmful to the environment, but also to the human health. Solar energy is by far the cleanest source among the renewable energies available. Solar energy in the form of photovoltaics offers a wide array of benefits such as having low maintenance cost, low carbon footprint, noise-free, and being decentralized as compared to wind, geothermal and tidal energy.

PV panel's output is dependent upon weather conditions. Under uniform irradiance on all PV panels, PV systems have only one global maximum power point (GMPP) however under non-uniform irradiance level, that is partial shading condition (PSC), multiple local maximum power points (LMPPs) exists with only one GMPP. Therefore the tracking of GMPP is very critical for harvesting the maximum power out of the PV system and this tracking of GMPP is known as maximum power point tracking (MPPT).

The conventional gradient-based MPPT techniques such as Peturb and Observe (P&O) and Incremental Conductance (IC) perform well under uniform irradiance but fall into the local maxima trap under Partial Shading (PS). The soft computing or metaheuristic optimization algorithm based MPPT control techniques are also presented in the literature. Standard Particle Swarm Optimization (PSO) and its variants along with the recently proposed optimization algorithms lack voltage stability in the initial phase where the large voltage variance may cause safety and technical issues for grid-connected operations. Modern deep learning and machine learning algorithms provide a strong ability to draw cross-correlations between nonlinear inputs with respect to desired outputs. However they are computationally very expensive.

In this work, a standard PV system's MPPT problem is solved using reference voltage estimation by a hybrid Neural Network (NN) and Swarm Intelligence framework. In this thesis, particularly, a General Regression Neural Network (GRNN)

trained with Sailfish Optimization (SFO) algorithm is utilized. Considering the limitations of back propagation's (BP) inefficient training of feedforward NN, SFO is utilized to maximize NN training for PV systems' MPPT control application as a hybrid MPPT technique. The hybrid GRNN-SFO is highly effective to detect MPPT due to precise estimation capability of the GRNN combined with global optimization of SFO.

Comprehensive comparative study is done with PSO and P&O which are trained using GRNN and Radial Basis Function Network (RBFN) to check the performance of the proposed MPPT technique. Moreover, RBFN trained using SFO is also compared against the proposed GRNN-SFO to determine the superior performance of the proposed technique. In total, five techniques are compared against the proposed GRNN-SFO. Designed case studies are comprehensive enough to test and validate the superior performance of GRNN-SFO under challenging test patterns. The results exhibit superior performance of GRNN-SFO showing global maxima tracking with upto 99.9% efficiency and comparatively 12ms faster tracking time under PSC. The analysis of statistical data has also been performed to examine the robustness and responsiveness of the proposed technique.

Keywords: Maximum Power Point Tracking (MPPT), Photovoltaic (PV), General Regression Neural Network (GRNN), Partial Shading (PS), Complex Partial Shading (CPS), Sailfish Optimizer (SFO).

Contents

List of Figures

List of Tables

Abbreviations

ANN	Artificial Neural Network
BoT	Boosted Tree
CPS	Complex Partial Shading Condition
FFO	Fruit Fly Optimization
FSCC	Fractional Short Circuit Current
FVOC	Fractional Open Circuit Voltage
G	Solar Irradiance
GRNN	General Regression Neural Network
GMPP	Global Maximum Power Point
IMPP	Current at Maximum Power Point
LMPP	Local Maximum Power Point
MAE	Mean Absolute Error
P&O	Perturb and Observe
PSC	Partial Shading Condtion
PSO	Particle Swarm Optimization
PV	PhotoVoltaic
RBFN	Radial Basis Function Network
SR	Success Rate
SSO	Salp Swarm Optimization
SVM	Support Vector Machine
T	Temperature

Symbols

$\boldsymbol{\alpha}$	Euclidean Distance
$\mathbf{d}$	search space
$\mathbf{dV}$	Change in Voltage
$\mathbf{D}$	Duty Cycle
$\mathbf{f}_{sw}$	Switching frequency
$\mathbf{G}_{best}$	Global best position
$\mathbf{I}$	Output Current
$\mathbf{I}_o$	Saturtion current in reverse
$\mathbf{I}_{sc}$	Short Cirrcuit Current
$\mathbf{K}$	Boltzmann constant
$\mathbf{max}_{iter}$	maximum number of iterations
$\mathbf{N}_P$	Number of cells connected in parallel
$\mathbf{N}_S$	Number of cells connected in series
$\mathbf{P}_{mpp}$	Maximum Power of PV panel
$\mathbf{P}_{PVI}$	Power at STC
$\mathbf{q}$	Charge on an electron
$\mathbf{t}_{sw}$	Switching time period
$\mathbf{T}$	Temperature of P-N junction of Solar Cell
$\mathbf{V}$	Output Voltage
$\mathbf{V}_{ref}$	Reference Voltage
$\mathbf{V}_{oc}$	Open Circuit Voltage
$\mathbf{V}_T$	PV cell thermal voltage
$\mathbf{w}$	weights of RBFN

Chapter 1

Introduction

In this chapter, a brief introduction of renewable energy along with its impact on solving future environmental problems is elaborated. The importance of solar energy as a significant electrical power source is highlighted and additionally, this chapter helps to scale the importance of the proposed study in the future with the pros and cons of the PV systems.

The mathematical model and characteristics of the PV systems are studied in detail. An overview of types of equivalent models, electrical characteristics of single-cell, effects of irradiance, and temperature on PV systems is given. The effects of scaling the PV system in a series-parallel combination and corresponding I-V and PV characteristic curves are elaborated. Different diode models are also studied and implemented in MATLAB along with the analysis of electrical parameters under PSC.

Finally the chapter shall elaborate on the thesis objectives, and overview.

1.1 Background

Energy is the backbone of a country's economic development. It is a crucial aspect of human life such as in agriculture, construction, electricity production and many other aspects are all fueled by energy. Energy is essential for economic

development. The demand-supply balance is shifting due to the fast expansion in industrial production and utilities. As a result, all available energy sources have been depleted. The amount of energy used by any country determines its progress. Moreover, the energy consumption per capita is higher in developed countries [2].

The usage of fossil fuels is rising compared to the rise in energy demand. The majority of the world's energy comes from the combustion of fossil fuels. It has resulted in a severe environmental crisis. It is also a significant contributor to global warming.

Non-renewable and renewable energy sources are the two primary categories of energy sources. Non-renewable energy sources include fossil fuels such as coal, oil, and gas whereas renewable energy sources include solar, geothermal, wind, and tidal energy. Numerous countries are making changes to include as many renewable energy sources as possible in national grids.

Since ancient times, we have relied on sun-oriented energy. Solar generated energy may be used in both direct and indirect ways. Solar based energy has a function in the maturation of crops, and evaporation.

The photoelectric phenomenon, thermoelectric, and concentrated solar power are three main sources of solar renewable techniques [3], [4] and these cells are quite adaptable. The heating frames make use of solar powered radiator converters and materials that store and transfer heat for indoor usage. Concentrated solar based power might be a future trend in utility scale power [5], [6].

1.2 Renewable Energy Statistics

Renewable energy's proportion of global energy consumption is expected to increase by one-fifth in the next five years, reaching 12.4% by 2023. Renewable energy will account for over 30% of total electricity consumption in 2023, making it the fastest-growing sector in the power industry. Renewable energy is expected to capture more than 70% of global power generation growth during this phase, with solar powered photovoltaic power generation leading the way, followed by

wind, hydro, and bio-energy. Hydropower will continue to be the most popular renewable energy source, accounting for 16% of global energy consumption by 2023, followed by wind energy (6%), solar powered photovoltaic power generation (4%), and biofuel (up to 3%) [7], [8].

1.3 PV Cell Modeling

Different PV cell models are covered in this section. PV cell acts as a constant current source with an anti-parallel diode to model the electrical behavior. This is referred to as the PV cell's ideal model. The difficulty with the ideal model is that it ignores non-linearity caused by the external factors. In order to tackle such non-linearities, the PV cell's practical models are also discussed [9], [10], [11].

1.3.1 Single Diode Model

PV panel acts as a current source when exposed to light. Photon current is produced by a PV panel in response to irradiance. Figure 2.1 depicts an ideal diode model with a current source and an anti-parallel diode. Eqation 1.1. shows the output current for the ideal diode type.

$$I = I_{ph} - I_{01} = I_{ph} - I_s \cdot e^{(\frac{V}{\eta N_s V_T})} \tag{1.1}$$

Where I denotes current for the ideal diode model, I_s represents the saturation current, I_o1 is the diode current, η is shows the diode ideality factor, V is the output voltage, and V_T is the thermal voltage. Total cells in series combination are represented by N_s [12], [13], [14].

The ideal diode model does not account non-linearity of I-V and PV curves. Therefore, the practical model is presented in Figure 1.1. The mathematical modeling of the practical single diode model is presented by Equation 1.2 whereas Equation 1.3 illustrates the thermal voltage.

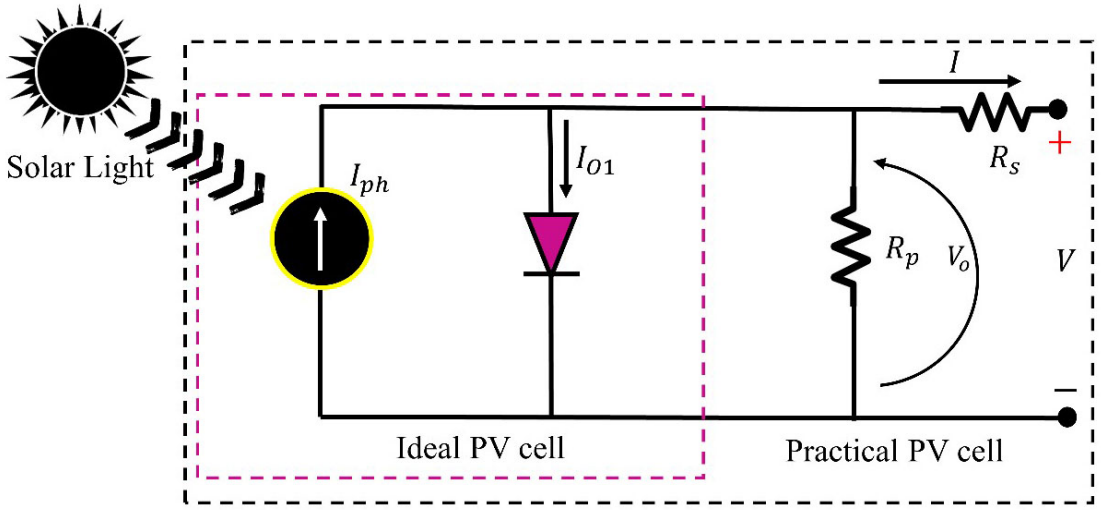

FIGURE 1.1: Single Diode Model of photovoltaic cell depicting ideal and practical photovoltaic cell(s)

$$I = I_{ph} - I_{01} = I_{ph} - I_s \cdot e^{(\frac{V+R_sI}{\eta N_s V_T})} - \frac{V + R_sI}{R_p} \tag{1.2}$$

$$V_T = \frac{N_s KT}{q} \tag{1.3}$$

Where I is the output current for the ideal diode model, I_{ph} is the photon current, I_s is the saturation current of diode, I_{o1} is the diode current, η is diode ideality factor, and V is the output voltage[15], [16].

The effect of R_s and R_p can be seen in the Equation (1.2). Modeling the I-V and PV curves of a PV cell using a single diode is relatively a simple design, however the single diode model doesn't properly reflect a practical PV cell.

1.3.2 Double Diode Model

To improvise the equivalent model a double diode model is another approach presented in the literature that modulates the PV cell properties [18]. Equation for double diode model is presented in Equation 1.4.

$$I = I_{ph} - \left(e^{(\frac{V}{\eta_1 N_{ph} V_T})} - 1\right) I_{s1} - I_{s2}\left(e^{(\frac{V}{\eta_1 N_{ph} V_T})} - 1\right) - \frac{V + R_sI}{R_p} \tag{1.4}$$

where I is the output current for the ideal diode model, I_{ph} is the photon current, I_{s1} is the saturation current for the first diode, I_{s2} is the saturation current for the second diode, I_{o1} is the first diode current, I_{o2} is the second diode current, η is diode ideality factor, and V_T is the thermal voltage [19], [20]. Figure 1.2 illustrates a double diode model.

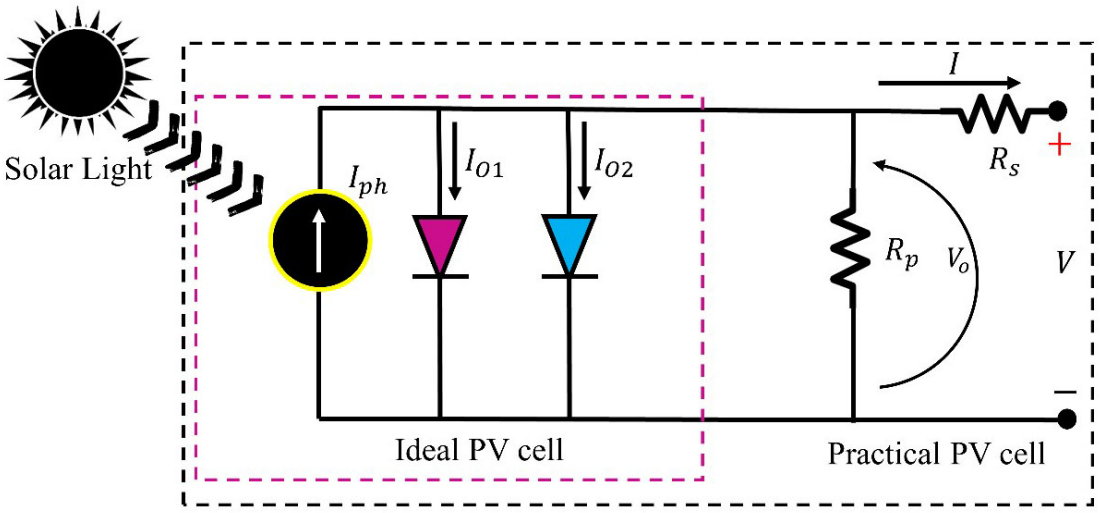

FIGURE 1.2: Double Diode Model of photovoltaic cell depicting ideal and practical photovoltaic cell(s)

Table 1.1 contains the description of the properties of the PV cell [17].

TABLE 1.1: PV cell symbols and description

Symbol	**Description**
$\mathbf{I}$	Output Current
$\mathbf{V}$	Output Voltage
$\mathbf{I}_o$	Reverse saturation current
$\mathbf{I}_{PV}$	Cell current generated by PV arrays
$\mathbf{I}_d$	Diode Current
$\mathbf{R}_s$	Series Resistance
$\mathbf{R}_p$	Parllel Resistance
$\mathbf{I}_{ph}$	Solar induced photovoltaic current
$\mathbf{N}_s$	Total series connected cells
$\mathbf{N}_p$	Total parallel connected cells
$\boldsymbol{\alpha}$	Diode Ideality Factor
$\mathbf{V}_T$	Thermal Voltage of PV module
$\mathbf{q}$	Electron Charge=1.6022×10^{-19} C
$\mathbf{k}$	Boltzmann Constant=$1.380\,73 \times 10^{-23}$ J/K
$\mathbf{T}$	P-N junction Temperature

1.3.3 Triple Diode Model

The triple diode model is also presented in the literature to successfully simulate the non-linearities of the I-V and PV curves in a more practical way [21]. The mathematical model of the triple diode model is presented in Equation 1.5.

$$I = \left(e^{\left(\frac{V}{\eta_1 N_{ph} V_T}\right)} - 1\right) I_{s1} - I_{s2}\left(e^{\left(\frac{V}{\eta_1 N_{ph} V_T}\right)} - 1\right) - I_{s3}\left(e^{\left(\frac{V}{\eta_1 N_{ph} V_T}\right)} - 1\right) \quad (1.5)$$

Where I is the output current for the ideal diode model, I_{ph} is the photon current, I_{o1} , I_{o2} and I_{o3} are the current of three diodes [22].

In triple diode model, the current source has three parallel diodes as illustrated in Figure 1.3.

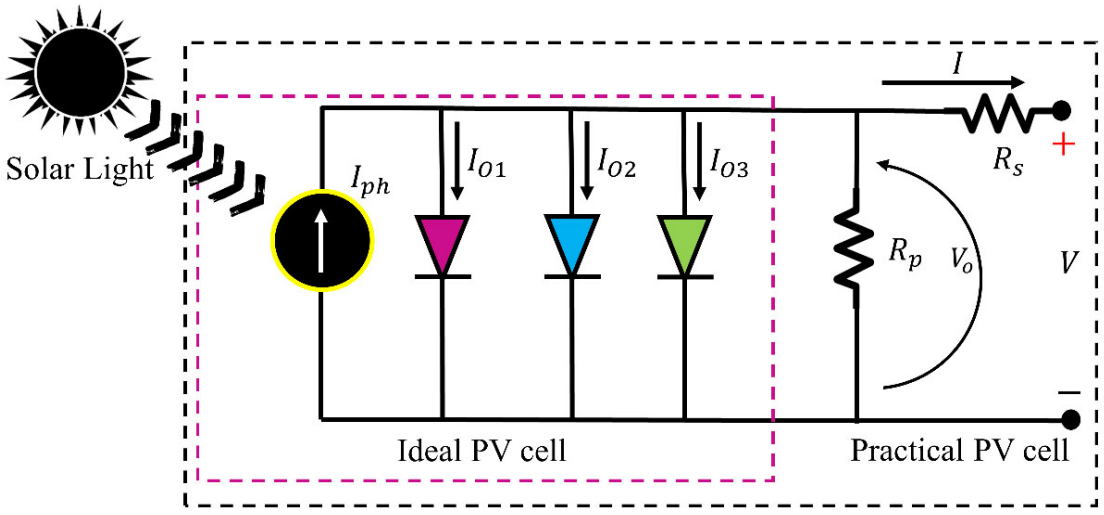

FIGURE 1.3: Triple Diode Model of photovoltaic cell depicting ideal and practical photovoltaic cell(s)

1.4 Characteristics of a PV Cell

The PV cell's I-V and PV properties are reviewed in this section. This section also covers the impact of dynamic environmental circumstances on I-V and PV curves. PV parameters are identified, which define the PV and I-V curves' properties [18], [23], [24].

1.4.1 I-V and PV Characteristics

Figure 1.4 shows I-V and PV curves of the PV module. PV cells are made up of PN junctions that generate current as soon as light strikes the PN junction. Variable load resistance at the output of the PV module can be used to generate an I-V curve [25], [26].

The basic principle is to short circuit the output primarily, which indicates that the load resistance is zero. The maximum current flows under these conditions, which is known as a short circuit current. After that, the resistance is changed from zero to maximum, resulting in an open circuit at the panel's output at zero current and max voltage called open-circuit voltage [27]. The I-V curve is a superposition of current source and diode action properties. Figure 1.4 represents an I-V and PV curve of a standard PV cell.

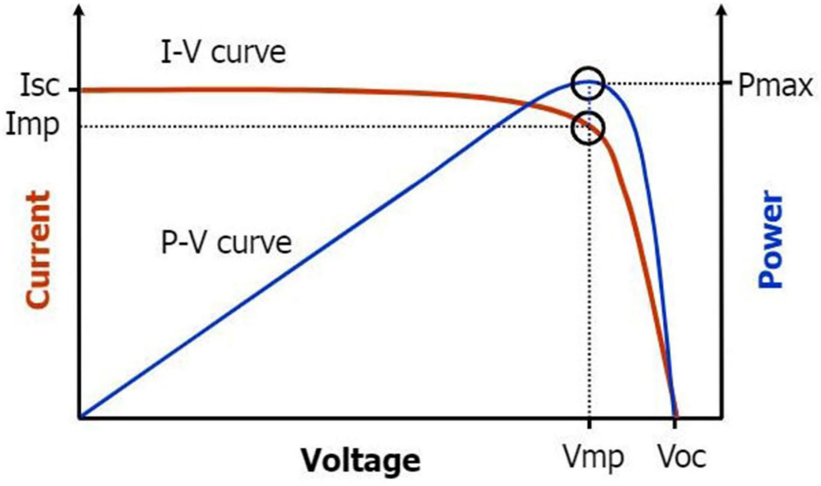

FIGURE 1.4: I-V and PV electrical characteristics of standard mono-crystalline silicon PV cell operating under normal conditions

1.4.2 Effects of Series and Parallel Modules

To achieve high power, scaled up systems require series-parallel configurations of PV panels. Series combination tends to increase the overall voltage whereas parallel combination increases the overall current. Figure 1.5 depicts PV modules coupled in series/parallel configurations under various environmental circumstances.

Changes in the I-V and PV curves are caused by dynamic environmental factors [20].

1.4.3 Description of PhotoVoltaic Parameters

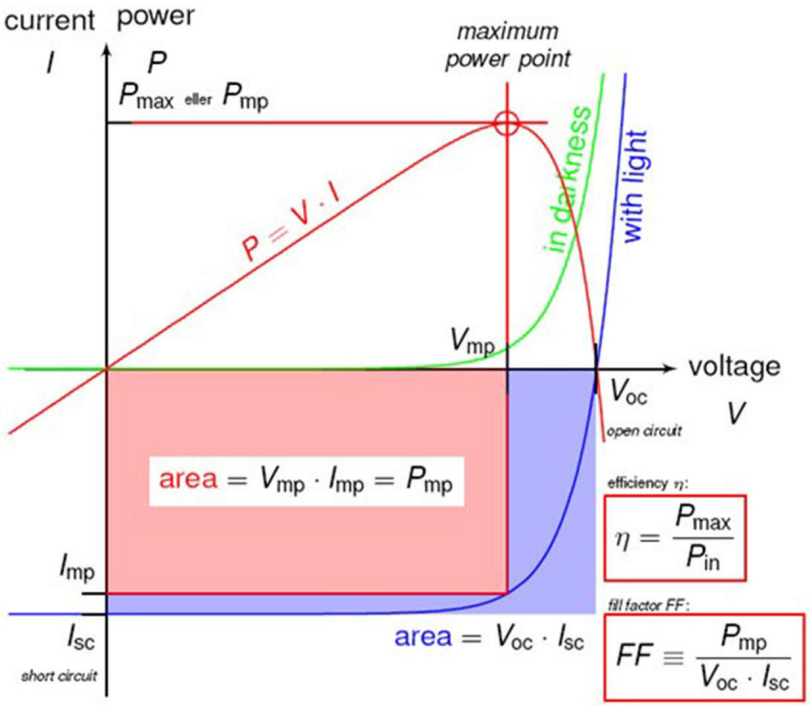

FIGURE 1.5: Description of Different Parameters such as fill factor, efficiency of Photo-Voltaic Cell

Figure 1.5 represents the different parameters of a PV panel which are described as below

- **Open circuit voltage (V_{oc}):** When the output resistance is infinite, voltage appearing at the load is called open-circuit voltage (V_{oc}).
- **Short circuit voltage (I_{sc}):** When the output load is zero, the current through the load is maximum and it is called short circuit current (I_{sc}).
- **Maximum power point (MMPT):** The point of operation at which maximum power is delivered to the load. It is the product of I_{mpp} and V_{mpp}.
- **Efficiency (η):** The efficiency of PV cells depends upon the properties of the material. η is the ratio of the practical and theoretical powers. Therefore

it is highly dependent upon the type of cell. Typically its value is between 9%-19%.

Figure 1.6 represents a series/parallel combination of PV panels. PV panels can get shaded due to shadows from fallen leaves, nearby buildings, clouds etc. This shading results in multiple LMPPs and only GMPP which makes it very challenging for any MPPT technique to track the GMPP.

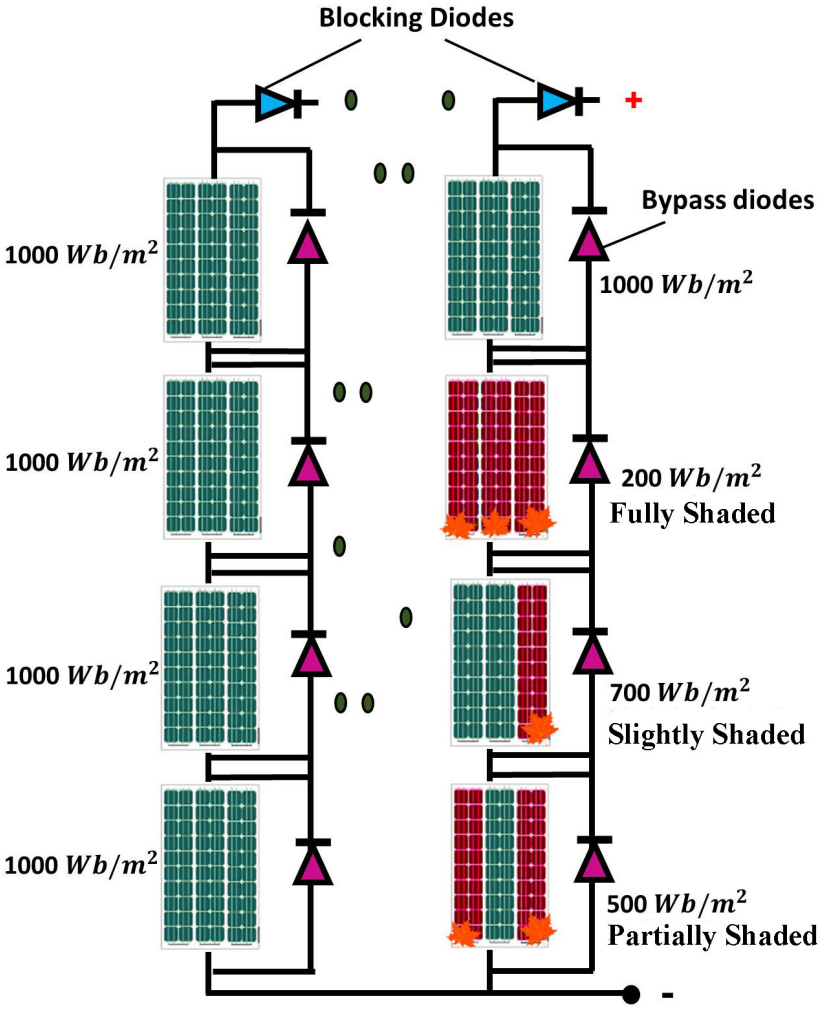

FIGURE 1.6: Series/Parallel photo-voltaic panels with uniform and non-uniform shading. Solar Irradiance significantly drops due to shading from either leaves, clouds, nearby buildings

In this work a "SunPower SPR-320E-WHT-D" panel is utilized. The parameters of the PV panel are given in Table 1.2. These parameters are taken from the PV module in MATLAB 2018a/Simulink.

TABLE 1.2: Electrical Parameters of SunPower SPR-320E-WHT-D

Parameters	**Values**
Power at MPP (P_{mpp})	300 W
Voltage at MPP (V_{mpp})	37.2 V
Current at MPP (I_{mpp})	7.79 A
Short Circuit Current (I_{sc})	8.85 A
Open Circuit Voltage (V_{oc})	44.72 V

1.5 Influence of Changing Solar Irradiance and Temperature on PV Curve

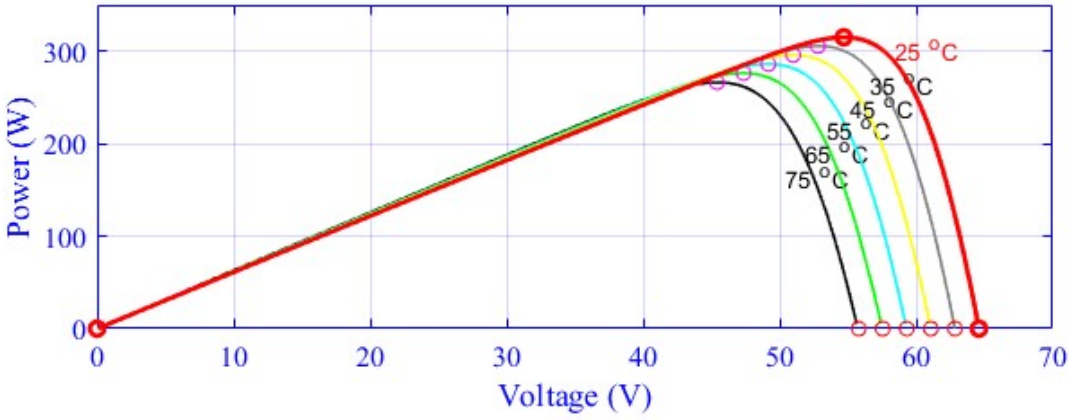

FIGURE 1.7: Variation on PV curve due to change in temperature

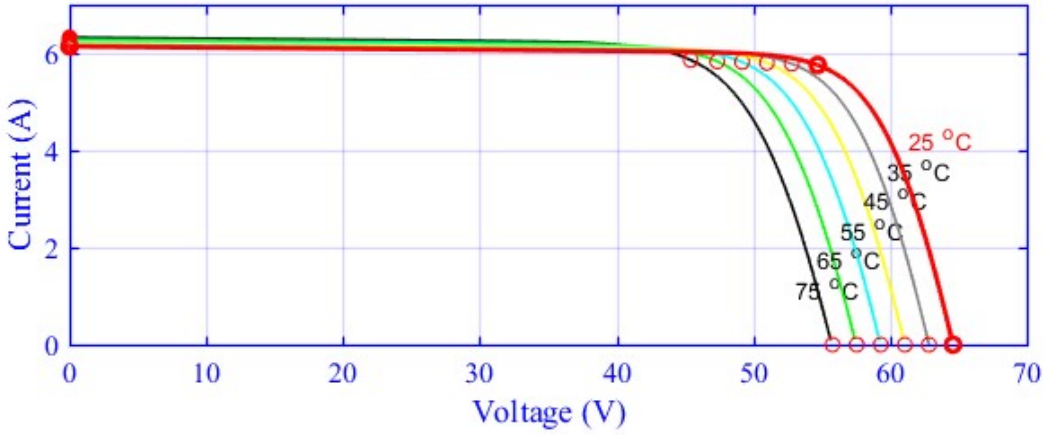

FIGURE 1.8: Variation on I-V curve due to change in temperature

To gauge the impact of temperature, the irradiance is maintained at Standard Testing Conditions (STC) and temperature is varied. A steady decrease in output

power is observed [28]. The panel's temperature and power are inversely related, as illustrated in Figure 1.7.

The deviation in temperature effects the change in PV curve very minutely. However, temperature has a significant impact on voltage, as seen in Figure 1.8. The MPPT on the PV curve shifts as the temperature changes showing an inverse proportional mathematical relationship.

When the temperature is held constant and the irradiance varies, MPP shifts accordingly, as illustrated in Figure 1.9.

The change in irradiance, on the other hand, has no influence on the voltage but it does affect the current, as shown in Figure 1.10. The change in power is directly proportional to the change in irradiance [29].

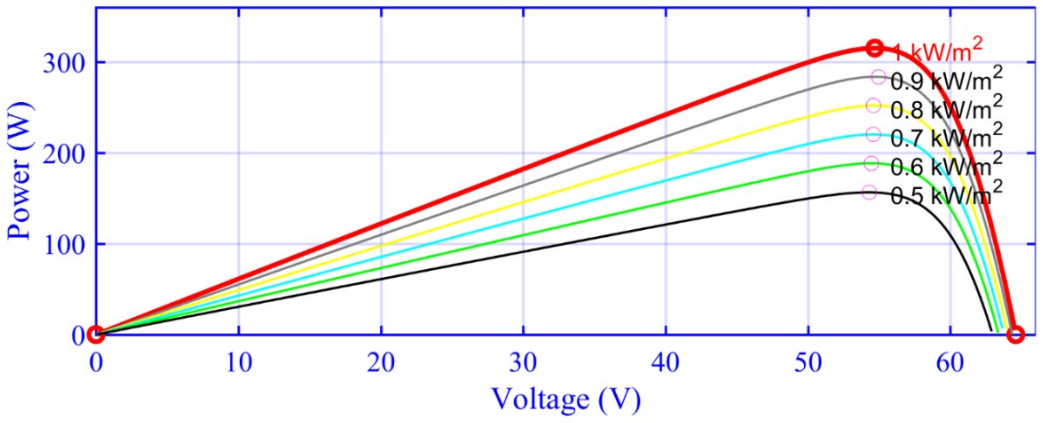

FIGURE 1.9: Variation on PV curve due to change in irradiance

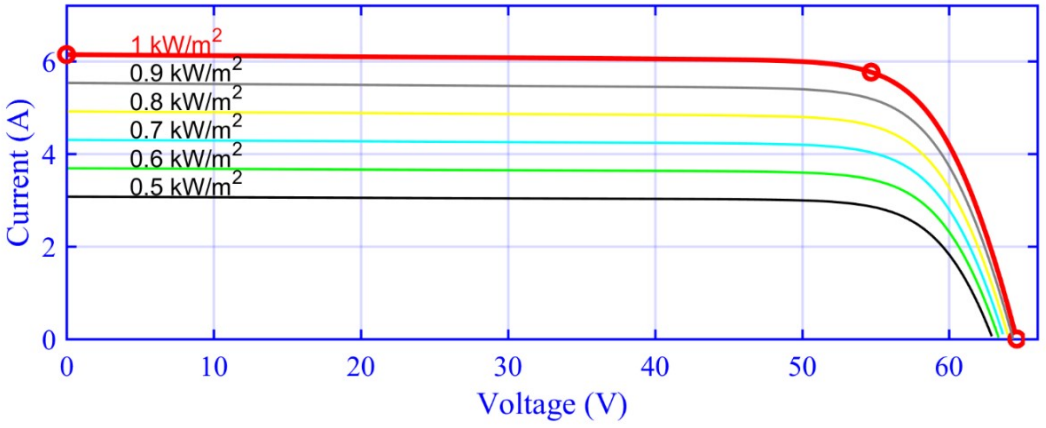

FIGURE 1.10: Variation on I-V curve due to change in irradiance

1.6 Effect of Partial Shading

Several panels are linked in series/parallel configuration for high power generation. Figure 1.6 depicts a 4x2 array of PV modules. Each PV module may or may not receive the same amount of irradiance. As demonstrated in Figure 1.6, the intensity level can change due to shadows from neighboring buildings, clouds, leaves, or dust [30]. This effect is known as PSC in PV panels. The modules that do not get equal irradiance become least productive, whereas the excess power is wasted in the PV panels. The PV panel might get irreparably damaged as a result of heat energy dissipation [31], [32].

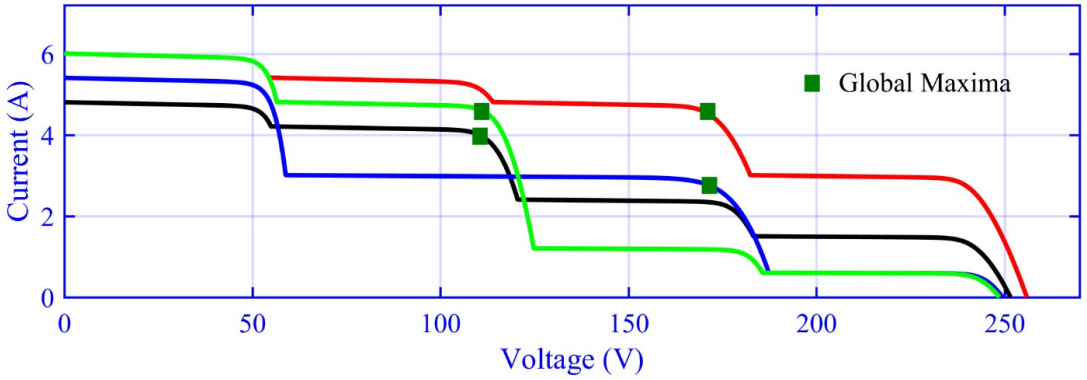

FIGURE 1.11: I-V curve consisting of multiple peaks under PSC

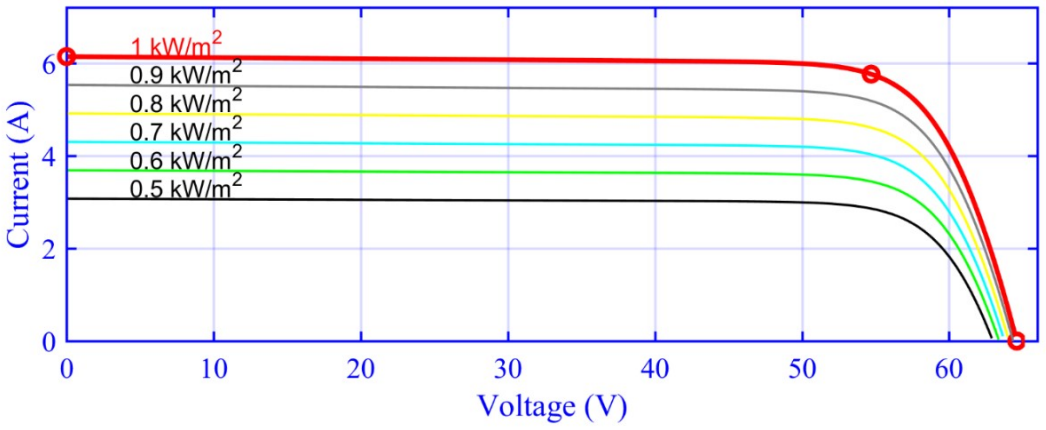

FIGURE 1.12: PV curve consisting of one GMPP and multiple LMPP's under PSC

To provide protection to PV panels against such hot spots, bypass diodes parallel to the PV module are connected to provide an alternate path for the current. One downside of these diodes is that the IV and PV curves become non-linear as shown

in Figure 1.11 and Figure 1.12 respectively [33]. The maximum power from this non-linear behavior cannot be extracted using typical MPPT procedures. Figure 1.12 depicts GMPP locations for MPPT control algorithms to attain [34].

1.7 Thesis Objectives

An exponential increase in demand for PV systems due to decreasing cost per watt and quick installation has made PV systems a popular source of energy. The changing weather conditions lowers the available energy harvest. There is a need for a control system to take advantage of available solar energy. This controller is referred to as MPPT control of the PV systems. The cost of an MPPT controller is trivial as compared to the benefits of stable output, more energy, and cost-benefit surplus.

The MPPT control suffers from PSC problems generating multiple solutions. Additionally, traditional controllers such as HC, I&C, and P&O cannot tackle PSC successfully. They suffer from the LM trap and produce large oscillations. Some modern controllers such as PSO, PSOGS, and SSO tend to track the GMPP however they produce undesired oscillations and random fluctuations. These issues accumulate power losses. Effective MPPT control is essential which can balance the trade-off between tracking time and power loss caused by slow convergence and random fluctuations around GMPP.

In technical terms, the modern Neural Networks (NNs) possess the capabilities of nonlinear control strategies. The added benefit of being model-free optimization makes it suitable for existing and new PV installations and plug and play capabilities [35].

The need to improve the performance using novel ideas for MPPT control is high in demand. Renewable resources such as solar energy PV systems are crucial to counter global warming. The masses can only adopt the renewable energy if the source is economically viable. Higher yield makes the PV system economically affordable and technically practical. The existing research gap and benefit of

humanity are the main motivation behind this work [36]. The objectives of this thesis are listed below:

- Implementation of Novel Sailfish optimizer Tuned General Regression Neural Network based Maximum Power Point Tracking (MPPT) Technique for PV systems.
- Testing under varying irradiance, PSC, and especially CPS.
- The proposed technique achieves greater than 99.9% power tracking efficiency with less than 100 *ms* tracking time and less than 130 *ms* settling time.
- GRNN-SFO extracts 10% more energy as compared to competing techniques.

1.8 Thesis Overview

This dissertation consists of 5 chapters.

Chapter 1 presents a brief introduction to renewable energy, PV systems, applications, advantages, PV cell models, and future aspects.

Chapter 2 discusses the literature review of the MPPT techniques that are available in the literature. Moreover, the components of PV systems such as the layout and functionality of DC converters, PV arrays inverters, controllers, and their properties are discussed.

Chapter 3 presents a GRNN and RBFN based MPPT controller which is trained using a novel Sailfish Optimization algorithm. The mathematical modeling is elaborated for PV systems and its ability to handle PS and CPS is emphasized.

Chapter 4 introduces a detailed result comparison of GRNN-SFO based MPPT controller which is proposed for variable weather conditions. A comparative study is made against PSO and P&O hybrid models with GRNN and RBF based NN models. The results of several studies are presented in Chapter 4. Moreover, the findings are discussed and new problem statements are formulated for future work.

Chapter 5 summarizes the dissertation with achieved results and future research direction.

1.9 Chapter Summary

This chapter focuses on the rapidly shifting trends away from traditional energy sources and towards renewable energy sources. The advantages of PV systems are reviewed, as well as the impact of partial shading (PS) on PV system performance, in order to demonstrate the need for a sophisticated maximum power point tracking (MPPT) management approach.

Different PV panel modelling methodologies, such as the single diode model, double diode model, and triple diode model, are also described. Due to the use of a single diode, the single diode model is fairly simple to design, but it does not account for all non-linarites of the I-V and PV curves. The double diode model compensates for these flaws, but the triple diode model provides a more exact description of the I-V and PV curves. The effect of temperature and irradiance variations on the I-V and PV curves is then studied, demonstrating that changes in environmental variables have an impact on PV power. Only one global peak is detected in the PV curve under uniform irradiation and temperature. These multiple peaks make tracking of MPP very challenging.

Finally this chapter discusses the objectives and overview of this thesis.

Chapter 2

Literature Review

In this chapter, a detailed literature review has been put forth, which discusses the techniques and work that has been done in the domain of MPPT. This section is to discusses the details of work that has been done in the field of MPPT and discuss the research gap that the existing techniques have left behind where there is gap for improvement.

2.1 Introduction

Multiple techniques and methodologies are used to manufacture PV panels. PV cells are the building blocks of PV systems. The cell's efficiency is highly dependent upon the manufacturing technology. PV fabrication is a sophisticated and complex technology. The efficiency depends upon the materials and their purity. The foundries use materials such as monocrystalline, polycrystalline, and amorphous silicon. These PV cells have conversion efficiencies of upto 27%. The low cost and high power PV cells are the focus of academic research and manufacturing [37], [38].

The highest efficiency in the lab for thin-film technology for CIGS and CdTe is 23.4% and 21.0% respectively. With the concentrated solar technology upto 38.9% efficiency is achieved. The new high concentration multi-junction solar cells achieve 47.1% efficiency. Multiple layer cells and multi-junction cells of up to 43%

efficiency have been made but these cells are costly to produce. Germanium is used for manufacturing which is a rare element. So there is a tradeoff between cost, efficiency, and power. The largest producers of PV cells are China, Japan, South Korea, Malaysia, Germany, India, and the USA [39].

It is quite up-front that shading limits current generation. PV systems can experience shading due to nearby buildings, trees, cloudy weather or dust upon them or mountains if panels are installed in the fields with mountains nearby. In any case, shading will impact the efficiency of the solar systems. Since solar panels are connected in series to form strings, any shading on any panel will force the PV panels, including the shaded ones, to carry the same current. Consequently, the shaded panels might get reversed biased and may act as a load and they will draw power which will rapidly minimize the yield of the PV systems [40].

Solar systems are the need of the hour due to exponential growth in energy consumption. With ever increasing power hungry devices and the inevitable depletion of fossil fuels along with rapidly increasing fuel prices and degradation of the environment due to global warming is pushing researchers and organizations to move towards more environment friendly energy sources such as solar, wind, geothermal, and biomass. Renewable energy sources have their own merits and demerits [41].

PV systems are increasingly being utilized in stand-alone and grid-connected applications across the world. A lot of work is being carried out to extract the maximum power out of them. The non-linear nature of PV systems renders their output insufficient for dynamic loads. To increase their performance, MPP needs to be tracked since the output of PV systems depends upon the ambient conditions [42], [43].

Non-uniform solar irradiance caused by nearby trees, buildings, dust, or clouds results in PS problems. However, there is only one point that corresponds to the global maximum power point (GMPP) where system output is at its maximum. Amongst all energy sources, solar energy, particularly photovoltaic systems are the most popular since they're highly reliable, have low operational and maintenance costs, and are noise-free [44], [45], [46].

To actively track GMPP and make the best use of the PV systems, the output of the PV system is connected to a load via a suitable power converter. The low power from the microcontroller needs to be normalized for driving the control signal. Usually, a weak controller is not adequate for driving power MOSFET. Therefore a MOSFET driver circuit is used with DC converter switching. The shading of PV modules causes the PV modules to fall into a PS condition. The irregular solar irradiance due to PS result in the hot spot effect on the PV panels, therefore bypass diodes are used to provide an alternative path for high current [47].

2.2 Trends in Implementation of PV Techniques

Several MPPT algorithms and techniques have been proposed for direct and indirect methods [48]. In the direct control methods, MPP is tracked using either mathematical functions or pre-calculated data such as in Open Circuit Voltage (OV) and Short Circuit Current (SC) methods. These techniques offer a simple implementation, however they cannot modify themselves based upon changes in the weather conditions. Contrary to these methods, voltage and current measurements are used such in techniques such as in P&O [49], Incremental Conductance (INC) [50], and hill-climbing [51] algorithms. The first set of techniques are simple in structure and are only applicable under uniform conditions or equal change on all PV modules [2].

The difficulty in tracking the direction of operation towards the improved power and oscillations at peak points is overcome by bio-inspired meta-heuristic algorithms such as Cuckoos Search (CS) [52], Grasshopper Optimization (GHO) [31], Moth flame optimization (MFO) [53], dragonfly optimization (DFO) [54], group teaching optimization algorithm (GTOA) [55], improved team game optimization [56] and particle swarm optimization gravity search (PSOGS) [57], [58].

The algorithms utilizing the chaos theory meta-heuristic operation are dependent upon several parameters including but not limited to the number of iterations, computation time, and exploration balancing variables. CS algorithm uses random

values to Levy flight, however even a small number of searching agents population can magnify the defects [59].

Another set of MPPT techniques are intelligence based techniques such as hybrid Neuro-Fuzzy controllers. Hybrid systems are accurate but require very fast sensors and costly micro controllers in order to affectively eliminate the oscillations around the MPP. The accuracy of these techniques is, however subject to failure if noise is added to the sensing input.

Fuzzy logic controller (FLC), are a new class of intelligent systems. However, they are dependent upon knowledge and fuzzy parameters such as error metrics and scaling factors including the rule base. Computational intelligence techniques such as fuzzy logic, neural networks, and evolutionary algorithms tackle the design problem with high accuracy but with increased computational expense [60], [61].

2.3 Maximum Power Point Tracking (MPPT) Techniques Review

In this chapter different MPPT techniques are studied under the following classifications:

- Conventional Techniques
- Intelligent Techniques
- Swarm Intelligence Techniques

The classification of all these MPPT techniques is presented in Figure 2.1.

The conventional MPPT techniques include a fractional short-circuit (FSCC), fractional open-circuit voltage (FOCV) [62], P&O [63], INC, hill climbing (HC), modified incremental conductance (Mod-INC), and lookup table method (LUT). The advantages of these techniques are their low complexity for implementation, quick tracking of MPP, and high efficiency under uniform irradiance and temperature.

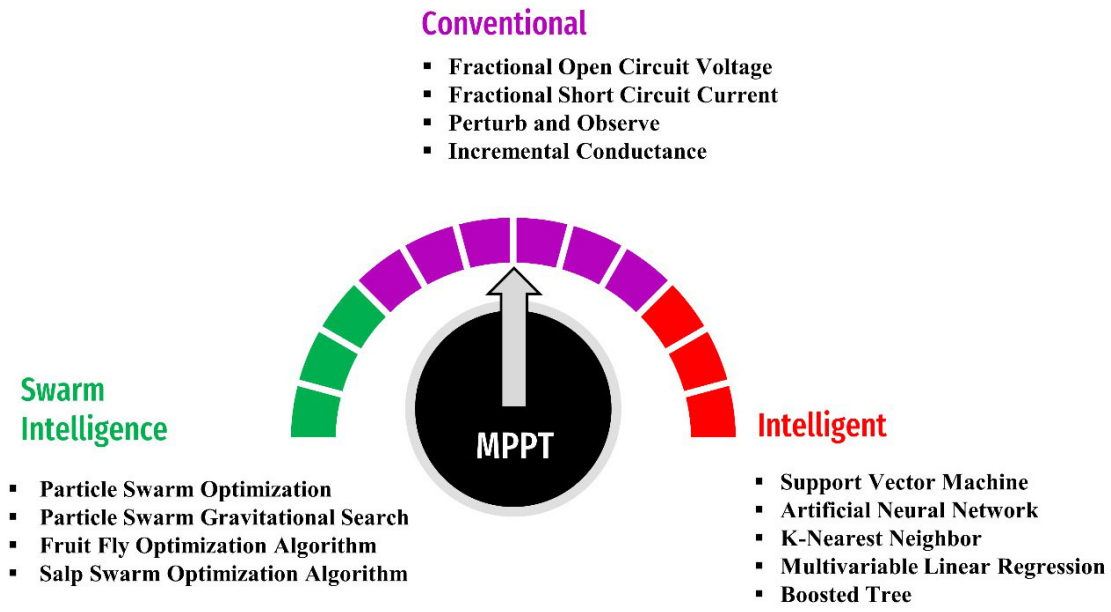

FIGURE 2.1: Set of MPPT techniques presented in the Literature

However, their disadvantage is the undesired oscillation at MPP which results in significant power losses. Also, under PSC conventional techniques do not possess the ability to differentiate between GMPP and LMPP and consequently they tend to get stuck in LMPP resulting in extensive power losses [64].

Another class of MPPT controllers that use meta-heuristic optimization algorithms is called swarm intelligence-based MPPT control. These MPPT control techniques use optimization algorithms which include PSO, Particle Swarm Gravitational Search (PSOGS), Salp Swarm Optimization (SSO), Fruit Fly Optimization (FFA), and Flower Pollination Algorithm (FPA). The low computation cost, high efficiency and medium time required for the MPPT are the main advantages of these MPPT control techniques. These control techniques can effectively differentiate between GMPP and LMPP and extract the maximum power [65], [66], [67]. However, they suffer from high settling and tracking time to attain oscillation free settling at higher power.

Intelligent MPPT techniques include Support Vector Machine (SVM) [68], Multivariable linear regression, KNN, and artificial neural networks. Under varying environmental conditions these techniques perform well with very high accuracy and less tracking time [69], [70], [71]. One of the problems with these techniques is

the requirement of large data set for training [72], [73]. However, ML algorithms combined with SI-based techniques can resolve these issues.

2.3.1 Conventional Techniques

In this sub-section, conventional MPPT techniques are presented and explained in briefly. These techniques are listed below:

- Fractional Open Circuit Voltage (FFCV)
- Fractional Short Circuit Current (FSCC)
- Perturb and Observe (P&O)
- Incremental Conductance (INC)

2.3.1.1 Fractional Open Circuit Voltage (FOCV)

FOCV is an approximation based technique. In this technique, a pilot PV cell of the same type of PV module is used. This cell is employed whose open circuit voltage is monitored every time. It is assumed that the same irradiance and temperature conditions are applied to the pilot cell. MPP using FOCV can be calculated using

$$V_{mpp} \cong KV_{oc} \tag{2.1}$$

Where V_{mpp} is the voltage at MPP and K is the scaling factor whose value is between 0.7-0.8. The Flowchart of the implementation of FOCV is shown below.

The advantage of FOCV is that it is very simple to implement. This technique can be implemented using the digital-analog circuit without any costly hardware. The drawback associated with this technique is that it is based upon the approximation of V_{oc} which is very inefficient and requires a pilot cell that needs to be operated under the same conditions. Moreover, this technique fails to perform under PSC [74].

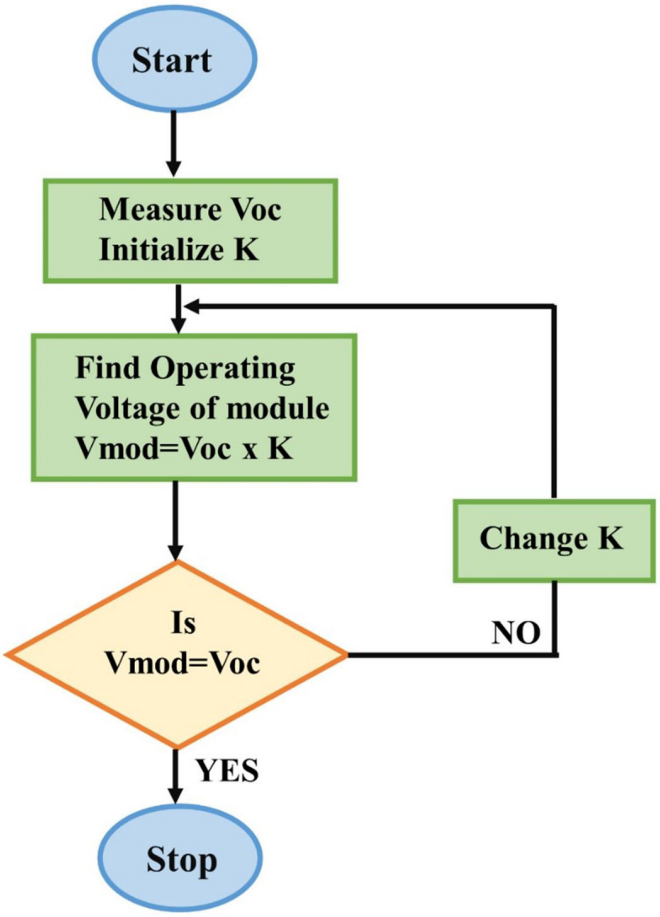

FIGURE 2.2: Flowchart depicting the working principle of Fractional Open Circuit Voltage (FOCV)

2.3.1.2 Fractional Short Circuit Current (FSCC)

This technique is similar to FOCV. Since MPP contains both I_{mpp} and V_{mpp} so, in this technique I_{mpp} is taken into account in the place of V_{mpp}. Pilot cell's short circuit current is multiplied by a factor K and is fed to the PI controller which maintains the duty cycle of the boost converter which can be calculated using Equation 2.2. The generic flowchart of FSCC is shown in Figure 2.3.

$$I_{mpp} \cong K I_{sc} \tag{2.2}$$

Where I_{sc} is the short circuit and K is the scaling factor whose value is between 0.7-0.8. similar to FOCV. The FSCC is also a simple technique to implement and no complex hardware is required. However, similar to FOCV, FSCC, also uses an

approximation therefore it fails to track GMPP effectively and also fails to track GMPP under PSC.

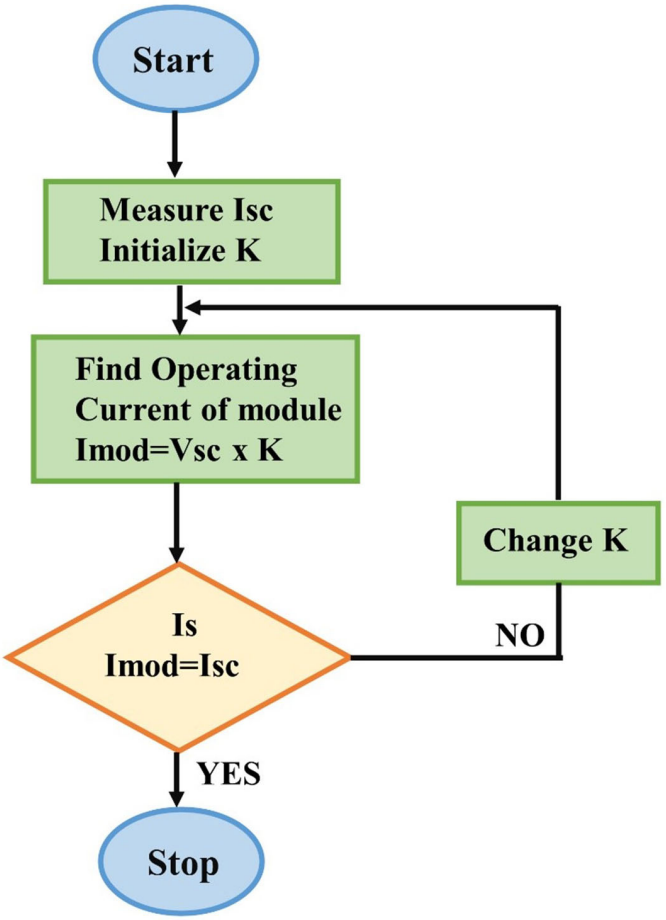

FIGURE 2.3: Flowchart depicting the working principle of FSCC Fractional Short Circuit Current (FSCC)

2.3.1.3 Perturb and Observe (P&O)

P&O is one of the simplest algorithms to implement on any microcontroller. Voltage and current sensors are required to calculate the fitness function in terms of power after each sample. As the name suggests, perturbation is made on power which decides the next perturbation of the duty cycle. The duty cycle is updated and the previous power is compared with the next power. If the current power is higher than the previous power, the duty cycle is increased whereas if the current power is less than the previous power, the duty cycle is decreased. This process continues and enables P&O to track GMPP. The flowchart of the P&O algorithm is shown in Figure 2.4.

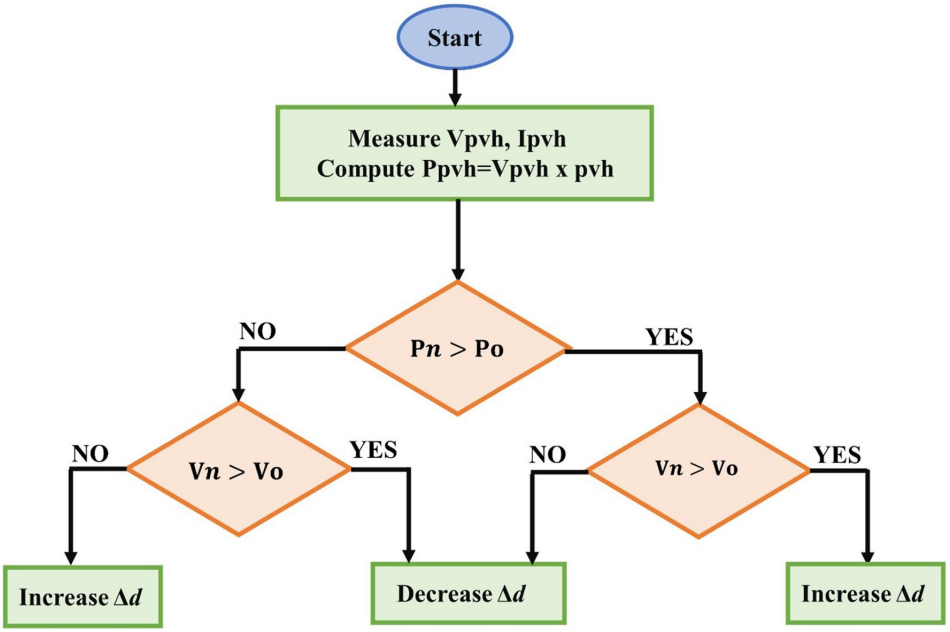

FIGURE 2.4: Flowchart depicting the working principle of (P&O)

Where dP_{PV} and dV_{PV} are the differential power and voltage of PV. P&O is also dependent upon the change in voltage of the PV module. The problem with P&O is the continuous oscillations around GMPP and under PSC, P&O tends to get stuck into the LM trap. As presented in the literature, under uniform irradiance, P&O has an efficiency of 92-98% [75].

If the power is increasing, then it perturbs the voltage in the same direction. If the power is decreasing, it starts perturbation in the reverse direction. P&O works fine when there is a single maximum power point on the PV curve. The mathematical formulation of P&O is shown in Equation 2.3 to Equation 2.5.

$$\frac{dP_{PV}}{dV_{PV}} = 0 = MPP \tag{2.3}$$

$$\frac{dP_{PV}}{dV_{PV}} > 0 \quad left \quad of \quad MPP \tag{2.4}$$

$$\frac{dP_{PV}}{dV_{PV}} < 0 \quad right \quad of \quad MPP \tag{2.5}$$

2.3.1.4 Incremental Conductance (INC)

In a 2D plane, the graph theory suggests that in any monotonic relationship the peak point on the graph has zero differential rate of the slope. As opposed to power in P&O, INC tracks MPP using the slope of the power curve which makes incremental conductance superior to P&O [76]. The flow chart shown in Figure2.5 explains the working of INC. We know that maximum power is defined by Equation 2.6.

$$P_{MPP} = V_{MPP} \times I_{MPP} \tag{2.6}$$

and instantaneous power is

$$P = V \times I \tag{2.7}$$

Taking derivatives of Equation 2.7 with respect to voltage

$$\frac{dP}{dV} = \frac{d}{dV}(V \times I) \tag{2.8}$$

$$\frac{dP}{dV} = 1 + \frac{d}{dV} \cdot V \tag{2.9}$$

At MPP

$$\frac{dP}{dV} = 0 \tag{2.10}$$

Therefore

$$\frac{dI}{dV} = -\frac{1}{V} \tag{2.11}$$

Where dI/dV is called differential incremental conductance, P_{MPP} is power at the MPP, V_{MPP} is the voltage at MPP, and I_{MPP} is current at MPP. Thus we can track MPP by using incremental conductance of the PV curve. From the flow chart, as shown in Figure 2.5, the conditions for incremental conductance are as follows

$$\frac{dP}{dV} = 0 \qquad \frac{\Delta I}{\Delta V} = -\frac{1}{V} \tag{2.12}$$

$$\frac{dP}{dV} > 0 \qquad \frac{\Delta I}{\Delta V} > -\frac{1}{V} \quad left \quad of \quad MPP \tag{2.13}$$

$$\frac{dP}{dV} < 0 \qquad \frac{\Delta I}{\Delta V} < -\frac{1}{V} \quad right \quad of \quad MPP \tag{2.14}$$

The Speed of INC depends upon the increments or decrements in V_{ref}. Larger increments lead to fast-tracking but cause more oscillations at GM which leads to power losses [77].

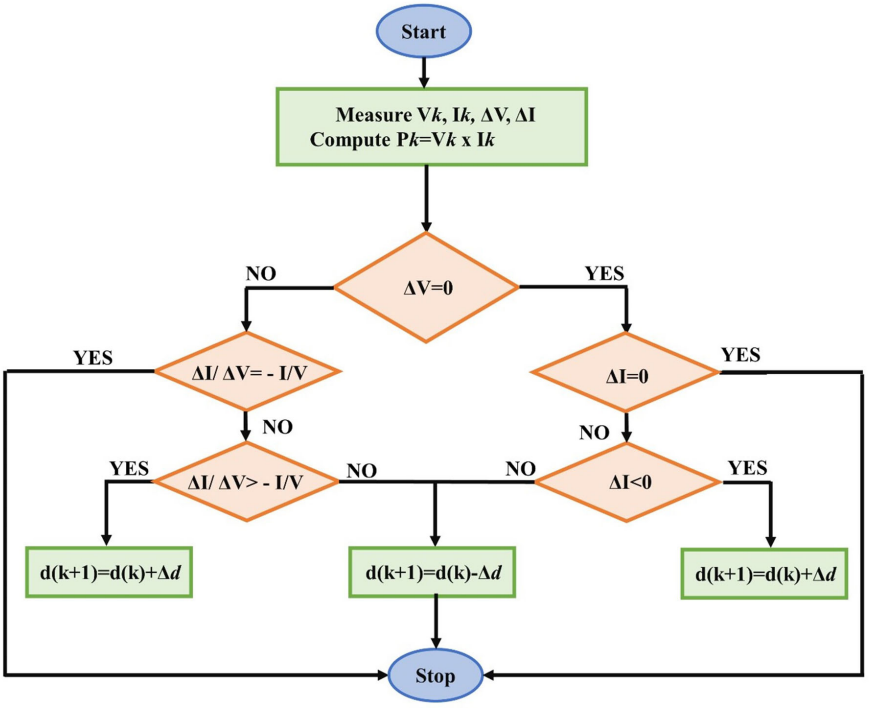

FIGURE 2.5: Flow Chart of the Incremental Conductance (INC) Scheme for MPPT

2.3.1.5 Performance Evaluation of Conventional MPPT Techniques

In this section, the comparison between conventional MPPT techniques is presented as shown in Table 2.1. The comparison is made in the form of advantages, disadvantages, and applications. The biggest problem with the conventional techniques is tracking of GMPP under PSC where these techniques get stuck in LMPP's and lose significant amount of power thereby reducing overall efficiency of the system [78].

TABLE 2.1: Comparative Evaluation of Conventional Techniques

Technology	Advantage	Disadvantage
FOCV	Suitable under low temperatures	In-efficient under PSC
FSCC	Simple Implementation	Significant Power loss under PSC
P&O	Best for uniform-irradiance conditions	Gets stuck in LMPP under PSC
INC	Better than P&O	Costly in terms of implementation

2.3.2 Intelligent Techniques (IT)

In this section IT based MPPT techniques are discussed which are as follows:

- Support Vector Machine (SVM)
- Artificial Neural Network (ANN)
- K-Nearest Neighbour (KNN)
- Multivariable Linear Regression (MLR)
- Boosted Tree (BoT)

2.3.2.1 Support Vector Machine (SVM)

SVM is a data categorization, pattern identification, regression, and prediction approach that uses machine learning. The categorization is formally represented by Equation 2.15 [79].

$$Y_{fit} = train\_classifier \cdot predictcn(x) \tag{2.15}$$

SVM may be used to solve two distinct classes by identifying the best hyperplane. A hyperplane distinguishes the positive data set from the negative data set with the maximum distance. The margin is the greatest possible gap between two locations. Figure 2.6 depicts a margin, and hyperplane between positive and negative data sets [80].

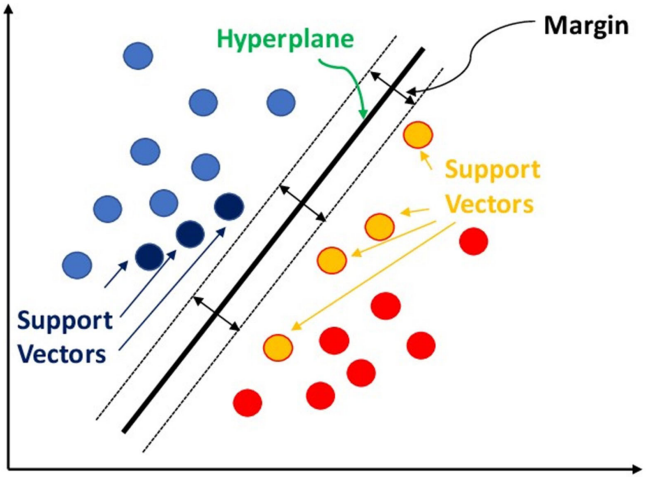

FIGURE 2.6: Support Vector Machine Visualization with hyperplane and support vectors

Where the positive data is represented as $w\ .\ X + b \geq 1$ and the negative data as $w\ .\ X - b \leq -1$. w is the hyperplane normal vector whereas x is the input vector. The separating hyperplane u is equal to zero. The margin is given as 2.16.

$$M = \frac{(x^{+} - x^{-}) \cdot w}{|w|} \tag{2.16}$$

Maximizing margin is given by Equation 2.17.

$$Maximize(m) = \frac{2}{|w|} \tag{2.17}$$

Since solar irradiation and temperature pose a non-linear characterization therefore SVM is highly suitable to estimate the voltage across MPP.

MPPT problem poses a regression task for SVM. The linear regression is represented using the Equation 2.18 as:

$$f(x) = (w.\phi(x)) + b \tag{2.18}$$

Where $\phi(x)$ is column vector functions mapping the input sample data to the higher dimensional feature space, w represents parameter column vector, and b is the threshold from the low dimensional input feature space.

2.3.2.2 Artificial Neural Network (ANN)

With the development of artificial intelligence, a new field emerges which is called Deep Learning (DL). No detailed system modeling is required by ANN based intelligent techniques. By proper input-output mapping, ANN based techniques can handle extremely complex problems [81],[82],[83],[84].

ANN uses the concept of neurons connectivity in the brain of the human body similar to Figure 2.7. The structure of the human brain neuron is shown in Figure 2.7 (a) which is very similar to the structure of perceptron as shown in Figure 2.7 (b). ANN with hidden layers is shown in Figure 2.7 (cc). ANN typically consists of three layers, that is, input, hidden, and output layer. The first layer takes inputs and passes them to the next layer. The weights and biases are connected that define the relation of the previous layer with the next layer. The weights connected between the input and hidden layers are termed as w_{ij}. The second layer is called the hidden layer which originally maps the input with output.

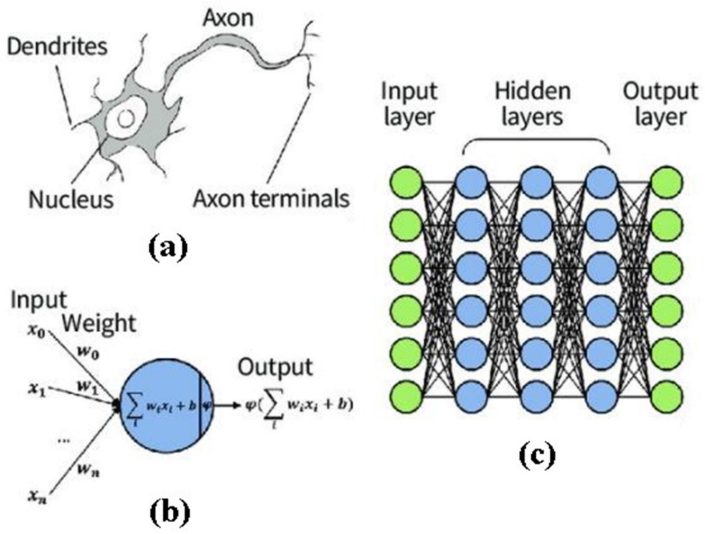

FIGURE 2.7: General structure of ANN. (a) A biological neuron which inspired ANN (b) Mathematical model of perceptron (c) Multilayer perceptron with all layers associated with ANNs

There are two important factors in ANN:

- Learning Mode
- Activation Mode

Another important function in an ANN is the selection of an activation function. This selection is mainly dependent upon whether the problem is classification or regression. There are different types of activation functions, such as RELU, sigmoid, and RBF.

The NN training can also be done using the data of I-V plots. The I_{pv} and V_{pv} is fed to ANN with the duty cycle as the output. In this method, the dataset is generated using conventional or swarm intelligence-based MPPT techniques. As discussed above the input features of this dataset can be irradiance, temperature, humidity, I_{pv}, and V_{pv} etc. and the class is the duty cycle d. With a proper learning method and activation function, ANN gets trained on the given dataset and a generated model is employed to track the MPP.

In literature, the most commonly used ML techniques utilize irradiance (G) and temperature (T) as input vectors but this technique includes system modeling. If

the system parameters change, that is, the module configuration shading pattern etc, then the ANN will not be able to perform accurately, and under such cases, retraining of ANN would be required. However, research is being conducted to implement ANN under PSC by training ANN under different shading conditions, different modules, and different configurations.

Another technique is employed in which GRNN is trained by FFOA. In this method, multiple shading patterns are considered and the dataset of current, voltage and duty cycle is generated using FFOA. This technique also achieves higher efficiency with less convergence time. Also, ANN trained with Genetic Algorithm (GA-ANN) based hybrid technique is presented in the literature which tracks GMPP with high efficiency. MPPT control structure of ANN is presented in Figure 2.8.

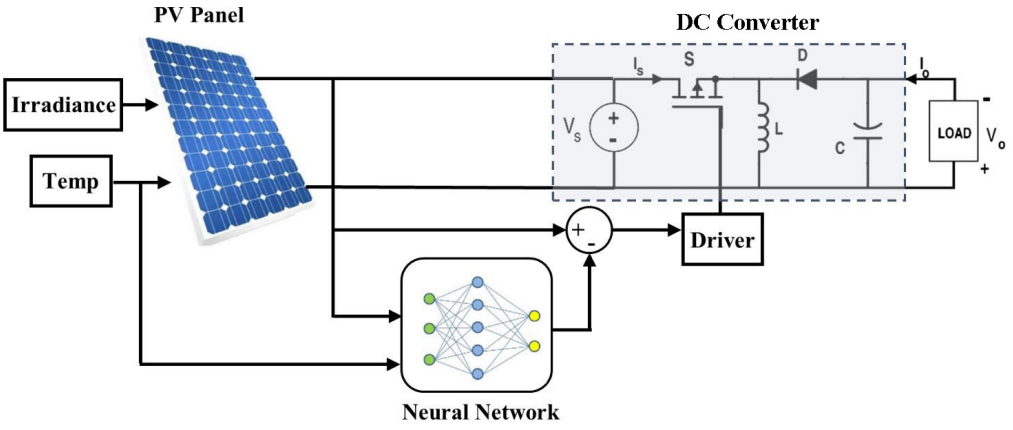

FIGURE 2.8: ANN based MPPT Control Implementation

2.3.2.3 K-Nearest Neighbours (KNN)

Among several ML techniques, KNN is one of most simple and easy algorithm to implement. Regardless of simplicity, KNN is highly effective for classification and control applications. KNN is applicable to both classification and regression tasks. KNN's popularity in classification problems is exceedingly well known. Still KNN is equally applicable to any regression problem.

The first step is to calculate the distance between the new point and each training point. Commonly known methods to calculate the distance: Euclidian, Manhattan (for continuous) and Hamming distance (for categorical) are as follows:

- **Eculidean Distance:** The square root of the sum of the squared differences between a new point (x) and an old point (y) is used to compute Euclidean distance (y).
- **Manhattan Distance:** This is the distance between two real vectors calculated by adding their absolute differences.
- **Hamming Distance:** It is used to represent categorical variables. If the values (x) and (y) are the same, the distance D is equals to zero. Otherwise, D equals one.

2.3.2.4 Multivariable Linear Regression (MLR)

MLR is a regression algorithm with one or more predictor variables that impact the output response. It is frequently utilized in uncertain datasets or complex large dataset learning challenges. If the response (Y) has a linear relationship with the predictors $(x_1,x_2,\ldots\ ,x_m)$, MLR will be given by Equation 2.19:

$$Y = \beta_o + \beta_1 x_1 + \ldots + \beta_k x_o + \varepsilon \tag{2.19}$$

Where β is a regression coefficient and ϵ is the training error $E(\epsilon) = 0$.

The main goal is to get the anticipated coefficients by plugging the observation values into Equation 2.20.

$$\begin{aligned} Y_1 &= \beta_o + \beta_1 x_{11} + \ldots + \beta_k x_{1k} + \varepsilon_1 \\ Y_2 &= \beta_o + \beta_1 x_{21} + \ldots + \beta_k x_{2k} + \varepsilon_2 \\ Y_3 &= \beta_o + \beta_1 x_{31} + \ldots + \beta_k x_{3k} + \varepsilon_3 \end{aligned} \tag{2.20}$$

MLR should be able to lower the LR model's sum of squares.

$$Q(\beta) = \sum_{i=1}^{n} \varepsilon i^2 = \sum_{i=1}^{n} (y_i - \beta_o - \beta_1 x_{i1} - \ldots - \beta_k x_{ik})^2 \tag{2.21}$$

The regression coefficient matrix is then given by:

$$\beta = (X'X)^{-1} X'Y \tag{2.22}$$

2.3.2.5 Boosted Tree (BoT)

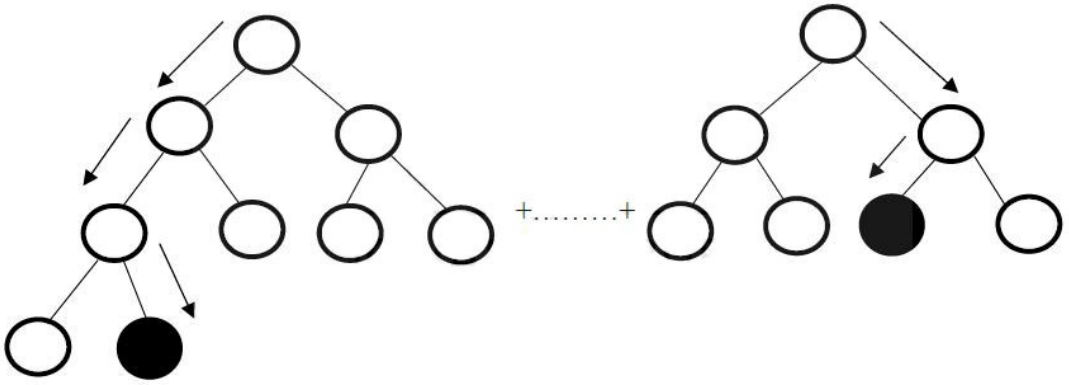

FIGURE 2.9: A general structure of BoT

BoT is a member of the ensemble family of algorithms. It is an approach that combines a large number of infirm learners (tree) into a strong classifier. As seen in Figure 2.9, this method employs many models to improve prediction accuracy. It is mathematically expressed as

$$\hat{g}(x) = \sum_{t} wtyt(x) \tag{2.23}$$

Where w is the weight in proportion to its accuracy and $\hat{g}(x)$ is the ensemble output. Weight is given to each data sample after each iteration based on misclassification. The aim is to reduce the objective function.

$$0f(x) = \sum_{l} l\left(\hat{g}_i, g_i\right) + \sum_{t} \Omega(ft) \tag{2.24}$$

Where $l(\hat{g}_i, g_i)$ is the loss function, which represents the difference between the actual and predicted i^{th} sample. $\Omega(ft)$ is regularization function, it corrects the complex of the (ft) tree.

2.3.2.6 Performance Evaluation of Intelligent MPPT Techniques

Intelligent ML-based MPPT techniques are very efficient and achieve high efficiency under dynamic atmospheric conditions. These MPPT techniques are system-dependent which increases the overall computation cost. The comparison of intelligent MPPT techniques is presented in Table 2.2.

TABLE 2.2: Comparative Evaluation of Intelligent Techniques

Technology	**Advantage**	**Disadvantage**
SVM	Eliminates ripples in the output voltage	Low efficiency
ANN	Highly efficient under PSC	Large dataset required for training purposes
KNN	Simple and easy to implement	Poor efficiency
MLR	Fast tracking of GMPP	In-efficient under PSC
Boosted Tree	Accurate tracking of GMPP	Complex calculations are required

2.3.3 Swarm Intelligence (SI) Based MPPT

SI algorithms use the behavior of animals or swarm to solve complex optimization problems. In recent decades optimization algorithms are being used as MPPT control techniques and they can effectively track the GMPP under dynamic environmental conditions using exploration and exploitation strategy by updating the duty cycle. In this section different SI based MPPT based techniques are discussed and at the end, an evaluation comparison is made [85]. The SI based MPPT techniques discussed are listed below:

- Particle Swarm Optimization (PSO)

- Particle Swarm Gravitational Search Optimization (PSOGSO)
- Fruit Fly Optimization (FFO)
- Salp Swarm Optimization (SSO)

2.3.3.1 Particle Swarm Optimization (PSO)

PSO [86],[87] is used for solving complex engineering problems. This algorithm uses the concept of swarm intelligence. Its operation is based on the behavior of flying birds and fish pools. These flock of birds (particles) search for the food (global best) in a specific area (search space) and the birds update their position in search of food according to the bird that finds the food. This method is applied to engineering problems where particles update position and velocity using the current best and global best position. PSO offers a variety of applications in the engineering problems. Mathematically PSO is represented as

$$X(i+1) = X(i) + V(i) \tag{2.25}$$

$$V(i) = W(V(i)) + C_1 \times r_1 \times (P_{best} - X(i)) + C_2 \times r_2 \times (G_{best} - X(i)) \tag{2.26}$$

where $x(i)$ is the current position $x(i+1)$ is the next position. $V(i)$ is the velocity. W is the weight, C_1, and C_2 are the controlling parameters and r_1 and r_2 are random numbers [88].

PSO can be used for MPPT control as well. In MPPT applications, the position of the duty cycle is going to be updated using the PSO algorithm. First, the particles or duty cycles are initialized in the search space, that is, between 0-100%. Then power is checked at every particle which is known as the fitness of the duty cycle [89].

In literature, PSO is implemented as an MPPT in PV systems. There are different variants of PSO which are proposed for tracking GMPP with high efficiency. Due to random numbers in the velocity vector, oscillations are caused even after achieving the GMPP which results in power losses. The effort is made to reduce the oscillation by improvising the PSO and achieve high efficiency. Another technique is presented which combines the PSO with INC. This hybrid technique achieves a high efficiency >98.5% with a high tracking time during the initial stage. Another effort is made which implements PSO on a low-cost controller.

2.3.3.2 Particle Swarm Gravitational Search Optimization (PSOGSO)

PSOGS is a popular heuristic technique used for optimization problems. PSOGS has been incorporated with PSO. Equation of PSOGS is shown as

$$F_k^d = G(z)\frac{M_{pt}(z) \times M_{ak}(z)}{R_k + \varepsilon}(x_n^i(z) - x_m^i(z)) \tag{2.27}$$

Where G(t) is instantaneous gravity, M_{pt}, M_{ak} are active gravitation and passive gravitation respectively. To avoid division by zero insertion of ε is necessary. (x_n^i (z)-x_m^i (z)) gives distances of active agents' positions. Instantaneous gravitational constant is represented as

$$G(z) = G_o \times e^{(\frac{\alpha \times iter}{\max_{iter}})} \tag{2.28}$$

Where, G_o is the initial value of gravity. α is the descending coefficient. Iter is the current iteration, max_{iter} is the maximum number of iterations. As a result, the total force exerted on candidate l is given by

$$F_l^d = \sum_{k=1,1\neq k}^{N\alpha} r_k f_l^d(z) \tag{2.29}$$

Where, r_k is an arbitrary number in the d dimensional search space. Acceleration is calculated as

$$F = \frac{m}{a} \qquad a = \frac{F}{m} \tag{2.30}$$

$$\alpha_l^d(t) = \frac{F_l^d(t)}{M_l^d(t)} \tag{2.31}$$

$$d_k^{it+1} = d_k^{it} - \Delta d_k^{it} \tag{2.32}$$

$$\Delta d_k^{it+1} = w d_k^{it} + c_1 r_1 \times \alpha_l^d(t) \times (P_{best} - d_k^{it}) + c_2 r_2 (G_{best} - d_k^{it}) \tag{2.33}$$

2.3.3.3 Fruit Fly Optimization Algorithm (FFOA)

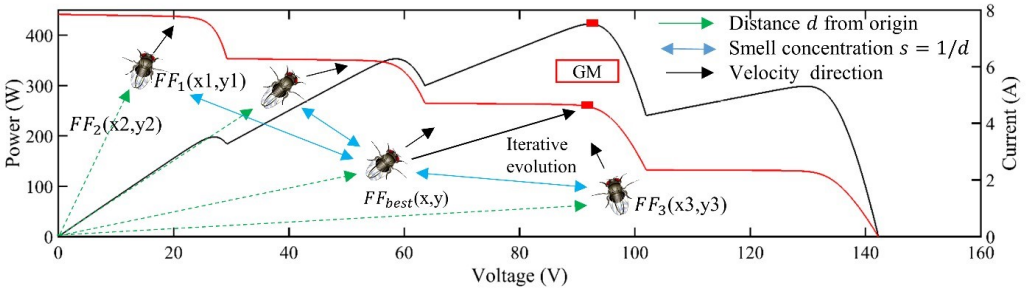

FIGURE 2.10: Fruit Flies finding target food iterative process

FFOA population is initiated randomly in a confined region bounded by I_{mpp} and V_{mpp} (5% to 95%). Fitness of each particles depends on the best smell and best value stored in every iteration. F_{best} is depicted visually in Figure 2.10. It shows I-V and PV curves of a PS system. Randomly initiated population does figurative exploitation and exploration in individual manner. Movement of individual particles is governed by its velocity vectors and smell concentrations. Smell concentration has inverse relation with distance from origin. This inverse relationship ensures fast initial velocity and a gradual decrease in velocity with respect to iteration number. This behavior results in smoother steady-state convergence of particles around GM with highest efficiency and least power loss oscillations. Step by step working of FFOA is discussed as follows:

Step 1: Define the location of the Fruit fly.

$$X_i = X_{axis} + rand() \tag{2.34}$$

$$Y_i = Y_{axis} + rand() \tag{2.35}$$

Step 2: Start the evolution by setting gen=0.

Step 3: Find D_{ist}. After finding D_{ist}, calculate smell intensification value S_i.

Step 4: After getting the $best_{indx}$ value and using Equation 2.35, the fitness function is defined as the maximum Output power V_{pv} x I_{pv}.

$$X_{axis} = X(bestIndx) \tag{2.36}$$

$$Y_{axis} = Y(bestIndx) \tag{2.37}$$

2.3.3.4 Salp Swarm Optimization (SSO)

Salps are marine animals as seen in Figure 2.11 (a). Their mobility is accomplished using water jet propulsion. They construct spiral-like chains for food discovery and sustainability, as seen in Figure 2.11 (b). SSA was first introduced by [1] for optimization purposes. Salp chains are comprised of a leader and followers.

The purpose of a heuristic algorithm in MPPT is to identify GM in its transient state as quickly as feasible and to limit oscillations in the steady state around GM to minimize power loss. SSA is used to optimize MPPT by taking these two properties into consideration. In this approach, duty cycle represents the search space, with values ranging from [0 to 1]. Equation 2.38 and Equation 2.39 are used in order to update the location of leader and follower particles.

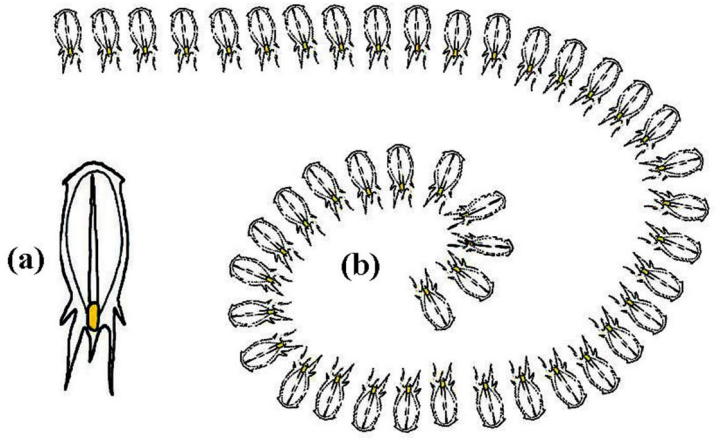

FIGURE 2.11: (a) Single salp (b) Salp chain [1]

$$x_j^i = F_i + c_i \left(\left(ub_j - lb_j \right) c_2 + lb_j \right) c_3 \geq 0 \tag{2.38}$$

$$x_j^i = F_i + c_i \left(\left(ub_j - lb_j \right) c_2 - lb_j \right) c_3 \leq 0 \tag{2.39}$$

where x_j^1 is the position of swarm leader, F_j is the food position, ub_j and l_j are upper and lower bound respectively. The weights c_1,c_2 and c_3 are random numbers. Exploration increases convergence rate around MPP, whereas exploitation is used to reduce power loss, hence the weight c_1 becomes crucial to balance between exploitation and exploration phenomenon is given by Equation 2.40.

$$c_1 = 2e^{-\left(\frac{4l}{L}\right)^2} \tag{2.40}$$

Where L the total number of iterations, l is the current iteration, c_1 and c_2 are randomly generated within the interval [0 to 1]. Position of follower particles is updated by Equation 2.41.

$$x_j^i = \frac{1}{2}\alpha t^2 + v_o t \tag{2.41}$$

Where x_j^i gives the position of ith particle in j^{th} dimension. New Equation 2.42 is obtained to update follower particles positions.

$$x_j^i = \frac{1}{2}(x_j^i + x_j^{i-1}) \tag{2.42}$$

Where x_j^i is the position of i^{th} follower salp in j^{th} dimension. Fitness function is given by Equation 2.43.

$$fitness = \frac{P_{\max}}{P_{availables}} \left(\left| \frac{i_{iter}}{\max_{iter}} \right| \right) \tag{2.43}$$

2.3.3.5 Performance Evaluation of SI Based MPPT Techniques

SI based MPPT techniques effectively track GMPP under various environmental conditions and low-cost hardware required, but the high settling time causes power loss. The comparative analysis of SI-based MPPT techniques is shown in Table. 2.3.

TABLE 2.3: Comparative Analysis of Swarm Intelligent Techniques

Technology	Advantage	Disadvantage
PSO	Performs well under PSC	High Tracking time
PSOGS	More efficient than PSO	Low efficiency
FFOA	High efficiency of upto about 99.5%	Costly hardware
SSO	Quick and robust tracking of GMPP	Oscillation around GMPP

2.3.4 Gap Analysis

Solar energy is one of most popular solutions for clean energy due to its zero operational carbon footprint, low maintenance and it's abundant nature. For high-energy production, multiple solar panels are required in series/parallel combinations. However, in dynamic environmental conditions, such as non-uniform irradiance and temperature on the solar panels, photovoltaic systems fall into the category of PS condition. The control problem in PV systems is highly non-linear and time sensitive.

Conventional MPPT techniques such as P&O, INC, Mod-INC don't have the ability to distinguish between LM and GM, therefore they tend to get stuck in the LM's. Also, numerous oscillations around the MPP result in significant loss of power.

Swarm intelligence-based MPPT techniques have the ability to solve the problems presented by the conventional techniques however, high tracking time, slow convergence, low tracking efficiency, low power tracked and low extracted energy makes them unstable for MPPT purposes.

Intelligent MPPT techniques. i.e. (Machine learning-based MPPT techniques) are presented in the literature as well however these techniques are system dependent and computationally very expensive. In order to mitigate the problems of earlier mentioned techniques, a hybrid solution which uses a combination of SI and ML based technique is proposed in this work. SI based technique helps to generate a dataset consisting of duty cycle and corresponding values of voltage and curent for different irradiances, upon which the Neural Network (NN) trains itself and predicts the duty cycle with respect to MPP.

The research gap analysis shows three main areas of improvement. First is the fast tracking of GM under dynamic operations. Second is the minimization of the fluctuation in the initial phase of GM tracking and zero oscillation at the GM in a steady state. The third objective is the utility of intelligent control to tackle PSC and CPS problems. The proposed techniques fulfills all three objectives with high responsiveness and robustness.

2.3.5 Problem Statement

The amount of electricity generated by a PV system is determined by the amount of solar irradiation and the temperature conditions in which it is operated. The PV panel current and voltage tend to vary without the MPPT controllers, which can be dangerous for the PV panels. Solar irradiance non-uniformity causes numerous power peaks in a PV curve, which are referred to as LMPP and GMPP. LMPP becomes very critical for MPPT techniques as techniques tend to get stuck in

LMPP or oscillate around GMPP, as a result, efficiency of the PV system is significantly affected.

The tracking time, settling time, tracking efficiency, energy extraction, and implementation cost, all factors into the choice of MPPT control mechanism. The literature suggests that MPPT control approaches have a high tracking and settling time, and low tracking efficiency. An intelligent technique which is a hybrid of swarm intelligence and machine learning that can minimize such issues needs to be implemented. ML algorithms are data hungry techniques and training on large datasets consume a lot of computational power and time which makes these techniques hard to use. Therefore the suggested MPPT control strategy should be able to generate a smaller dataset and train itself on it while generating efficient results.

For this purpose, GRNN trained with Sailfish Optimizer, i.e. a hybrid MPPT technique has been presented in this work. GRNN-SFO has the ability to generate a dataset of duty cycle, voltage and current, train itself. GRNN-SFO is quick, easy to implement, and offers magnificent power tracking capability.

2.3.6 Chapter Summary

This chapter provides an in-depth overview of MPPT techniques. Conventional MPPT techniques include FOCV, FSCC, P&O, and INC. Conventional MPPT techniques perform better under uniform irradiance conditions. P&O offers simple implementation, however the oscillations around the MPP is the major drawback of the P&O. INC reduces ripples at the MPP however under PSC, conventional MPPT techniques do not perform well and are unable to differentiate between GMPP and LMPP.

SI based techniques namely PSO, PSOGS, FFA, and SSO have a good ability to track the GMPP however slow convergence, high tracking and settling time makes them inadequate for tracking MPP under PS Conditions.

Intelligent MPPT techniques are presented which include ANN, SVM, KNN, BoT and MVR. These techniques perform with high efficiency under PS Conditions but high training data and high computational power is required for the implementation of these techniques which makes them difficult to use for MPPT. As a solution, bio-inspired metaheuristic optimization algorithms are proposed for the MPPT which perform with higher efficiency and takes less computational power for MPPT implementation.

Chapter 3

Proposed Technique(s) and Implementation

This chapter deals with the mathematical model and characteristics of the PV system components in detail. The purpose of this chapter is to discuss the hardware components and proposed machine learning algorithm, optimization algorithm, and PV system integration as MPPT control.

3.1 PhotoVoltaic (PV) System and its Components

A standalone PV system, as seen in Figure 3.1, is made up of the following components:

- PV module
- Boost Converter
- MPPT control
- Load

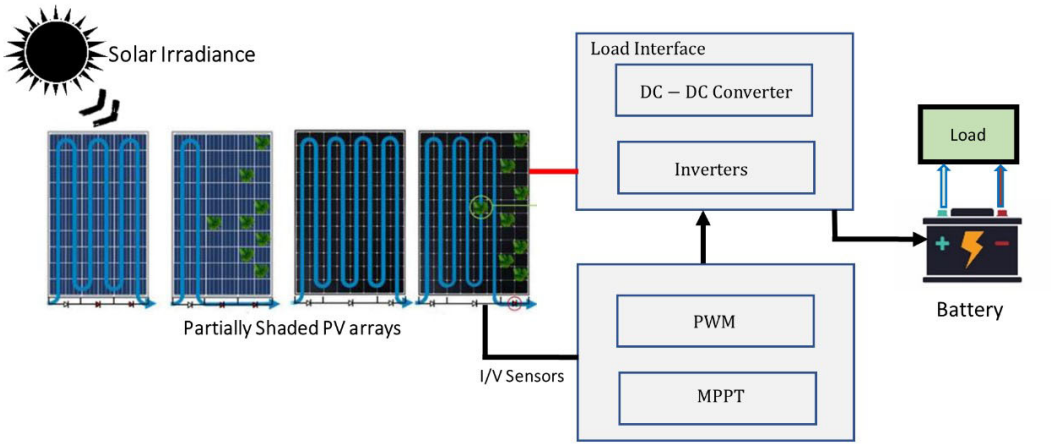

FIGURE 3.1: Components of a typical Photo-Voltaic (PV) system consisting of PV panels, load interface, controller and load

Load interfacing and control application is provided by the DC boost converter in this section. Current and voltage is fed into the MPPT controller which calculates PV power by product of current and voltage. The stabilized output power depends upon the efficient design of boost converter's components, that is, inductor, capacitors, and frequency of switching. The microcontroller generates PWM signal given to MOSFET driver and controls the voltage of the PV panel.

3.1.1 Boost Converter

Since DC power is transferred to the load via converter or inverter circuits therefore efficiency plays a critical role in PV systems. Among numerous DC converter topologies discussed in the literature, the DC-DC boost converter [90] is preferred because the output voltage greater than the input voltage reduces heat dissipation losses in this converter.

The simulation and practical implementation has been done using boost converter in this thesis. The relationship of duty cycle is given in Equation 3.1. Figure 3.2 depicts an example of a boost converter.

$$D = \frac{T_{on}}{T_{sw}} \tag{3.1}$$

where T_{sw} is the switching time, D is the duty cycle, T_{on} is the switch on time, T_{off} switch off time.

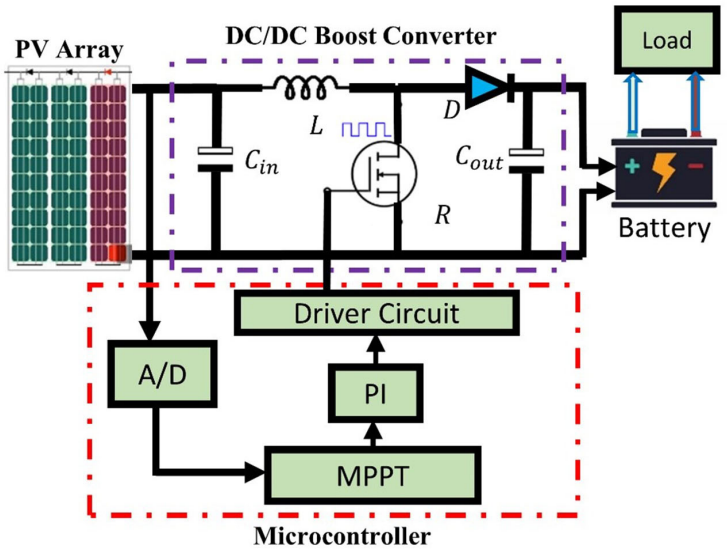

FIGURE 3.2: MPPT control using Boost Converter

3.1.1.1 Mathematical Model of Boost Converter

The mathematical modeling provides design of circuit components using mathematical correlations. The output voltage is dependent upon the variation in duty cycle, which varies between 0%-100%. The input capacitor (C_{in}) is dependent upon switching frequency and current ripples whereas the output capacitor (C_{out}) depends upon the duty cycle. Inductor is an important component whose design depends upon the PV voltage range and ripple tolerances. The inductor controls the current ripples at the output. The design of all the components depends upon the following equations

$$C_{in} = \frac{\Delta I_d}{8\Delta V_d f_{sw}} \tag{3.2}$$

$$C_{out} = \frac{I_o D}{8\Delta V_d f_{sw}} \tag{3.3}$$

$$L = \frac{V_{PV} D}{2\Delta I_d f_{sw}} \tag{3.4}$$

Where C_{in} is the input capacitor, C_{out} is the output capacitor, I_{out} is the output current, $D$is the duty cycle, V_{PV} is the voltage of photovoltaic system, L is the inductance, δI_d and δV_d are the ripples of current and voltage. The switching frequency is represented by f_{sw}.

3.1.1.2 Boost Converter Application for MPPT

PV system differs from conventional energy sources mainly due to storage issues unlike hydro power, and chemical energy. Therefore continuous extraction of power is required which is done by interfacing DC-DC converter between PV panel and load. In order to maximize the power transferred to load from the PV module, the maximum power transfer theorem is applied which states that the maximum efficiency is achieved when resistive mismatch is equal to zero between the load and the power source. If the load resistance at the PV panel is kept at maximum power then the change in environmental conditions will affect the operating point. Therefore maximum power will not be delivered to the load. The resistance of load and boost converter will change the duty cycle and will be maintained at that value where maximum power is delivered to the load.

This load variation capability provided by the boost converter is very effective [91].

TABLE 3.1: Specification of Electrical Components used in Simulation

Components	Values
Panel Power	300 W
Inductor	1.4 mH
Capacitor at input, Cin	10 uF
Capacitor at output, Cout	470 uF
Frequency of switching, f	50 kHz
Resistive load, RL	70 Ω

The equivalent resistance is given by Equation 3.5 as

$$R_{eq} = \frac{V_o}{I_o} = V\frac{(1-D)^2}{I_o} = R(1-D)^2 \tag{3.5}$$

Where R_{eq} is the equivalent resistance, R is the resistance, I_o is the output current, D is the duty cycle, and V_o is the output voltage.

The change in resistance is dependent on the change in duty cycle when R is kept constant. Change in the load resistance, or in environmental conditions will be catered for by the MPPT control technique by continuously monitoring the power of the PV panel. Table 3.1. provides DC converter design parameters.

3.1.2 MPPT Controller

Photovoltaic power generation is dependent upon manufacturing technology, weather conditions, irradiance, temperature, and configuration schemes. Photovoltaic are used in commercial scale solar parks and standalone PV systems. However PS reduces the efficiency of PV systems, therefore modern MPPT control is focused on minimizing these affects [92]. MPPT techniques can be classified into

- Offline control techniques (Classical)
- Online control techniques (Classical/Intelligent)
- Hybrid of classic-intelligent methods

The offline techniques use mathematical relationships among the operating conditions and optimum operating point. The output power is estimated and random duty cycle values are calculated. The limitations arise when irradiance or operating temperature changes significantly. Studies show that there are no real time adjustments to the operating conditions. As a solution, online methods, such as, P&O measure the instantaneous power and adjust the control signals accordingly in order to increase the output and minimize the mismatching between load and

power generation. Hence effective decision-making enhances the output power [93].

Although these approaches are useful for tracking MPPT, there are several issues that cannot be overcome, such as numerous power points, steady-state inaccuracies, and oscillations. Although heuristic algorithms such as PSO and PSOGS are successful in identifying GM, the time required to track the MPP and transients in the power curve are major drawbacks with these methods.

Advanced approaches are employed in hybrid MPPT models to maximize PV outputs. To efficiently use power management controllers with renewable energy resources, creating a control for MPPT must consider computing power, cost, efficiency, and complexity. After getting the design parameters, we go into the designing phase.

The real-time changes in electrical characteristics of PV system due to resistances, temperature, irradiance or resistive load makes the system least deterministic which is well accommodated by optimization algorithm because it can handle less accurate modeling of the nonlinear base system. The current source model and diode action are well suited for offline methods where variation in operations is very limited. Mainly fixed duty cycle, MPP locus Characterization, P&O and INC are utilized [93].

The progress in intelligent systems and nature-inspired optimization algorithms has enabled MPPT control techniques to deal with hot spot affects, non-uniformity, changing temperature hikes, PS, and failure to reach GMPP all of which affect the power of a PV system. A standard PID controller is applicable for control action in combination with conventional techniques to adaptively accommodate the step size to reduce the oscillations around GMPP. It not only enhances the steady-state and transient response but also lowers the undesired fluctuations at GMPP. However, conventional techniques are still unable to deal with CPS and PS problems. Therefore hybrid models are more valuable.

A hybrid model is enforced using two major steps. Firstly GRNN, GA, Fuzzy, or ANN is integrated with classical controller for the desired outcome. In second

step optimized parameters after extensive training are exported for online control action.

3.1.3 Load

An electrical load is a portion of a circuit that consumes active electrical power. A load of a PV system can be AC or DC. Therefore certain predefined criteria should be met before connecting the load to PV system supply. DC load compensation is simpler but the AC load increases the design complexity. Since grid-connected inverters pump electricity into the grid, they are expected to maintain very high power quality to ensure that acceptable power flows into the grid. As a result, inverters should have a very low harmonic content of line currents. Grid-connected inverters are also supposed to have active islanding detection capabilities, according to IEEE 1547 [94].

Modern PV systems in building integrated environment require inverter interfacing. In grid-tied setup, islanding affect may occur. This islanding causes safety concerns and therefore, anti-islanding capability is needed in inverters.

3.2 Proposed Technique(s)

In this work, a General Regression Neural Network has been proposed in order to track the MPP under changing environmental conditions, i.e. fast changing uniform irradiance, PS, and CPS. Also, Radial Basis Function Neural Network has been implemented in this work since both GRNN and RBFN belong to the same category of NN's. Therefore in order to analyze the performance of GRNN properly, RBFN has also been trained under same conditions. Sailfish Optimization Algorithm has also been proposed in this work.

The general flow of the proposed techniques is respreented in Fig. 3.3. The purpose of SFO is to generate a dataset and tune the hyperparameter of both NN's.

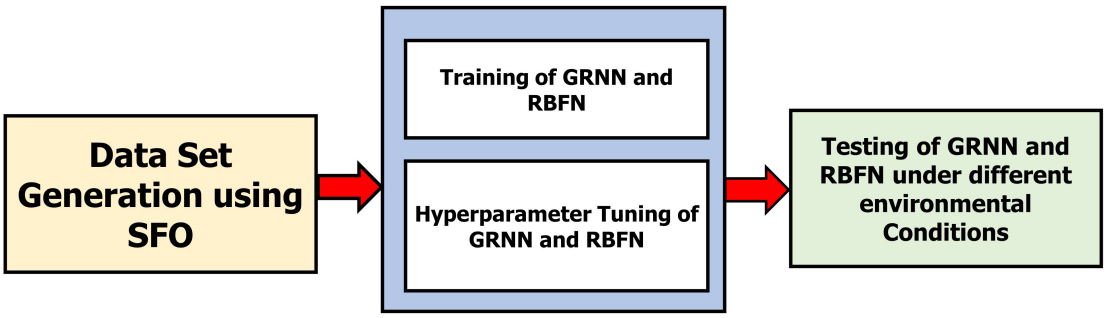

FIGURE 3.3: Block diagram representing the flow of the proposed MPPT technique.

In general, SFO algorithm is used to generate a dataset on which NN's are going to train themselves upon. Since, MPP is varied by varying the duty cycle of the boost converter, therefore this dataset consists of duty cycle as the output and voltage and current as its features. After the dataset generation, GRNN and RBFN is trained and tuned using the same SFO algorithm. Finally, both of the NN's are tested under different environmental conditions.

3.2.1 Machine Learning Algorithms

Two machine learning based algorithms have been implemented in this work.

- General Regression Neural Network (GRNN)
- Radial Basis Function Network (RBFN)

3.2.1.1 General Regression Neural Network (GRNN)

One of the most common neural network is GRNN, which is a form of supervised Feed Forward Neural Network (FFNN). GRNNs are famous for their ability to train themselves quickly on sparse data sets. GRNN networks can be trained quickly because the data only needs to propagate forward once, unlike most Back Propagation Neural Networks (BPNN), which may need to propagate data forward and backward multiple times before finding an acceptable error[13], [14],[16],[15],[17],[18].

Interpolation problems are well-suited for GRNNs. As with standard regression approaches, GRNN is used to estimate continuous variables. It employs a single smoothing parameter (σ) that has been fine-tuned for optimal learning.

Given an input vector x, it returns the most likely scalar Y. Let *f(x,y)* be the continuous probability density function of a vector and a scalar random variable, respectively. Let x be a particular random X measured value. The conditional mean of Y given x (also known as regression of T given x is given by:

$$E\left[Y/X\right] = \int_{-\infty}^{\infty} Y \cdot f(Y/x)dy \frac{\int_{-\infty}^{\infty} Y \cdot f(x,Y)dy}{\int_{-\infty}^{\infty} f(x,Y)dy} \tag{3.6}$$

The regression is parametric if the connection between independent *(X)* and dependent *(Y)* variables is described in a functional form with parameters. The nonparametric estimate approach will be utilized because there is no real knowledge of the functional form between x and y. Gaussian function is used as one of the consistent estimators for a nonparametric estimate of *f(x,y)*.

The key benefit of GRNN is that it has high convergence and only takes a few data samples to train. GRNN is separated into four levels, as seen in Figure 3.4. GRNN primarily analyses linear or non-linear regression on an input vector and produces the output represented by Equation 3.11

$$K_j^2 = (x - x_j)^T (x - x_j) \tag{3.7}$$

$$Y_j = e^{-\frac{\left(x-x_j\right)^T \left(x-x_j\right)}{2\sigma^2}} \tag{3.8}$$

$$S_w = \sum_{j=1} w_j Y_j \qquad S_\delta = \sum_{j=1} Y_j \tag{3.9}$$

$$Y = \frac{S_w}{S_\delta} \tag{3.10}$$

$$Y(x) = \frac{\sum_{j=1}^{m} w_j e^{\left(\frac{K_j^2}{2\sigma^2}\right)}}{\sum_{j=1}^{m} e^{\left(\frac{K_j^2}{2\sigma^2}\right)}} \tag{3.11}$$

The input layer of a GRNN is entirely connected to the second layer and is known as the first layer.

The first concealed layer is the second layer (also called the pattern layer). This layer is made up of N processing components or nodes, where N is the number of samples in a training data set and each node represents the input vector, X_i, that is connected with the j^{th} sample in the training data set. Each input vector is subtracted from the node's allocated vector, X_j. The node then squares this difference. The summing units receive the outputs from the pattern units.

It should be noted that the output layer always contains one more node than the second hidden layer. When you require a multidimensional (vector) output, all you have to do is add one more node to the second hidden layer, as well as one more node in the output layer for each member in the output vector.

The third layer is known as the summation layer, which consists of two nodes.The sum of the first hidden layer activations equals the second node's input. In Equation 3.7 and Equation 3.8 the term K_j^2 is the distance between the predicted sample and the trained sample x is referred to as the input vector for GRNN, x_j is the trained vector for the pattern layer. The pattern layer neuron is defined in terms of Gaussian function Y_j in Equation (3.10). The term w_j refers to the weight of neuron *(j)* in the pattern layer connected with the summation layer. Arithmetic summation S_δ and the weighted summation S_m represent the arithmetic and weighted sums of the inputs in the summation layer respectively. The only parameter which needs to be learned is the variance σ of the basis function.

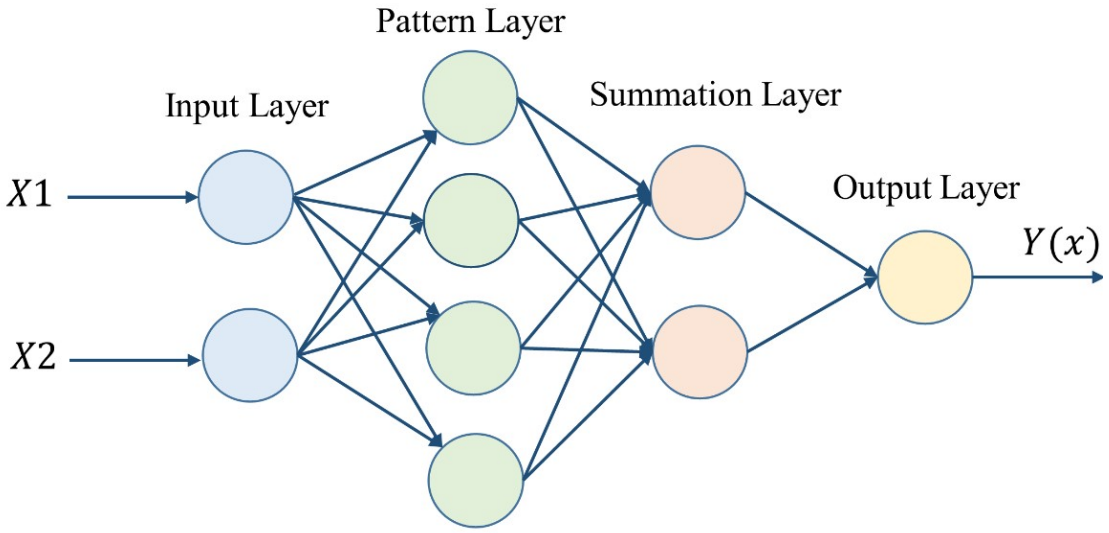

FIGURE 3.4: The structure of GRNN comprising of four layers, i.e. input, pattern, summation and output layer respectively.

3.2.1.2 Radial Basis Function Network (RBFN)

RBFNN is a popular alternative to Feed Forward Back Propagation Neural Network (FFBPNN), which was presented by Broomhead and Lowe in 1988. The weights and activation of a transfer function F provided for the units determine the network's behavior. The output of a processing node is determined by activation functions, which are mathematical formulas. By applying F to the output value, the activation function maps the sum of weighted values provided to them, which is then "fired" onto the next layer.

Linear function (LF), Threshold function (TF), Sigmoid Function (SF), and Radial Basis Function (RBF) are the four types of transfer or activation functions. RBFs are a type of activation function that consists of a collection of basis functions, one for each data set. RBF takes the following broad form as depicted in Equation 3.12.

$$G\left(\|X-u\|\right) \tag{3.12}$$

where G is a nonlinear symmetric radial function (kernel); X is the input pattern; and μ is the function's centre. RBF's output is also symmetric about the related

centre, which is a significant feature. As a result, $f(x_i)$ can be considered a linear combination of all the basis functions' outputs.

$$f(x) = \sum_{i=1}^{n} w_i G\left(\|X - u\|\right) \tag{3.13}$$

There are several common types of radial basis functions as represented in Table 3.2.

TABLE 3.2: List of Common RBF's

Symbol	**Description**
Thin Plate Spline	$G(x) = (x-\mu)^2\ log(x-\mu)$
Multiquadric	$G(x) = \sqrt{(x-\mu)^2 + \sigma^2}$
Inverse Multiquadric	$G(x) = \frac{1}{\sqrt{(x-\mu)^2+\sigma^2}}$
Gaussian	$G(x) = \frac{1}{\sigma\sqrt{2\pi}} e^{-(x-\mu)^2/2\sigma^2}$

μ and σ^2 are the function parameters which represent center and radius. A Gaussian function, often known as a "bell-shaped curve" or normal distribution, is the most prevalent kind of RBF. It may be used to generalize a global mapping as well as fine-tune local features. Since the Gaussian function has a more local effect, it is more physiologically acceptable than other functions. RBF differs from the others such that it decreases monotonically with distance from the center, generating the well-known bell-shaped curve that converts high values into low values and mid-range values into high ones. Figure 3.2.1.2 depicts the plot of a Gaussian function.

Gaussian function is mathematically represented as

$$f(t) = \frac{1}{\sqrt{2\pi\sigma^2}} e^{-\left(\frac{t-u}{2\sigma^2}\right)} \tag{3.14}$$

Where t is the current value of input.

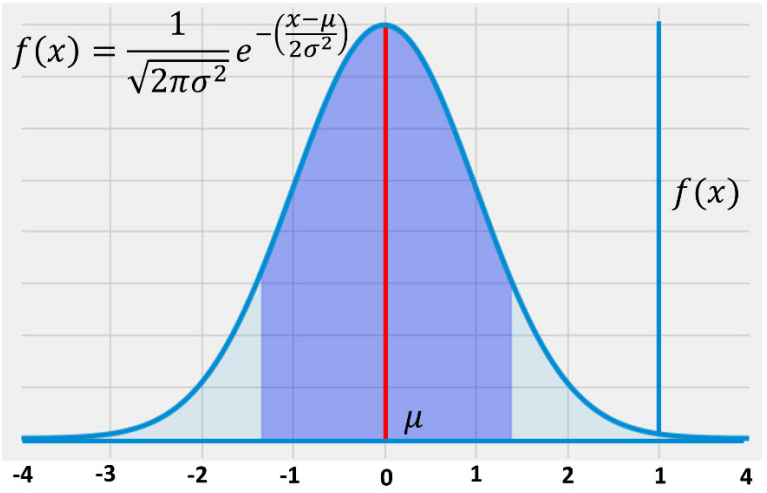

FIGURE 3.5: Illustration of Gaussian Function

$$u = E(T) = \int_{-\infty}^{\infty} x \cdot f(t)d(t) \tag{3.15}$$

$$\sigma^2 = E(T-u)^2 = \int_{-\infty}^{\infty} x \cdot (t-u)^2 \cdot f(t)d(t) \tag{3.16}$$

where μ is the distribution's mean (center) and σ^2 is the variance of the distribution (width or radius).

We may get the universal Gaussian probability density by extending Equation 3.16 to multiple dimensions:

$$f(t) = \frac{1}{(2\pi)^{p/2}} e^{\left(-\frac{1}{2}(t-u)^K \sum_{-1} (t-u)\right)} \tag{3.17}$$

where p is the number of dimensions, and μ is the mean p-dimensional vector.

RBFs are effective for estimating functions and recognizing patterns [24] and can be used to solve situations where the input data is distorted by additive noise. The output layer has a single neuron with a node y_k which generates the control signal d with an activation function as shown in Figure .

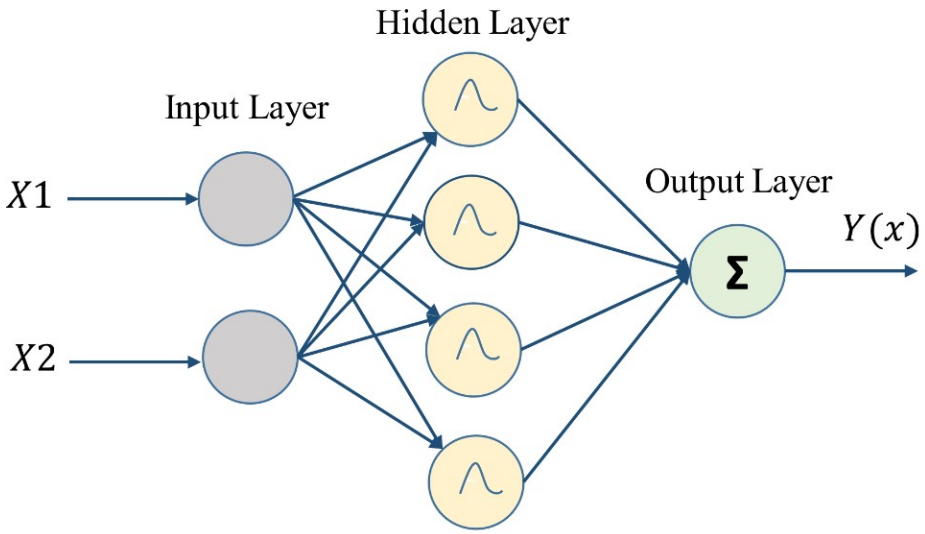

FIGURE 3.6: Extended diagram illustrating the architecture of RBFN with hidden functions

The distance between the input vector and a prototype vector determines the activation function of the hidden unit in the RBFN feed-forward NN model. The controller that creates the duty cycle for the PV system's converter is built using RBFN. The proposed RBFN has three layers: an input layer, a concealed layer, and an output layer. Voltage and current are fed to the input layer whereas the output of the NN is duty cycle *d*. The net input and output data are sent to the next layer by the input layer.

$$x_k(z) = net_k \tag{3.18}$$

$$y_k(z) = f_k\left[net_k(z)\right] = net_k(z), k = 1, 2 \tag{3.19}$$

$$net_k(z) = -(x - M_j)^T \sum_j (x - M_j) \tag{3.20}$$

$$y_j(z) = f_j[net_j(z)]_2 e^{(net_j(z))} j = 1, 2 \tag{3.21}$$

where x_k is the input layer, net_k is the sum of the input layer and y_i is the hidden layer with node k. The hidden layer consisting of neurons uses Gaussian functions as a membership function for each node in RBFN.

3.2.2 Sailfish Optimzer (SFO)

SFO algorithm is inspired by natural behavior of sailfish in the wildlife. In this section a detailed mathematical model is provided [95].

3.2.2.1 SFO: Inspiration

The most prominent social behavior in hordes of mammals is group hunting. The group efforts of predators reduces the energy consumption, efforts and increases the chances to kill the prey comparatively. Some animals aim to kill their prey with little or no coordination of attack, but others devise intricate hunting techniques. The hunting process has evolved over millions of years.

This strategy helps to conserve energy. SF alternate their attacks on schooling sardine prey. Figure 3.7 shows each behavioral state of SF's group hunting. SF being the fastest ocean creature can reach speeds of upto 100 km/h. The prey such as sardines are pushed towards the surface (Figure 3.7 A, B). The maneuverability of sardines is challenging for SF (Figure 3.7 C). SF attacks to injure several sardines or tap a single sardine (Figure 3.7 D). Since SF acceleration is higher as compared to sardines, sardines cannot outswim the SF to avoid being captured. A segregated sardine can be easily captured (Figure 3.7 E).

SF fin and body rigidity helps to hunt the prey quickly (Figure 3.7 F). To avoid injury the SF use color changes to indicate attack modes. The attacking behavior of SFO can be mathematically used as an optimization algorithm.

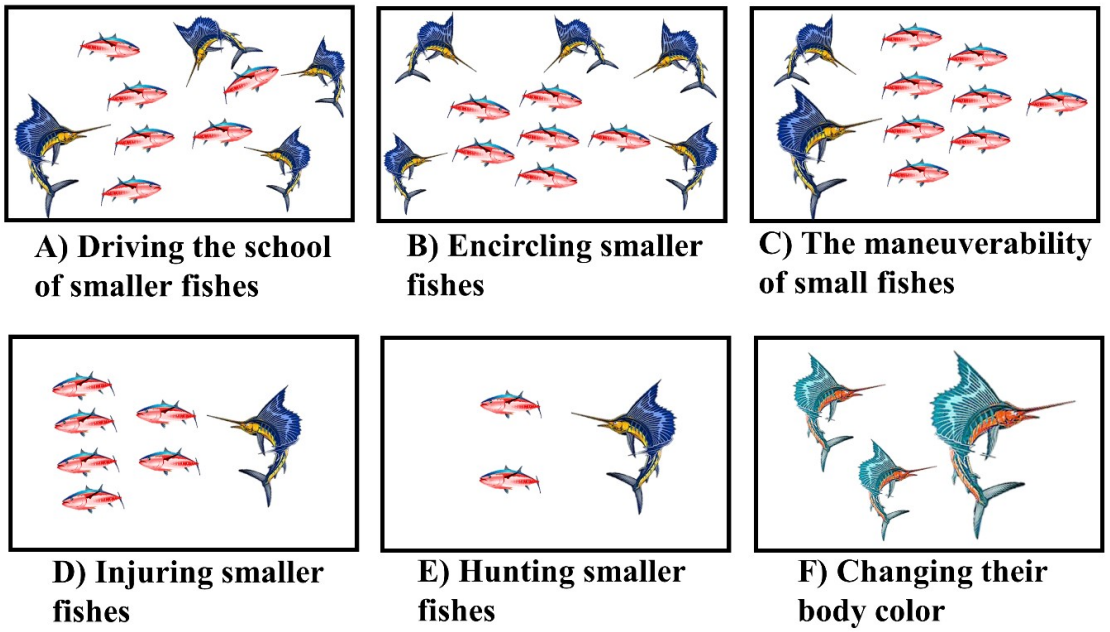

FIGURE 3.7: Sail Fish Hunting Behavior

3.2.2.2 SFO: Initialization

SFO is a meta-heuristic algorithm based upon population evolution over time. Each SF represents a candidate solution. The position of sailfish in the search space are the parameters to be optimized. The initial population is initiated randomly over the solution search space. In a d-dimensional search space, the i^{th} member at the k^{th} search has a current position SF_i,k ϵR (i=1,2,...,m).

3.2.2.3 SFO: Elitism

The position of search agents in the space is updated periodically during which good solution may be lost. Elitist selection is employed to minimize this loss. It is done by transferring the best solutions in the next iteration. The best position of SF is saved and transferred as an elite solution. In each iteration the position of injured sardine is also preserved as the best target for cooperative hunting strategy representing the highest fitness at i^{th} iteration as $x^i_{elite_SF}$ and $x^i_{injured_SF}$ respectively. This scheme is useful to avoid repeated exploration and avoid discarded solutions.

3.2.2.4 SFO: Attack Alteration Strategy

The SF attack the prey one after the other to avoid injuries and enhanced efficiency. This strategy promotes the rate of success using well organized coordinated attack. The herding prey adjusts their position according to the location of predator SF. The SFO algorithm mimics attack-alteration strategy of SF. As illustrated in Figure 3.6, the SF searches a wide section of the search space during the exploration phase to locate the best alternatives for further refining. The SF do not attack haphazardly. They can attack in particular directions while continuing to shrinking the attack circle. SF update their hunting position according to the best probability of success around the prey fish pool. In SFO algorithm, the updated SF position denoted by $x^i_{new_SF}$ is calculated using Equation 3.22 as

$$X^i_{new\_SF} = X^i_{elite\_SF} - \lambda_i \times (rand\,[0,1]) \times \left(\frac{X^i_{new\_SF} + X^i_{injured\_s}}{2} \right) \tag{3.22}$$

where $x^i_{elite_SF}$ is the elite sailfish position that has been formed up to this point, $X^i_{injured_s}$ calculates the injured sardine position recorded so far. $x^i_{old_SF}$ is the current SF position, rand [0,1] is the random number, λ_i is the coefficient at the i^{th} iteration that is generated as follows

$$PD = 1 - \left(\frac{N_{SF}}{N_{SF} + N_S} \right) \tag{3.23}$$

where N_{SF} and N_{SF} are the number of sailfish and number of sardines respectively. The value of λ influences the position of SF around prey. λ parameter will be 1 when rand [0,1]>0.5 while it tends to be -1 when rand[0,1]<0.5 and will go to zero if rand[0,1]=0.5. Fluctuations of λ and new position devise the divergence of SF while iteratively converging towards the globally best solution while maximizing the exploration process.

3.2.2.5 SFO: Hunting and Catching Prey

During the start of group hunting, the prey is seldom killed. In 95% of the cases, the prey, that is, sardines only suffer from scales loss and injuries. Initially the prey and predators have high energy levels for hunting and escaping. Sardines show high mobility and escape agility. Gradually this process slows down as both prey and predator's energy drops. The sardine lose the sense of directional attack loosing escape maneuverability.

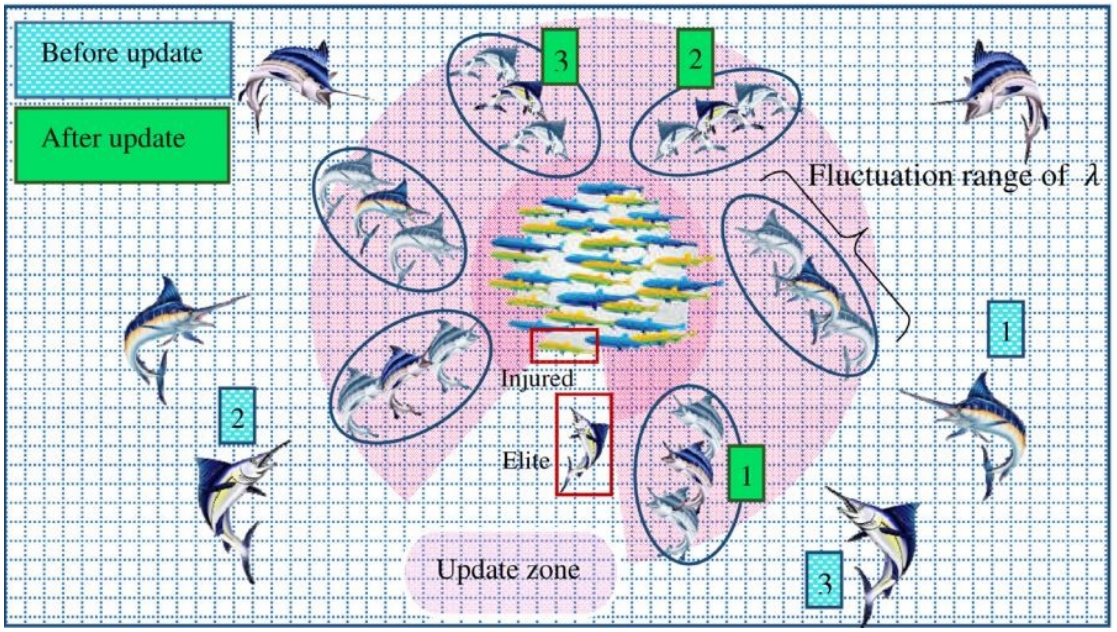

FIGURE 3.8: Swimming Sailfish around the prey school in the search space

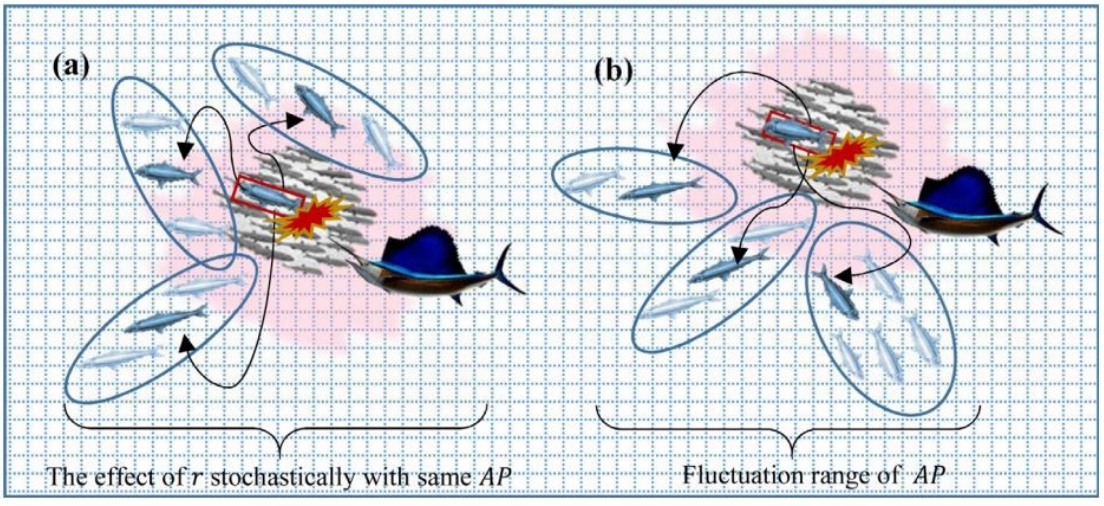

FIGURE 3.9: Slashing the prey school by Sailfish and update the position of sardines in the search space

Prey hit by SF's, break off the prey from the school. This behavior is mimicked as attack power of SF that is obliged by the position of the SF and sardine. The updated position of sardine $x^i_{new_s}$ in new iteration is given by Equation 3.24.

$$X^i_{new\_s} = r \times \left(X^i_{new\_s} - X^i_{old\_s} + AP\right) \tag{3.24}$$

where $X^i_{elite_SF}$ is the best position of the elite sailfish formed.$X^i_{old_s}$ is the current position of the sardine. r is a random number between 0 and 1 and the AP shows the amount of sailfish attack power which can be calculated as

$$AP = A \times (1 - (2 \times Itr \times \varepsilon)) \tag{3.25}$$

where A and ϵ are the coefficients for decreasing the value of power attack linearly from A to 0. Using AP, α number of prey update their location and the number of variables β.

$$\alpha = N_S \times AP \tag{3.26}$$

$$\beta = d_i \times AP \tag{3.27}$$

where N_s is the number of sardines in each cycle and d_i is the number of variables at the i^{th} iteration. According to AP parameter, if the intensity of the sailfish's tap is low. such as AP¡0.5, only α sardines with β variables will be updated. However if the sailfish's tap is high such as $AP \geq 0.5$, then the position of all sardines will be updated. Basically AP and r parameters assist SFO in order to show a more random behavior throughout optimization.

The position of wounded prey must be taken into account to maximize the likelihood of hunting the new prey. This is achieved using the position of sardines and is shown by Equation 3.28.

$$X_{SF}^{i} = X_{S}^{i}; iff(S_i) < f(SF_i) \tag{3.28}$$

where X_s^i is the current position of the sardine and X_{SF}^i represents the current position of the sailfish.

3.2.3 Dataset Generation using Proposed SFO Algorithm

Since MPPT problem is the problem of regression, that means there is going to be only one value in the output. In this work, we are interested in calculating the value of duty cycle, since by varying the value of duty cycle of the boost converter, the operating point of PV array can be changed accordingly. Therefore, the output value of the dataset is duty cycle. The output of the PV panel is voltage and current. These values are then used as an input to the MPPT controller, therefore the input features of the NN's are voltage and current, against which the value of duty cycle is being predicted.

For dataset generation, for each case of environmental condition, i.e. fast changing uniform irradiance, PS and CPS, random sets of duty cycles are initialized. In this work, 4 random duty cycles are used as shown in Fig. 3.10 (a). For different values of irradiances, i.e. $100\frac{KW}{m^2}$ to $1000\frac{KW}{m^2}$ experiments has been conducted. For each value of irradiance, different values of duty cycles are updated using the Equation 3.24 and Equation 3.25 of SFO. In this work, the tuning parameter of SFO, i.e. the value of iter, which represents the number of iterations, has been selected to be 10.

In 10 iterations, all 4 values duty cycles update their positions as shown in Figure 3.10 (b) and finally reach the GMPP as shown in Figure 3.10 (c). This process is repeated for 10 different values of irradiances while keeping temperature at STC.

i.e.25^o. Since boost converter requires up to $20ms$ to settle at any given value of duty cycle, therefore each value of duty cycle is used for up to 20ms and value against each duty is stored after every $2.5ms$. Therefore after 10 iterations and 10 different values of irradiances we get 3200 samples.

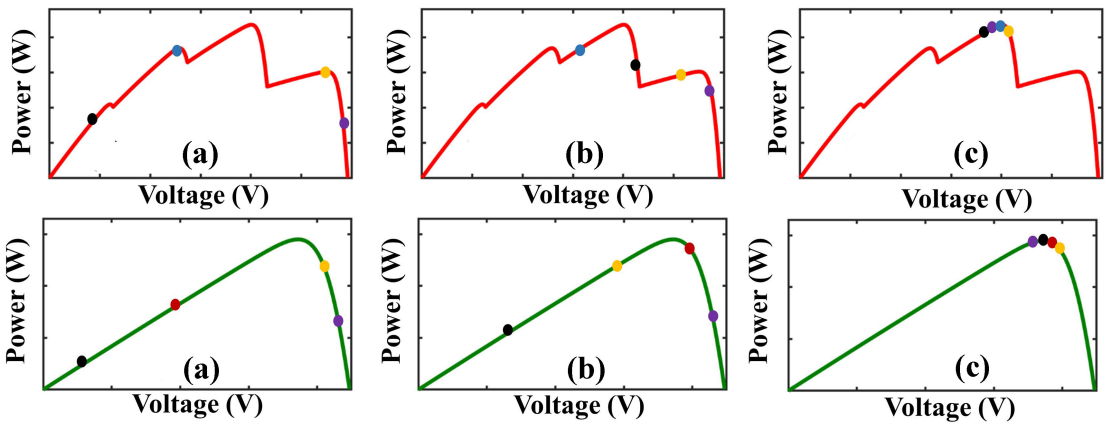

FIGURE 3.10: Duty cycle updation during several iterations under differnt environmental conditions

3.2.4 Training and Tuning of GRNN and RBFN

Figure 3.11 represents the flowchart showing the training of GRNN and RBFN. Since σ is the only free parameter in GRNN and RBFN and suitable values of it will improve the NN's accuracy, it should be estimated. GRNN and RBFN use gaussian activation function in their hidden layers therefore width of this activation function is very critical in generating a best fit model for both the NNs.

The value of σ, i.e. the spread factor can be set to 0.01 to 1. Figure 3.12 shows shape of gaussian activation function for different values of σ. A small value of σ as means that the model is going to underfit the training data as shown in Figure 3.13 (a), where as a large of σ, means that the model is going to overfit the training data as shown in Figure 3.13 (c).

Using an ideal σ value is critical in order to obtain the best fit model, as demonstrated in Figure. 3.13 (b). Since there is no ideal analytical solution for determining σ, numerical methods can be employed to approximate it. One of the used technique is the holdout method. In this technique, samples are deleted at random from the training dataset; next, using the GRNN with a fixed σ, the output is computed using the removed samples; and finally, the error between the network outputs and the sample targets is obtained. This technique is repeated for various σ values.

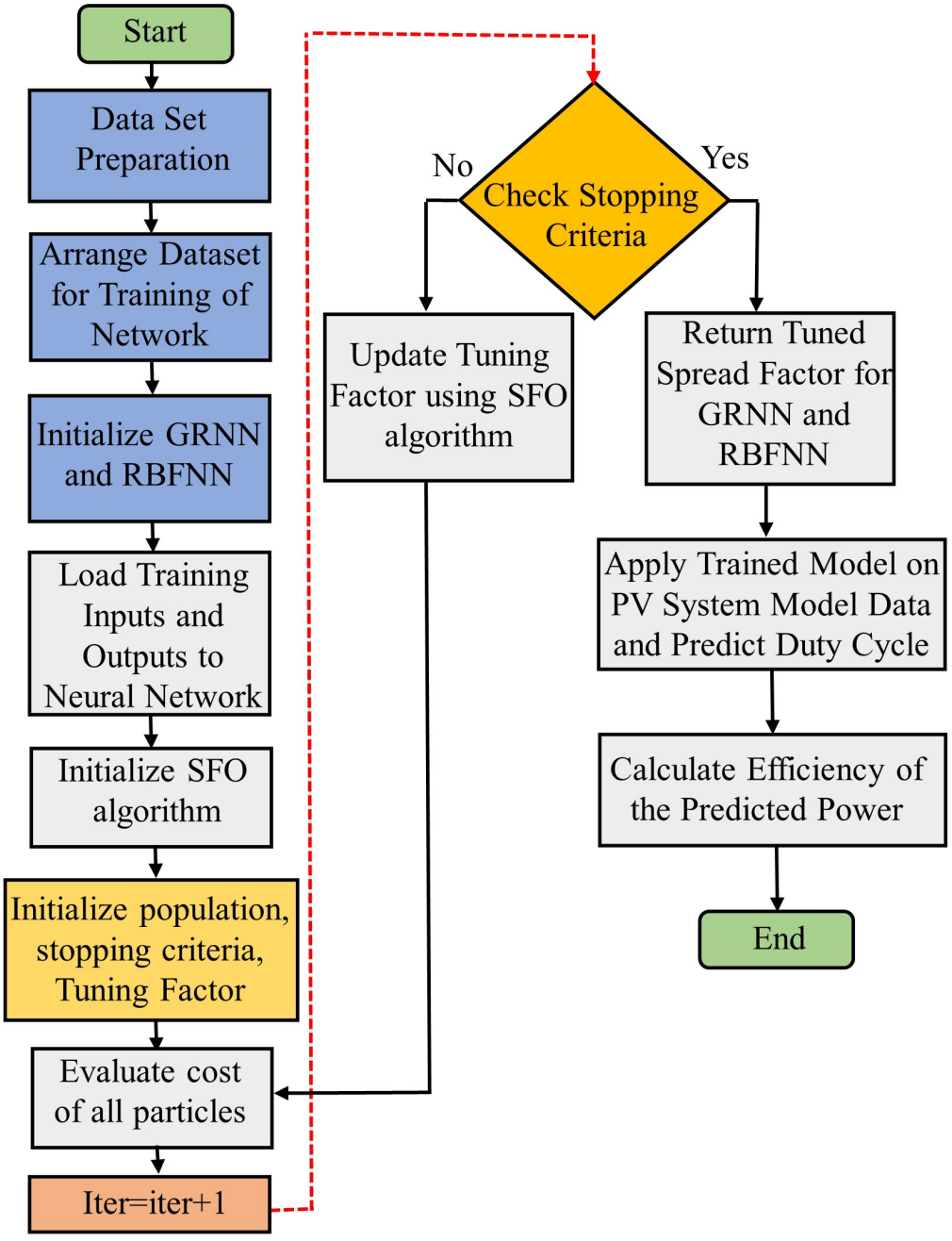

FIGURE 3.11: Flowchart of training of GRNN and RBFN using SFO

Different search and optimization strategies has also been used to find (σ). Genetic algorithms (GA) and differential evolution (DE), for example, are viable solutions. In this work, SFO has been proposed for proper tuning of σ. The value of σ is adjusted such that random values of σ are initialized (50 in this case), and NN's are trained on each of those values. Training errors are then calculated and each value of σ is updated for about 10 iterations. After 10 iterations an optimal value of σ is returned which in this case is 0.6.

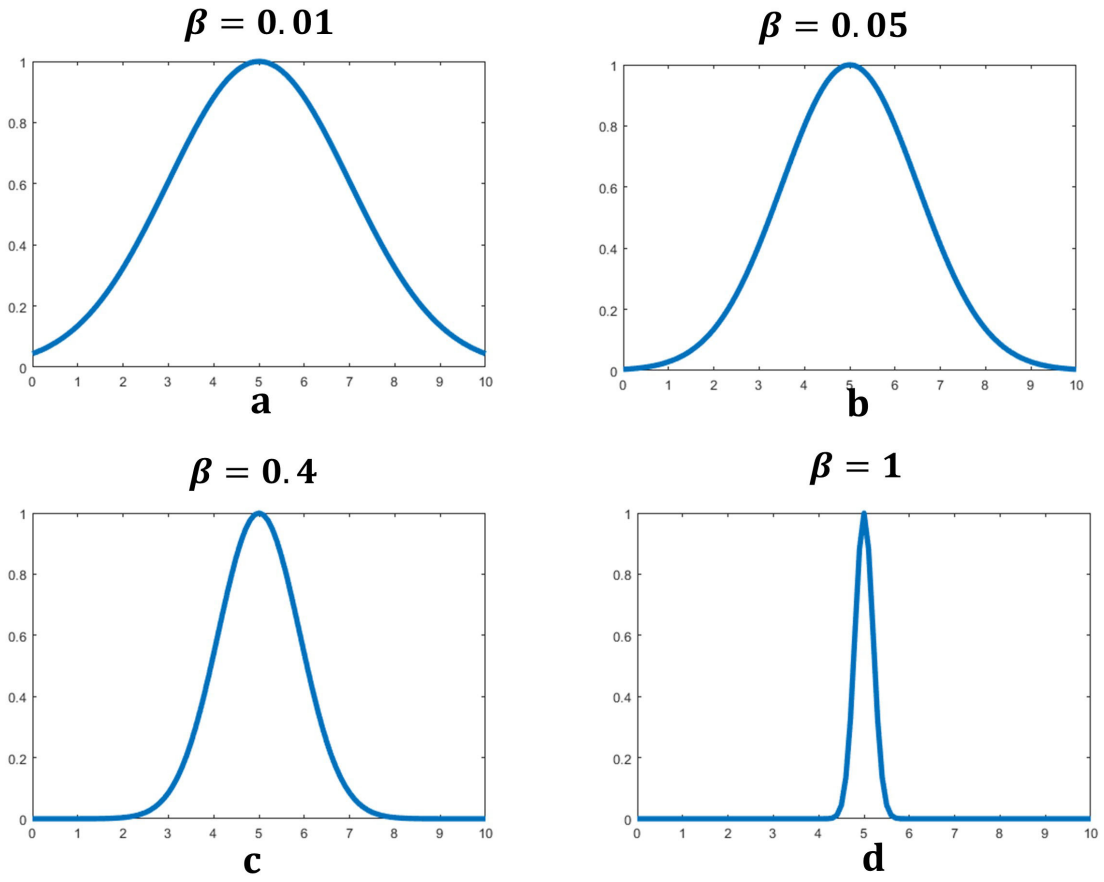

FIGURE 3.12: Variation in the widh of gaussian activation functions depending on values of β

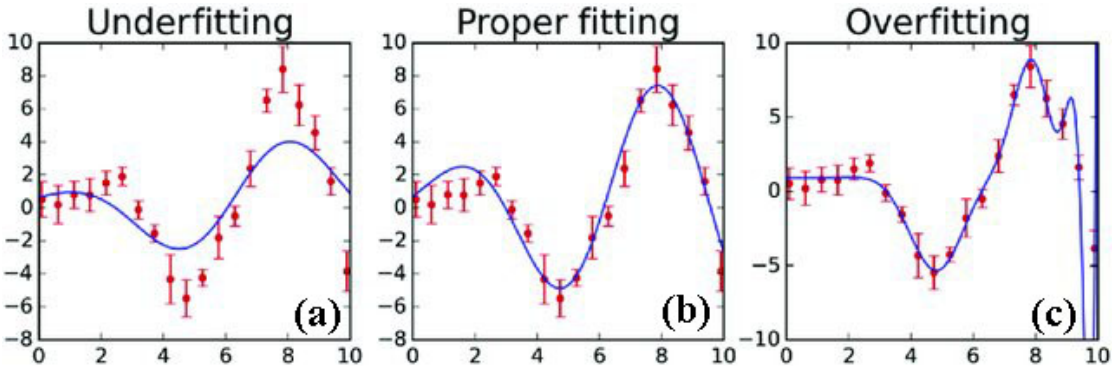

FIGURE 3.13: (a) Underfitted model (b) Best fit model (c) Overfitted model

In order to train the neural network, inputs with defined outputs are required. A neural network is trained with two inputs defined as $X_i = V_{pvh}$ and $X_2 = I_{pvh}$. Input vectors are just a way on the GRNN's input layer and the distance required for recording the pattern is obtained using the pattern node of the pattern layer.

The number of neurons of pattern layer are dependant on number of input samples which in this case is 3200. Therefore pattern layer of GRNN consists of 3200

neurons. The number of neurons in summation layer are dependat upon the nmumber of neurons in the outer layer. Summation layer contains one more neuron than the outer layer. Since MPPT problem in this work is a problem of regression which means that there will be only one neuron in the outer layer, there the summation layers consists of 2 neurons. The structure of GRNN used in this work is illustrated in the Figure 3.14.

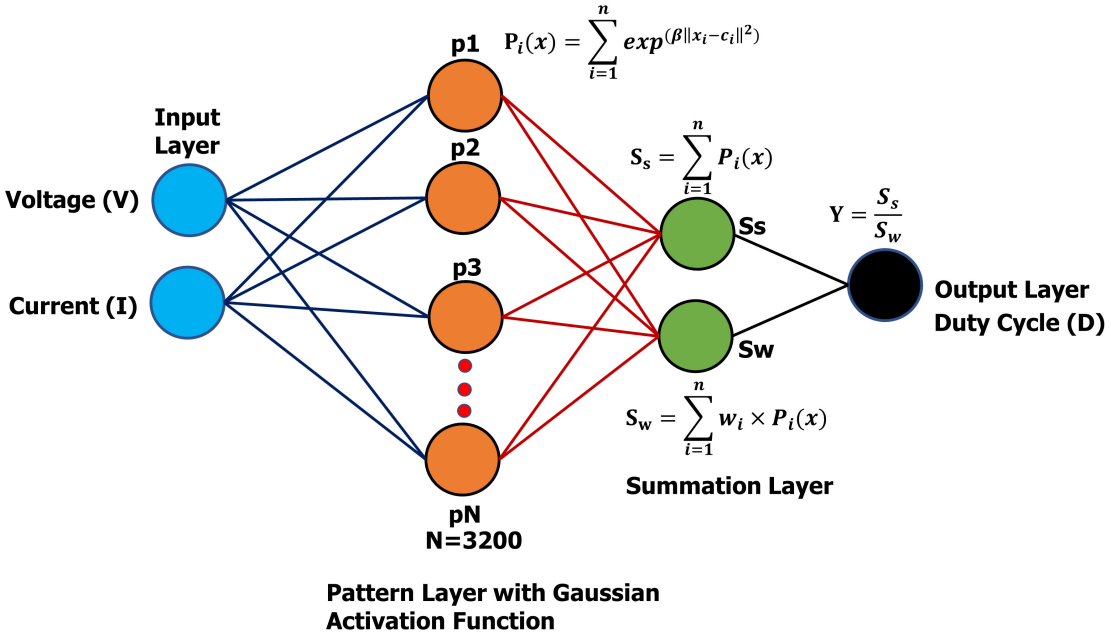

FIGURE 3.14: Structure of GRNN used in the proposed technique

RBFN consists of 3 layers. The hidden layer contains gaussian activation function. For selection of number of neurons in the hidden layer in RBFN, there are two possible approaches. The first approach is to use randomly k prototypes from the training data.

Given enough RBF neurons, an RBFN can define any arbitrarily complex decision boundary. In other words, you can always improve its accuracy by using more RBF neurons.

However, more neurons means more computation time, so it's ideal if we can achieve good accuracy using as few RBF neurons as possible. One of the approaches for making an intelligent selection of prototypes is to perform k-Means clustering on your training set and to use the cluster centers as the prototypes.

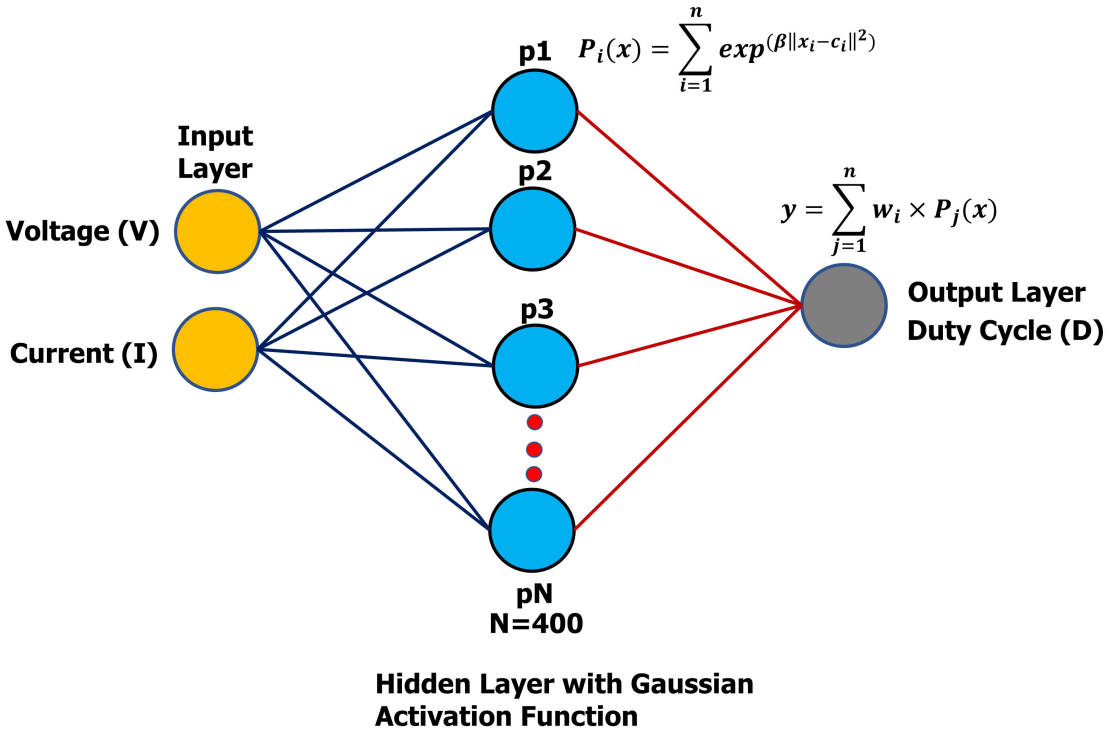

FIGURE 3.15: Structure of RBFN used in the proposed technique

The number of neurons used in this work are 400 which are selected using K-means clustering. The structure of RBFN used in this work is depicted in Figure 3.15.

3.2.5 Model Evaluation of GRNN and RBFN

ML algorithms typically work in three phases; training, validation and testing phases. After the training phase is completed it moves to the validation. A new set of data is used during the first pass. If the results are satisfactory, move on to the testing stage. If not, it's a good idea to let the machine learning program run through the data again until no new patterns emerge or the maximum number of passes has reached. As training progresses, the ML algorithm or whoever is in charge of it automatically modifies the parameters.

The testing stage is a "final phase" against a new batch of data, but without the "assist" data labels (for supervised learning only). It's a working model if the algorithm satisfies the success criterion test. If not, it's back to the drawing board.

AI machine learning is a rerun of ML software exposure to data, with parameters updated repeatedly by the ML software (and maybe by humans) to improve the

model after each pass of the data. ML software continues to run several runs over the data until it detects no new patterns or reaches its maximum number of passes, at which point it stops.

To evaluate the efficiency of GRNN and RBFN, the dataset has been split into 70-30 ratio. 70% of the data has been used for training the models, and 30 percent of the data is used for testing of the models. Since total number of samples used in this work are 3200, therefore 2240 samples are taken into account for training purposes whereas 960 samples are being used for testing of the models.

3.2.6 Tracking Mechanism of Proposed Technique

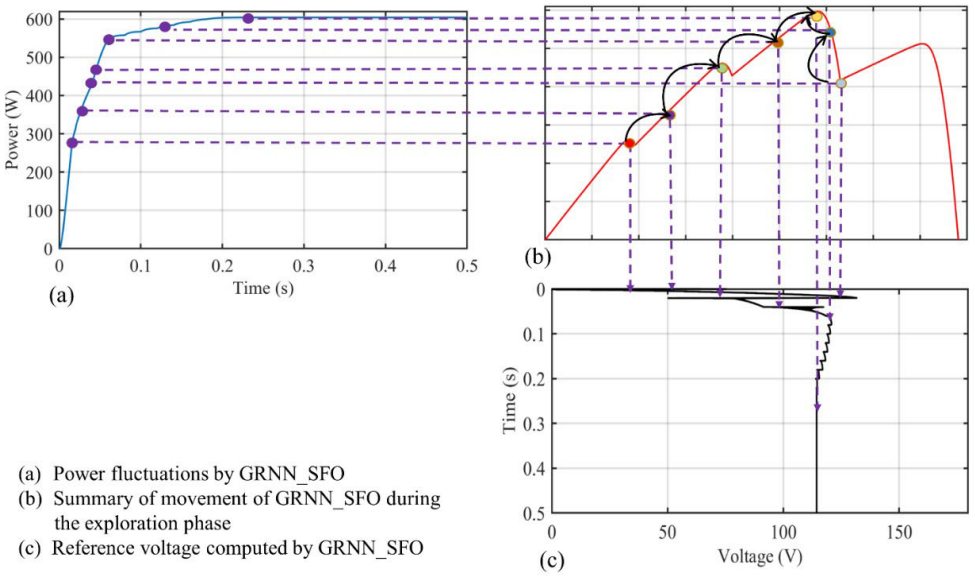

FIGURE 3.16: Tracking Mechanism of GRNN-SFO (General Regression Neural Network-Sail Fish Optimizer) (a) Power Fluctuations (b) Summary of GRNN-SFO during exploration phase (c) Reference voltage computed by GRNN-SFO

The tracking mechanism of GRNN-SFO is presented in Figure 3.16. Power transients during tracking of GM are shown in Figure 3.16 (a) whereas the prediction of duty cycle against V_{pv} and I_{pv} of PV panel is shown in Figure 3.16 (b). The reference voltage computed by GRNN-SFO is shown in Figure 3.16 (c). As V_{pv} increases, the predicted duty cycles moves toward the GM. GRNN-SFO predicts the duty cycle according to the behavior of V_{pv}. At $130ms$ all the predicted duty cycles reach GM and are stabilized.

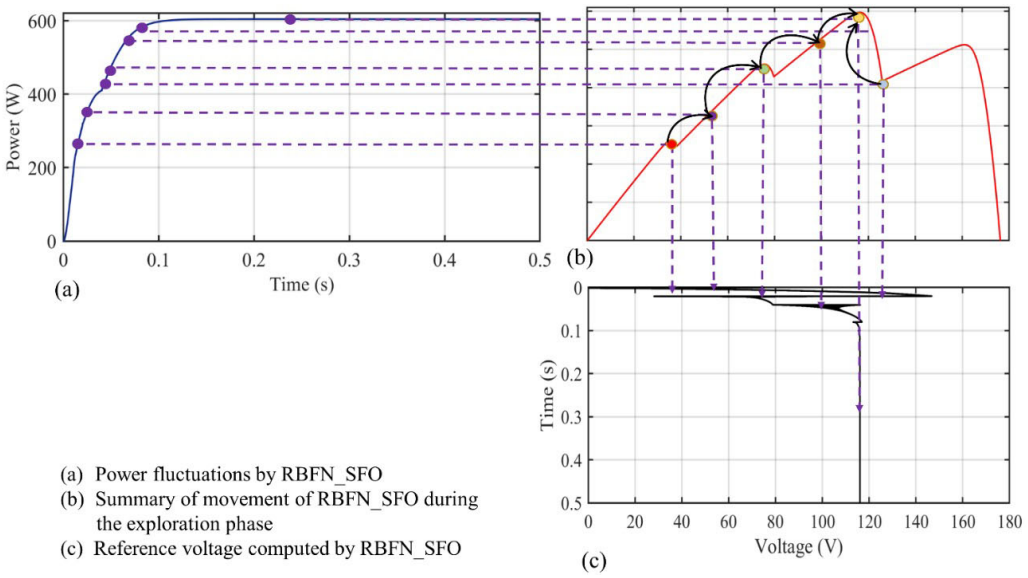

FIGURE 3.17: Tracking Mechanism of RBFN-SFO (Radial Basis Function Network-Sail Fish Optimizer)) (a) Power Fluctuations (b) Summary of RBF-SFO during exploration phase (c) Reference voltage computed by RBF-SFO

In the similar manner, the tracking mechanism of RBFN-SFO is presented in Figure 3.17. The power transients during tracking of GM are illustrated in Figure 3.17 (a) whereas the prediction of duty cycle against V_{pv} and I_{pv} of PV panel is shown in Figure3.17 (b). The reference voltage computed by RBFN-SFO is shown in Figure 3.17 (c). As V_{pv} increases, the predicted duty cycles move toward the GM. RBFN-SFO predicts the duty cycle according to the behavior of V_{pv}.

3.2.7 Proposed Technique Under CPS

When large numbers of PV modules undergo PS, several closely linked peaks are formed. This type of shading is known as complex PS. Cluster is the collection of local peaks and the Cluster Head Maxima (CHM). In Figure 3.18, CPS condition is shown. Cluster-1 exists in left half plane of PV curve which contains three MPPs. CHM occurs at the center. The global maxima which is just $17W$ less from cluster 1 has a close value with other MPPs in cluster 2.

In the last iterations, velocity vectors deliberately retard the movement of the particles. For better convergence and less oscillations, in the last iterative cycles, slower movement of particles is suitable. Around 6% power loss occurs in complex PS due to undetected GM. The loss becomes prominent due to non-proper tuning

of swarm based intelligence techniques. These techniques are effective when the GM is in the center but the problem becomes more prominent as the GMPP is tilted from the center. Using a large number of particles is a common approach to overcome the previously mentioned issue however this approach increases the resources to compute the social interaction. Therefore reduced ranged applications, complexity, and cost are the side effects. GRNN-SFO effectively deals with these issues by increasing the exploration phase and has a slow movement as the iterations increase in order to reduce the oscillations and track GMPP effectively.

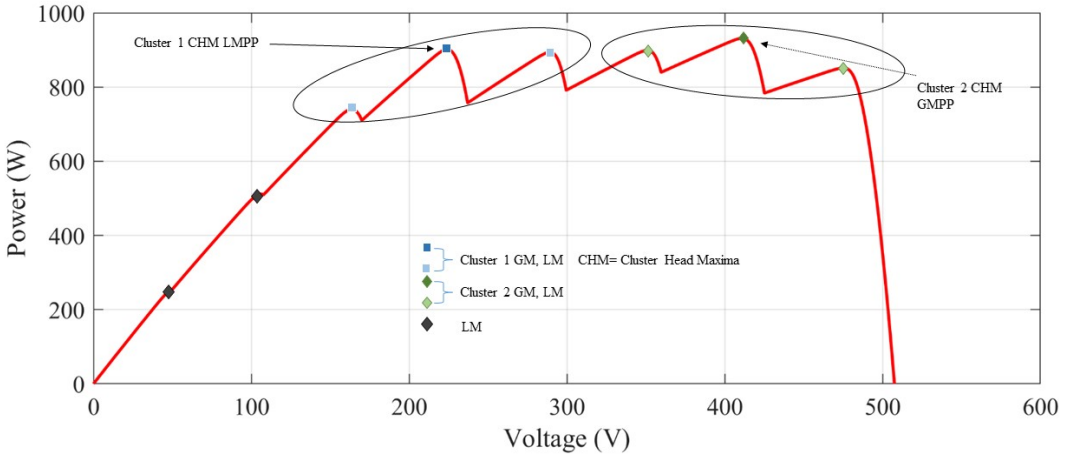

FIGURE 3.18: Complex partial shading with cluster formation denoting a very small difference between GMPP and LMPP

3.3 Chapter Summary

In this chapter, the components of the PV system from the converter to the load are discussed in detail. Also the proposed meta-heuristic algorithm, that is, SFO is explained. In addition, the Machine learning algorithms such as Generalized Regression Neural Network (GRNN) and Radial Basis Function Neural Network (RBFNN) are specified. SFO helps to generate a dataset of current and voltage over wide range of irradiance levels and at STC upon which GRNN and RBFN are trained to predict the duty cycle for MPPT. The tuning of GRNN and RBFNN is a great challenge which is also done using the proposed SFO. The other important thing to check is the working of the proposed technique under PSC and the proposed GRNN-SFO performs excellently under PSC.

Chapter 4

Simulation and Results

In this chapter, a Machine Learning based technique for MPPT control is presented under uniform irradiance condition, PS condition (PS), and complex PS condition (CPS). GRNN trained with Sailfish Optimizer (GRNN-SFO) is compared with GRNN trained with Perturb and Observe (GRNN-P&O) and Particle Swarm Optimization (GRNN-PSO), Radial Basis Function Network trained with Sail Fish Optimizer (RBF-SFO), Perturb and Observe (RBF-P&O) and Particle Swarm Optimization (RBF-PSO). Settling time, tracking time, oscillations reduction, power and energy harvested by each technique is compared. The superior performance of the proposed GRNN-SFO is achieved in all operating conditions including PS and CPS. Fast-tracking, high efficiency, and robustness are key features of the proposed study which is a novel addition to the MPPT of PV systems. It is evident from the results that GRNN-SFO is better in terms of convergence time, and power tracked for global maxima tracking under various weather condition.

4.1 Introduction

This section covers three separate examples that illustrate the operating conditions of a PV panel. The simulation setup for MPPT control based on hybrid MPPT technique is shown in Figure 4.1, which is simulated using MATLAB/SIMULINK

2018a. Performance of GRNN-SFO, is compared with GRNN-P&O, GRNN-PSO, RBF-SFO, RBF-PSO, RBF-P&O under three different cases.

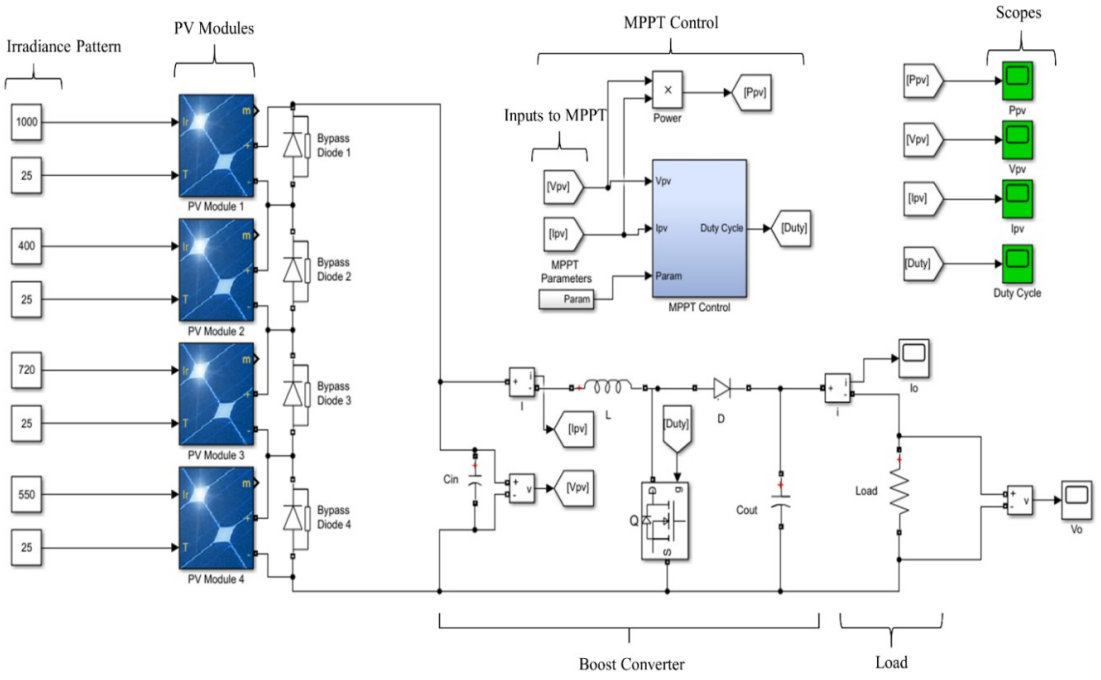

FIGURE 4.1: Simulation Setup of Machine Learning Based MPPT Control of a PV System

Case 1 depicts the situation of rapidly changing irradiance where environmental conditions are changing quickly but all PV panels are experiencing the same environmental effects. Case 2 represents the PS and CPS condition is presented in Case 3. Getting stuck in LMPP, oscillations around GMPP, power tracked, tracking time, settling time, transients in current, duty cycle, and power efficiency are the terms used for analysis.

In order to compare the performance strength of all techniques mean absolute error (MAE), relative error (RE) and root mean square error (RMSE), statistical analysis is also presented. The specifications of the components used for the simulations are presented in Table 4.1. Due to high switching frequency of the boost converter, the design value of the inductor and capacitor is low which reduces the size of the circuit and makes use of little hardware for the implementation. The PV module used has a maximum power of $300\,W$ and load resistance selected for the MPPT implementation is 70 *ohms*.

TABLE 4.1: Specification of Electrical Components used in Simulation

Components	**Values**
Panel Power	300 W
Inductor	1.4 mH
Capacitor at input, Cin	10 uF
Capacitor at output, Cout	470 uF
Frequency of switching, f	50 kHz
Resistive load, RL	70 Ω

4.2 Evaluation Criteria for MPPT Techniques

To evaluate the performance of MPPT techniques, the evaluation criteria is defined as follows:

- Oscillations at GMPP, Power tracked, tracking time, settling time, transients in current, duty cycle, and power efficiency are the terms used for comparative analysis.
- Tracking time is the time required to track the GMPP. Low tracking time will lead to high efficiency and low power losses.
- Settling time is the time required to settle at the GMPP without oscillations. Less settling time also leads to the higher efficiency of PV system.
- Efficiency of the technique determines how well a given technique performs in terms of tracking the MPP.
- Robustness and sensitivity of MPPT techniques can be validated using the statistical analysis such as Root mean square error (RMSE), Mean absolute error (MAE), relative error (RE).

4.3 Case 1: Fast Changing Irradiance

Irradiance levels as observed by PV systems depend upon external environmental conditions. In this case, the irradiance on all panels is kept same, however the weather conditions are changing quickly.

4.3.1 Testing: Case 1

Performance of MPPT techniques under rapidly varying irradiance is shown in Table 4.2, whereas power comparison amongst GRNN-SFO, GRNN-PSO, GRNN-P&O, RBF-SFO, RBF-PSO, and RBF-P&O is shown in Table 4.3.

Due to sailfish and sardines movement for the search of the optimal solution, SFO effectively tracks the GM with high efficiency and tracks GM in less time as compared to other meta-heuristics techniques. This helps to generate a fine data set of duty cycle and their corresponding values of power. Therefore SFO effectively trains GRNN and achieves high efficiency in MPP tracking. Due to random numbers embedded in PSO velocity vectors, PSO tracks GM with large time and settles at less time at GM, as a result GRNN and RBF trained PSO also settles at a low value along with power losses. Perturb and Observes lack of ability to distinguish between LM and GM, results in poor performance and power yield.

In order to determine the performance under changing irradiance, an average value is best suited which is taken into account in this work.

TABLE 4.2: Fast Changing Irradiance Pattern for Case 1 consisting of 4 Photo-Voltaic Panels

Cases	**Irradiance S_i ($\frac{KW}{m^2}$)**				
Case 1	PV1	1	0.8	0.65	0.4
	PV2	1	0.8	0.65	0.4
	PV3	1	0.8	0.65	0.4
	PV4	1	0.8	0.65	0.4

Case 1 deals with fast changing irradiance conditions, that is, the irradiance that each PV panel experience is changing quickly however each PV Panel receives the same amount of irradiance at all times. In this case, four panels have been used in order to test 6 different techniques and a comparison has been made amongst them. Figure 4.2 illustrates a graph which depicts four different types of irradiances, that is $1\frac{KW}{m^2}$, $0.8\frac{KW}{m^2}$, $0.4\frac{KW}{m^2}$, and $0.65\frac{KW}{m^2}$ have been used for experimental purposes in this case.

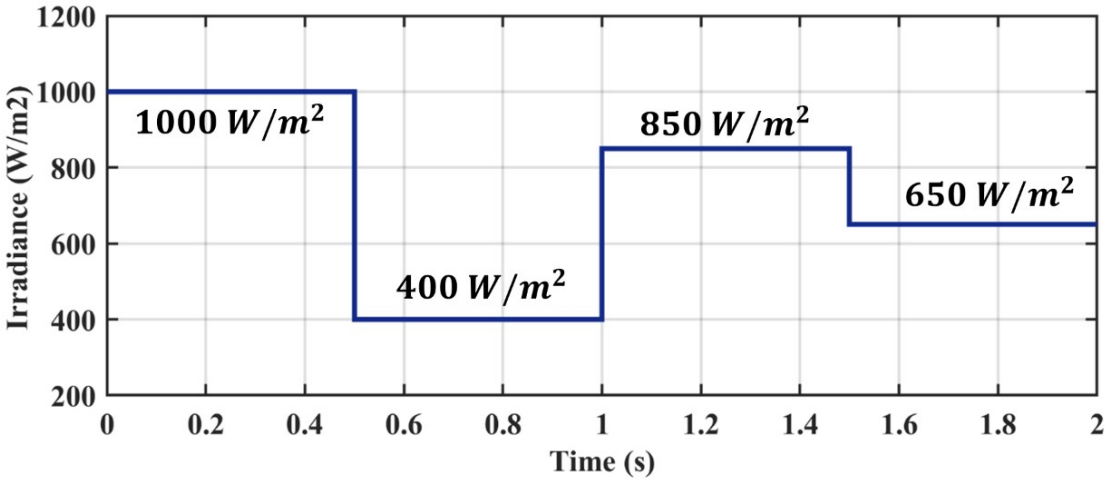

FIGURE 4.2: Irradiance Pattern on PV Panels for Case 1 illustrating that all 4 panels receive changing but same irradiance at all times

The irradiance on PV panels change quickly as mentioned above which gives the effect of fast varying irradiance. Figure 4.2 shows the irradiance pattern on four panels under fast changing irradiance condition. Figure 4.3 illustrates the power for given irradiances that are shown in Table 4.2.

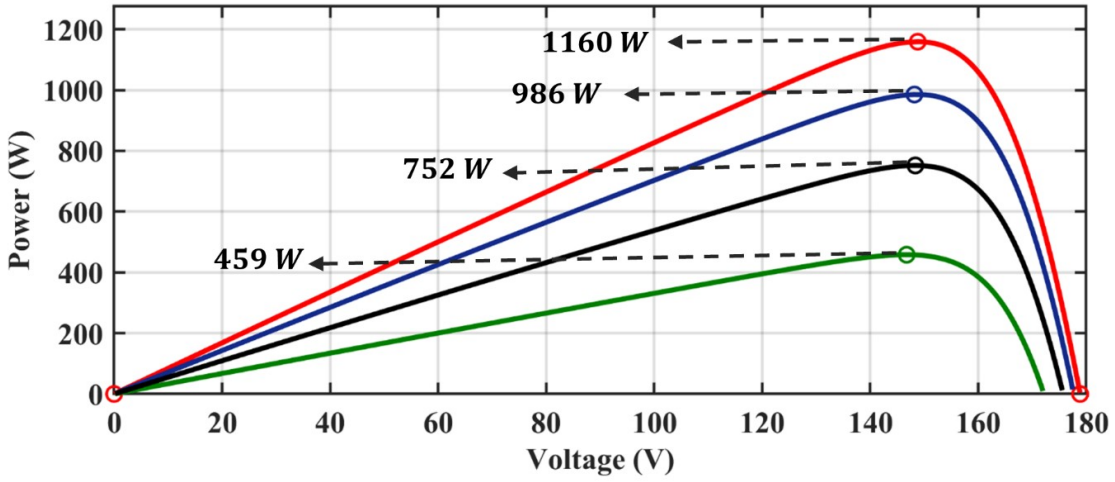

FIGURE 4.3: Maximum Power Point for different irradiance patterns

This means that for irradiance of $1\frac{KW}{m^2}$, the maximum power that can be extracted is $1160\,W$, for $0.8\frac{KW}{m^2}$ $986\,W$ can be extracted, for $0.4\frac{KW}{m^2}$, the maximum power lies at $459\,W$, and $752\,W$ power can be extracted for the irradiance of $0.65\frac{KW}{m^2}$.

4.3.2 Results: Case 1

Figure 4.4 to Figure 4.7 represent the power, and duty cycle variations tracked by all six techniques that have been presented in this work. The results indicate that the power levels as observed by PV systems depend upon external environmental conditions. The rapid change in irradiance level is referred to as a rapid variation of irradiance. The comparison amongst GRNN-SFO, GRNN-PSO, GRNN-P&O, RBF-SFO, RBF-PSO, and RBF-P&O states that the highest performance is achieved by GRNN-SFO.

Figure 4.4 represents the power tracking curve for GRNN trained with SFO, PSO, and Perturb and P&O (GRNN-SFO, GRNN-PSO, GRNN-P&O) under fast changing irradiance conditions. The proposed technique has been compared against one of the conventional MPPT technique that is P&O, and one SI based MPPT technique, that is PSO.

GRNN-SFO is highly capable to track the power under fast changing irradiance condition and tracks power in $81ms$ as opposed to GRNN-PSO's $97ms$ and GRNN-P&O's $66ms$. Integration of SFO with GRNN makes it very proficient for the MPPT. GRNN-SFO tracks an average power of $835.595\,W$ with an exceptional efficiency of 99.89% which shows the superiority of GRNN-SFO. The results conclude that GRNN-SFO is quick, robust and suitable in order to track MPP under rapidly changing irradiance levels.

The second set of techniques with which GRNN-SFO is compared with is RBFN trained with same conventional and swarm based techniques. Figure 4.5 illustrates the power tracking curve for GRNN and RBFN trained by SFO, PSO and P&O (RBF-SFO, RBF-PSO, RBF-P&O) under fast changing irradiance conditions.

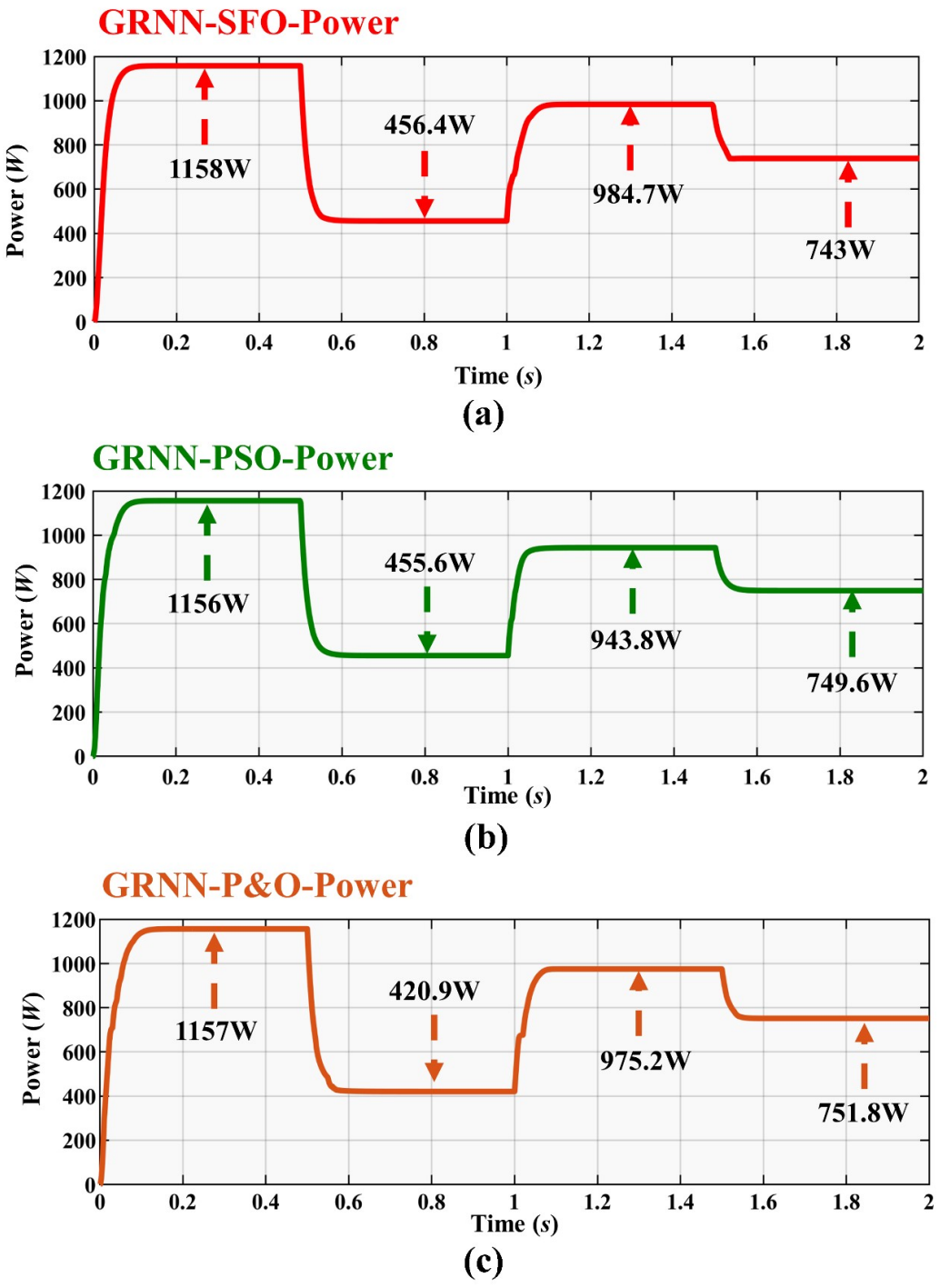

FIGURE 4.4: Power Tracking for PV panels for (a) Sail Fish Optimizer (b) Particle Swarm Optimization (c) Perturb and Observe trained by GRNN(GRNN-SFO, GRNN-PSO, GRNN-P&O) under fast changing irradiance conditions

RBF-SFO tracks the power in fast changing irradiance condition in 88ms, RBF-PSO in 101ms, and RBF-P&O in 69ms. RBF-SFO takes more time as compared to RBF-P&O.

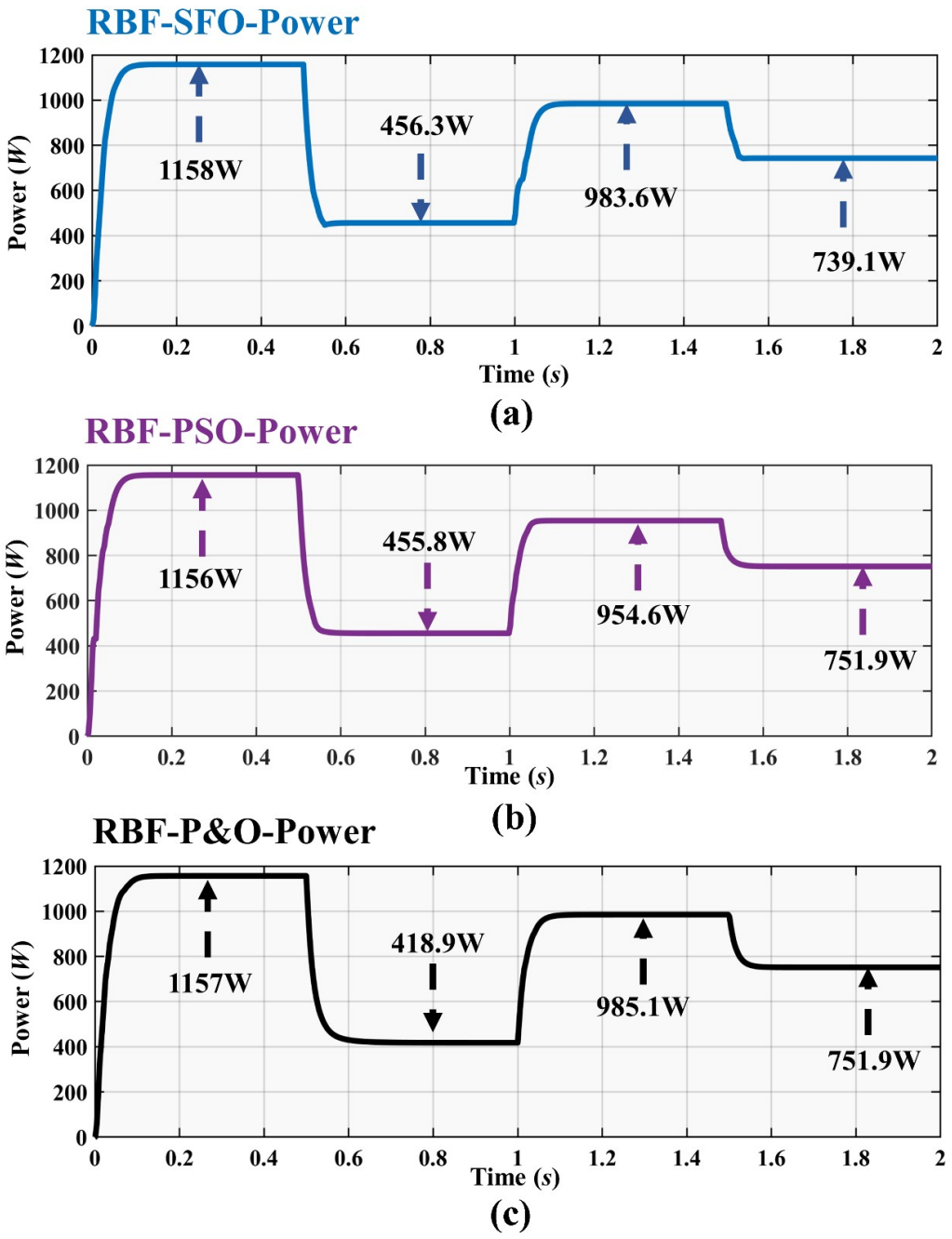

FIGURE 4.5: Power Tracking for PV panels for (a) Sail Fish Optimizer (b) Particle Swarm Optimization (c) Perturb and Observe trained by Radial Basis Function (RBF-SFO, RBF-PSO, RBF-P&O) under fast changing irradiance conditions

However it harvests more average power than the compared techniques, that is, 834.5 W.

Results show, that amongst all 6 techniques GRNN-SFO works exceptionally well, that is, it is even superior to RBFN. GRNN offers a swift ability in traking the MPP.

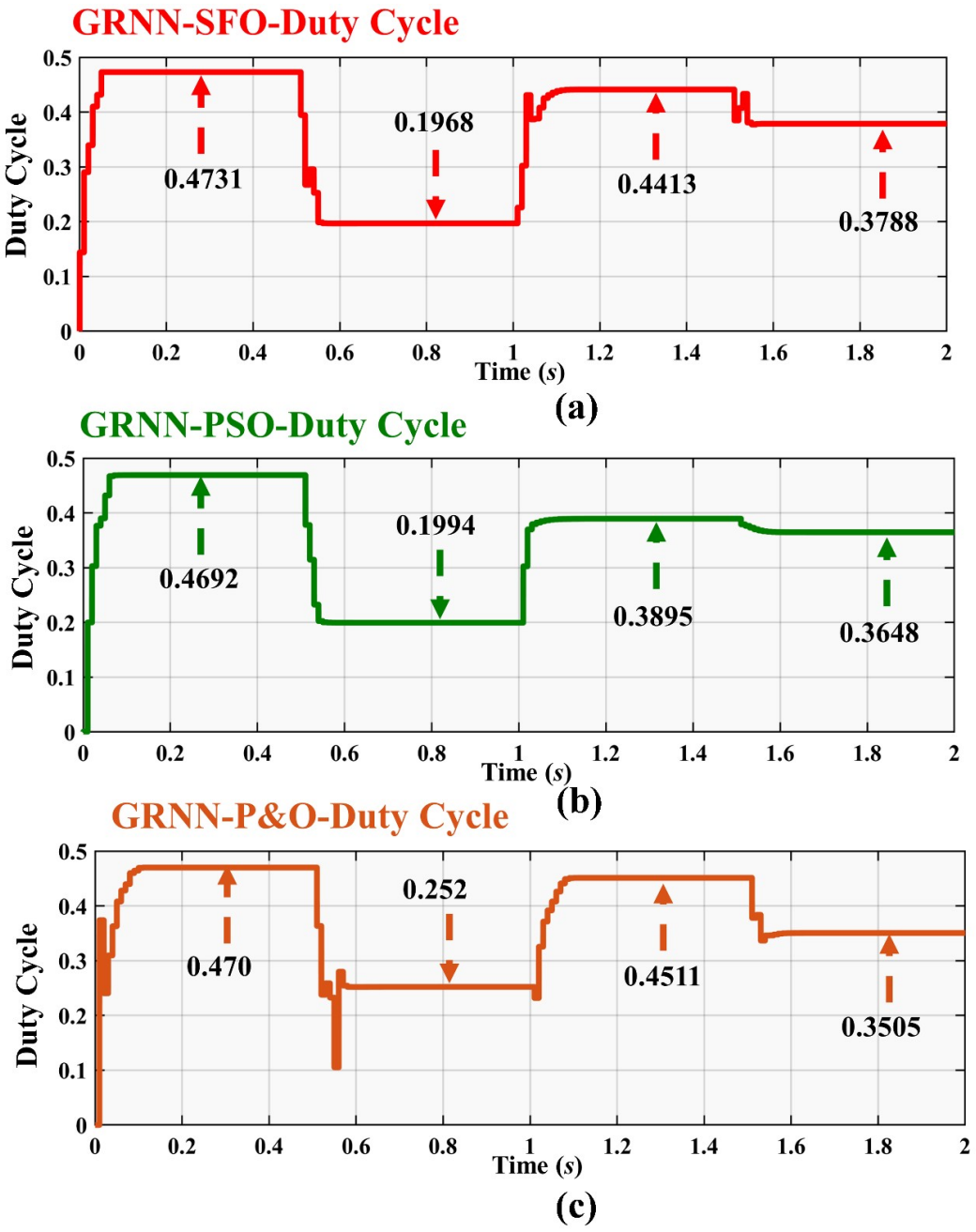

FIGURE 4.6: Duty Cycle variation for PV panels for (a) Sail Fish Optimizer (b) Particle Swarm Optimization (c) Perturb and Observe trained by GRNN(GRNN-SFO, GRNN-PSO, GRNN-P&O) under fast changing irradiance conditions

The results illustrate that the order of performance is such that GRNN-SFO > RBF-SFO > GRNN-PSO > RBF-PSO > GRNN-P&O > RBF-P&O.

Figure 4.6 represents the duty cycle variation for GRNN trained by SFO, PSO and P&O (GRNN-SFO, GRNN-PSO, GRNN-P&O) under fast changing irradiance conditions.

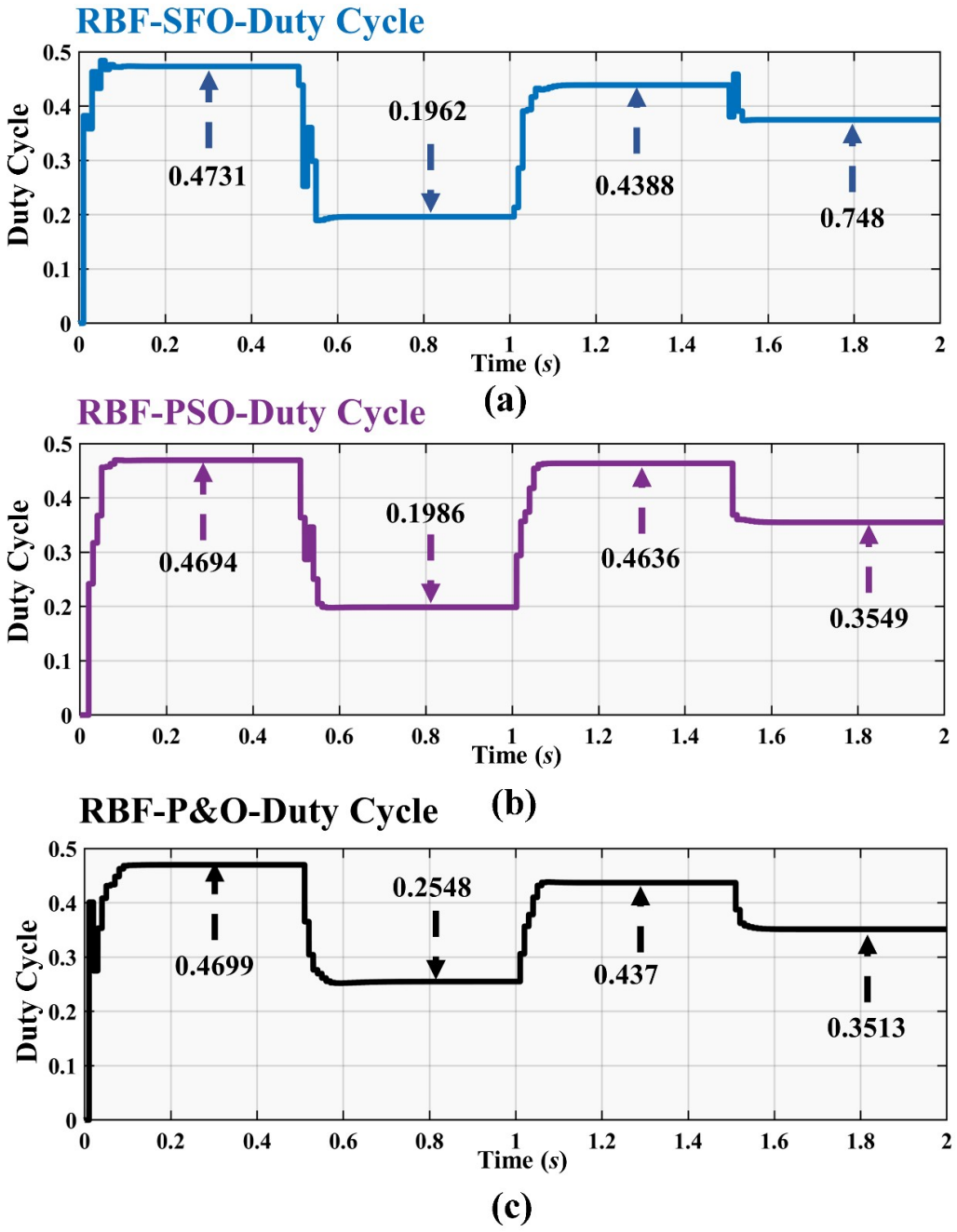

FIGURE 4.7: Duty Cycle variation for PV panels for (a) Sail Fish Optimizer (b) Particle Swarm Optimization (c) Perturb and Observe trained by Radial Basis Function (RBF-SFO, RBF-PSO, RBF-P&O) under fast changing irradiance conditions

The proposed technique has been compared against P&O, and PSO based GRNN and RBFN. GRNN-SFO is very quick to adjust the duty cycle to reach MPP as compared to GRNN-PSO and GRNN-P&O. SFO trains GRNN in such a way that it makes it very proficient for the MPPT. GRNN-SFO's ability to extract $1.633KJ$ energy makes it an excellent choice for tracking the MPP.

Figure 4.7 illustrates the duty cycle variation of RBFN trained by SFO, PSO and P&O (RBF-SFO, RBF-PSO, RBF-P&O) under fast-changing irradiance conditions. RBF-SFO adjusts its duty cycle in fast changing irradiance condition whilst harvesting the energy of $1.631KJ$ which is more as compared to RBF-PSO and RBF-P&O.

GRNN-SFO in terms of duty cycle in a similar manner to power works better as compared to RBF-SFO illustrating the high functionality of GRNN-SFO. Results denote that for duty cycle the order of performance is such that GRNN-SFO > RBF-SFO > GRNN-PSO > RBF-PSO > GRNN-P&O > RBF-P&O.

4.3.3 Performance Evaluation: Case 1

In case 1, GRNN and RBFN trained with SFO have been compared with P&O and PSO also trained by GRNN an RBFN. The cumulative set of results in terms of tracking time, settling time, energy, average power tracked, and efficiency has been illustrated in Table 4.3. From the results, it is evident that GRNN-SFO bypasses all other techniques in terms of performance and MPPT.

TABLE 4.3: Combined Performance Analysis for Case 1: Fast Changing Irradiance

Tech	**Tracking Time(ms)**	**Settling Time (ms)**	**Energy (KJ)**	**Avg. Power Tracked W**	**Efficiency (%)**
GRNN-SFO	81	119	1.633	835.595	99.89
GRNN-PSO	97	136	1.632	829.650	99.18
GRNN-P&O	66	100	1.630	827.930	98.97
RBF-SFO	88	124	1.631	834.500	99.76
RBF-PSO	101	139	1.630	828.150	99.00
RBF-P&O	69	105	1.629	827.100	98.86

Figure 4.8 illustrates the settling time of all six techniques. The results show that GRNN-SFO settles at $119ms$, GRNN-PSO settles at $136ms$, GRNN-P&O settles at $100ms$, RBF-SFO settles at $124ms$, RBF-PSO settles at $139ms$, and RBF-P&O settles at $105ms$

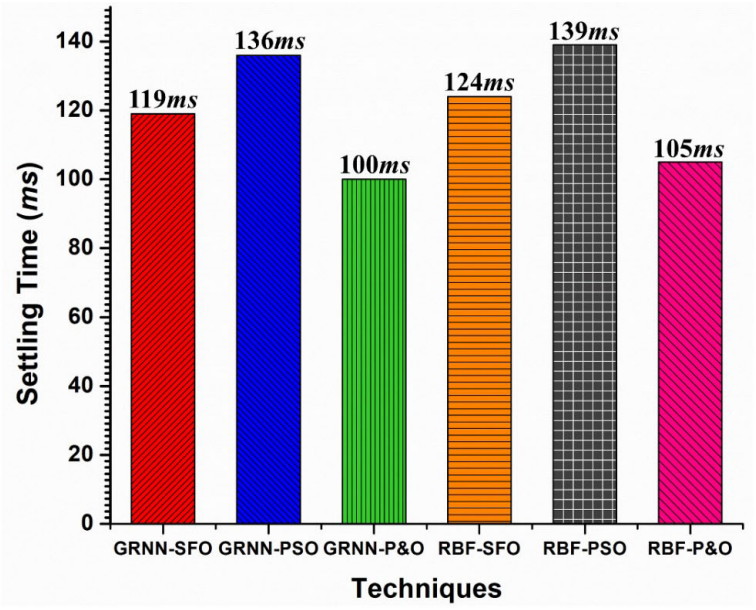

FIGURE 4.8: Settling Time comparative analysis of all techniques for case 1

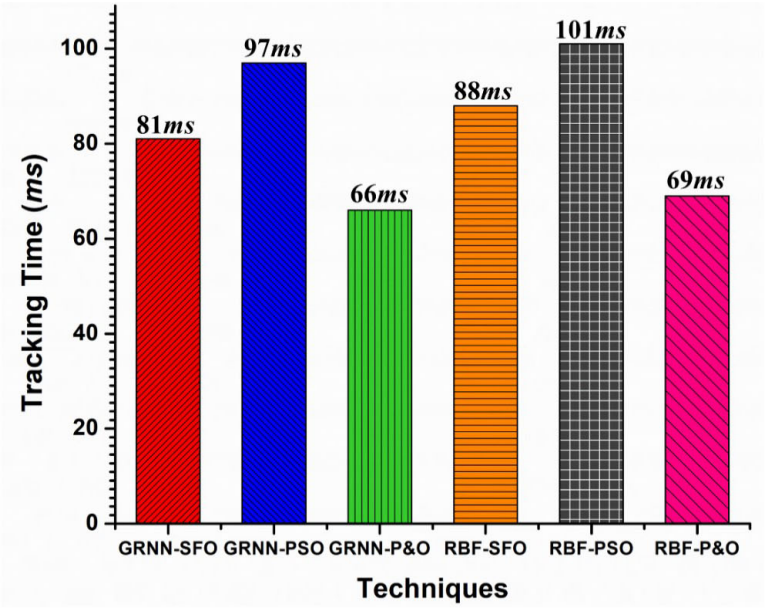

FIGURE 4.9: Tracking Time comparative analysis of all techniques for case 1

The second evaluation criterion that is used in this thesis is tracking time. Tracking time corresponds to better efficiency. Figure 4.9 shows the tracking time of all six techniques. The results show that GRNN-SFO tracks power in $81ms$, GRNN-PSO in $97ms$, GRNN-P&O in $66ms$, RBF-SFO in $88ms$, RBF-PSO in $101ms$, and RBF-P&O in $69ms$.

The third criterion to test the performance of all techniques is efficiency. Figure 4.7 and Figure 4.8 give an impression some techniques are better than GRNN-SFO.

However, the efficiency of techniques is based on the evaluation of all the parameters combined. The objective is to achieve high efficiency. Figure 4.10 shows a comparative analysis of efficiencies achieved by all six techniques which clearly shows the superior performance of GRNN-SFO under fast changing irradiance.

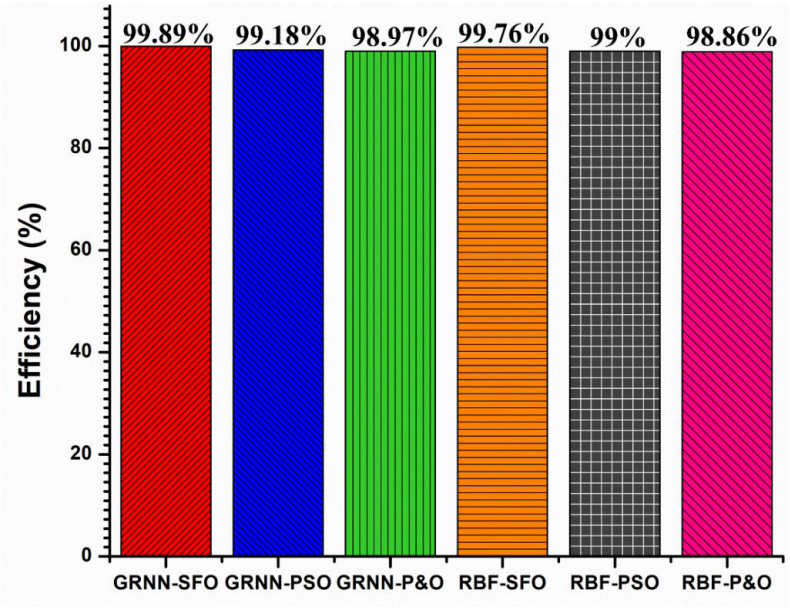

FIGURE 4.10: Efficiency comparison of all techniques for case 1

Figure 4.11 is a comparative graphical illustration of all the techniques that have been presented. The graph shows the superior performances of GRNN-SFO in terms of tracking time, average power tracked and efficiency. It can be clearly seen that GRNN-SFO tracks power in $81ms$, and RBF-SFO in $88ms$ with average power tracked of $835.56\,W$ and $834.5\,W$ respectively. GRNN-SFO tracks MPP with 99.89% efficiency whereas RBF-SFO tracks MPP with 99.76% efficiency. The high efficiency of GRNN-SFO fast tracking time makes it a much better choice in tracking MPP since GRNN-SFO offers better results more so than RBF-SFO.

Case 1 deals with fast changing irradiance on PV panels. Based on these results, it is concluded that GRNN-SFO > RBF-SFO > GRNN-PSO > RBF-PSO > GRNN-P&O > RBF-P&O. GRNN-SFO settles 15% faster at GM which justifies its superior performance. One of the major areas of problem is oscillations around GM offered by MPPT techniques which costs the efficiency of PV systems and reduce the power tracked. These issues have been significantly softened and reduced using GRNN-SFO.

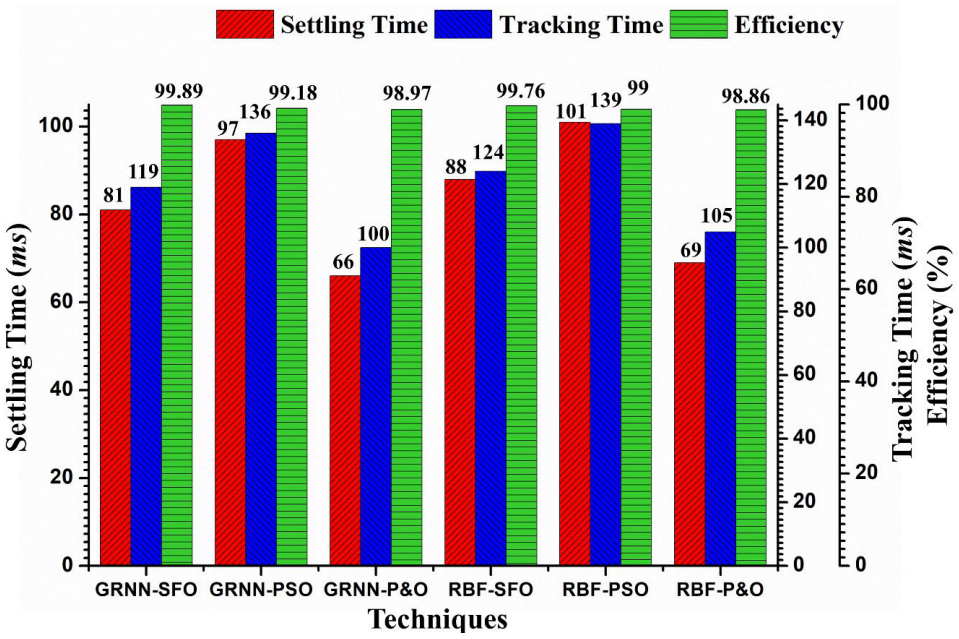

FIGURE 4.11: Comparative analysis of all 6 techniques in terms of settling time, tracking time, and efficiency for case 1: Fast Changing Irradiance

4.4 Case 2: Partial Shading Condition (PSC)

Case 2 deals with PS condition. All PV panels receive different irradiances which result in a non-linear curve. Under this condition, the PV curve consists of a multiple peaks. Only one peak is considered as a GMPP, while other peaks are known as LMPP. The MPPT techniques have a tendency to either oscillate or get stuck at LM as a result of these multiple peaks. In order to test the performance of any technique, PS condition is an ideal scenario.

Under PS, GMPP is at $604.7\,W$ for our presented sets of irradiance. Table 4.4 represents irradiance patterns.

4.4.1 Testing: Case 2

Four PV panels are utilized to evaluate the performance of all six approaches. All PV panels receive changing irradiances which replicates the condition of PS. Table 4.4 illustrates the irradiances that is received by all panels. Figure 4.12 depicts the graphical representation of the irradiance levels on PV panels.

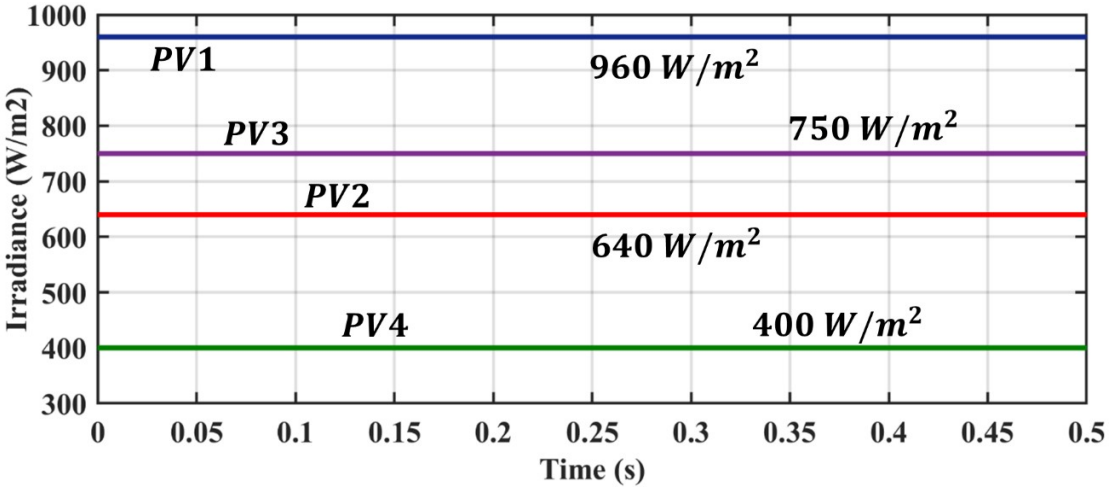

FIGURE 4.12: Irradiance Pattern on Photo-Voltaic (PV) Panels for Case 2 illustrating that all 4 panels receive different irradiance creating a condition of partial shading

TABLE 4.4: Partial Shading Condition Pattern for Case 2 consisting of 4 Photo-Voltaic Panels

Cases	**Irradiance S_i $(\frac{KW}{m^2})$**	
Case 2	PV1	0.96
	PV2	0.75
	PV3	0.64
	PV4	0.40

Case 2 deals with PS condition. This is a special case, where an array of PV system gets partially shaded. This PS can be caused by the shadows of nearby trees, buildings, mountains, or dust. PV panels are installed with built-in protection diodes knows as bypass diodes. These diodes are installed in order to protect the PV panel from getting hotspots which can be caused by PS.

The main idea behind PS is such that, as soon as one or more panels in an array of PV panels get shaded, a current mismatch is created between the shaded and unshaded panels. Had it not been for the bypass diodes which provide an alternate path for current, the shaded panels would heat up to the point of damage. While on one hand, bypass diodes provide protection during the current mismatch. On the other hand they result in a non-linear power curve that contains multiple power points rather than only one. In this curve, there is only one GMPP amongst several

LMPPs. These LMPPs makes it very hard and difficult to track the GMPP. This is where the conventional algorithms fail to perform as desired.

Figure 4.13 illustrates the maximum power that can be extracted under the given irradiance conditions shown in Table 4.4. This means that for the irradiance of $0.96\frac{KW}{m^2}$, $0.75\frac{KW}{m^2}$, $0.4\frac{KW}{m^2}$ and $0.64\frac{KW}{m^2}$ the maximum power that can be extracted is $604.7\,W$.

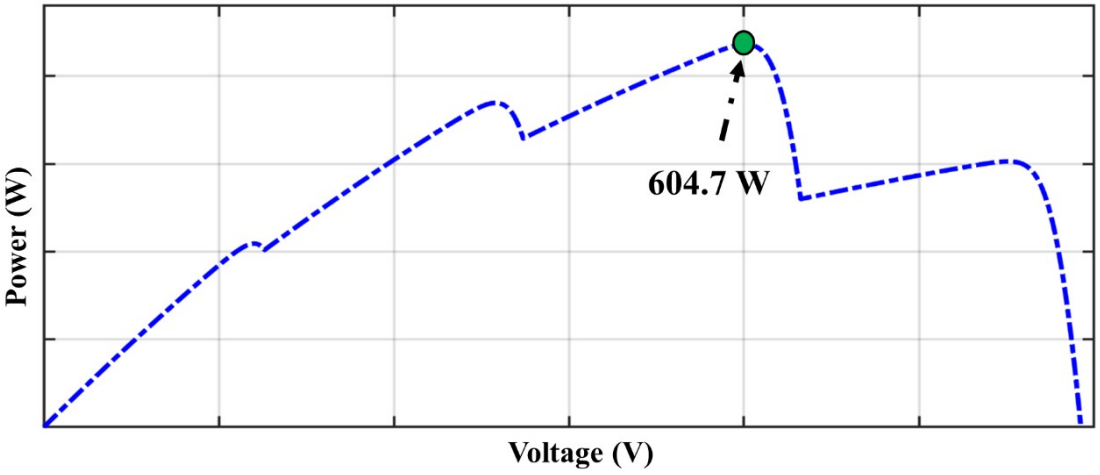

FIGURE 4.13: Maximum Power under PSC for the given irradiances

4.4.2 Results: Case 2

Figure 4.14 to Figure 4.17 represents the power, duty cycle and voltage tracked by 6 techniques that have been presented for case 2. The results indicates that the irradiance levels as observed by PV panels depend upon external environmental conditions. The comparison amongst GRNN-SFO, GRNN-P&O, GRNN-PSO, RBF-SFO, RBF-PSO and RBF-P&O states that the highest performance is achieved by GRNN-SFO.

Figure 4.14 represents the power tracking curve for GRNN trained with SFO, PSO and P&O (GRNN-SFO, GRNN-PSO, GRNN-P&O) under PSC.

GRNN-SFO's capability to track the power in 89ms under PS Condition as opposed to GRNN-PSO's $101ms$ and GRNN-P&O's $66ms$ makes it strong and top quality technique for MPPT. GRNN trained with SFO offers a quick MPPT solution that tracks $604.4\,W$ power with a high efficiency of 99.90%.

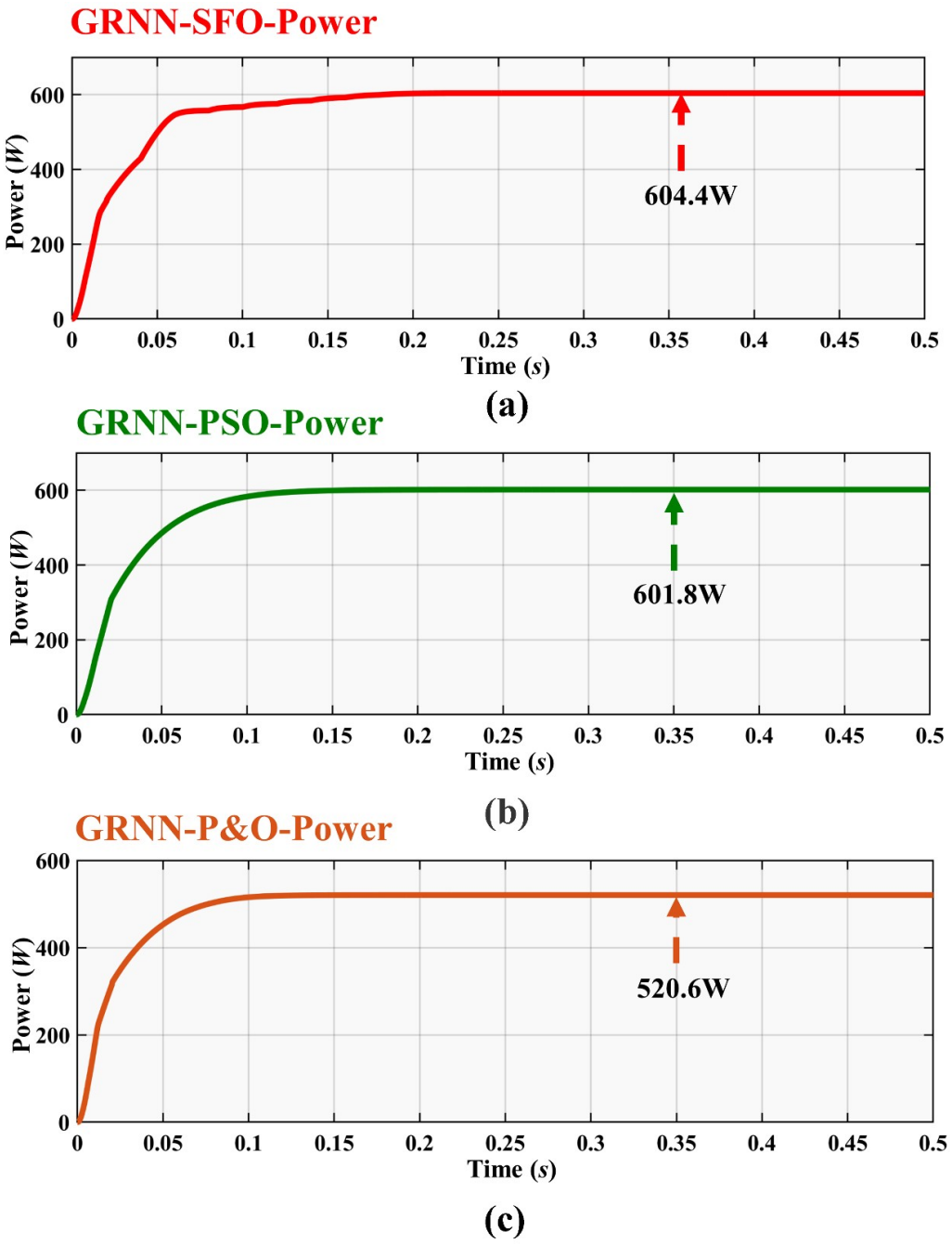

FIGURE 4.14: Power Tracking for PV panels for (a) Sail Fish Optimizer (b) Particle Swarm Optimization (c) Perturb and Observe trained by GRNN(GRNN-SFO, GRNN-PSO, GRNN-P&O) under Partial Shading Condition

The results conclude that GRNN-SFO is quick, robust and suitable for MPPT under PS condition.

The second set of technique with which GRNN-SFO is compared with includes the training of conventional and swarm based techniques with RBFN. Figure 4.15 illustrates the power tracking curve for RBFN trained with SFO, PSO and P&O

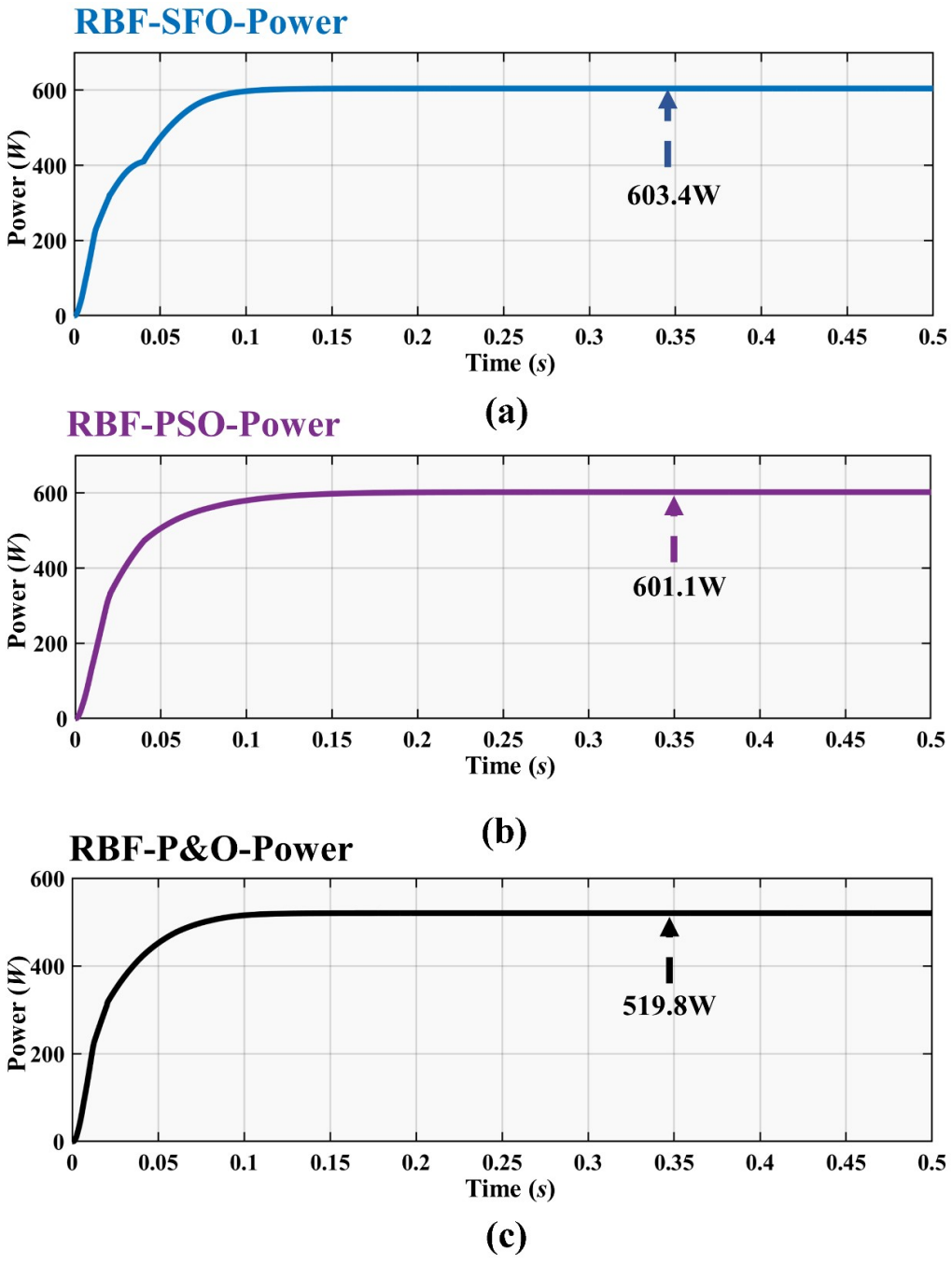

FIGURE 4.15: Power Tracking for PV panels for (a) Sail Fish Optimizer (b) Particle Swarm Optimization (c) Perturb and Observe trained by Radial Basis Function (RBF-SFO, RBF-PSO, RBF-P&O) under Partial Shading Condition

(RBF-SFO, RBF-PSO, RBF-P&O) under PS Condition.

RBF-SFO tracks the power in fast changing irradiance condition and tracks power in $92ms$, RBF-PSO in $105ms$, and RBF-P&O in $65ms$. Even with a high tracking power of RBF-SFO, from the results it can be deemed that GRNN-SFO is still a better choice in terms of tracking MPP even though RBF-SFO tracks $603.4\,W$

power which is just $1\,W$ off from GRNN-SFO.

It can be concluded that both proposed technique, that is, GRNN-SFO works exceptionally well for tracking the MPP under PS condition. The order of performance of all the techniques is concluded as: GRNN-SFO > RBF-SFO > GRNN-PSO > RBF-PSO > GRNN-P&O > RBF-P&O for PSC.

Figure 4.16 represents the duty cycle variation for GRNN trained with SFO, PSO and P&O (GRNN-SFO, GRNN-PSO, GRNN-P&O) under PS Condition (PSC).

GRNN trained with SFO is very proficient for the MPPT. GRNN-SFO's ability to extract $0.284KJ$ energy makes it an excellent choice for tracking the MPP. Figure 4.17 illustrates the duty cycle variation of RBF trained with SFO, PSO, and P&O (RBF-SFO, RBF-PSO, RBF-P&O) under PSC for the second set of technique that is used for comparison against GRNN-SFO.

RBF-SFO adjusts its duty cycle in fast changing irradiance condition whilst harvesting an energy of $0.2839KJ$ which is more as compared to RBF-PSO and RBF-P&O.

RBF-SFO adjusts its duty cycle in PS condition whilst harvesting an energy of 0.2839KJ which is more as compared to RBF-PSO and RBF-P&O.

GRNN-SFO in terms of Duty cycle in the similar manner to power works better as compared to RBF-SFO illustrating the high functionality of GRNN-SFO.

Even though RBF-SFO works better than GRNN-PSO, GRNN-P&O, RBF-PSO and RBF-P&O, results denote that for duty cycle the order of performance is such that GRNN-SFO > RBF-SFO > GRNN-PSO > RBF-PSO > GRNN-P&O > RBF-P&O.

Figure 4.17 shows that the highest efficiency is achieved by GRNN-SFO. The efficiency of GRNN-SFO, RBF-SFO, GRNN-PSO, RBF-PSO, GRNN-P&O, and RBF-P&O is 99.9%, 99.73%, 98.47%, 98.35%, 86.04%, and 85.91% respectively.

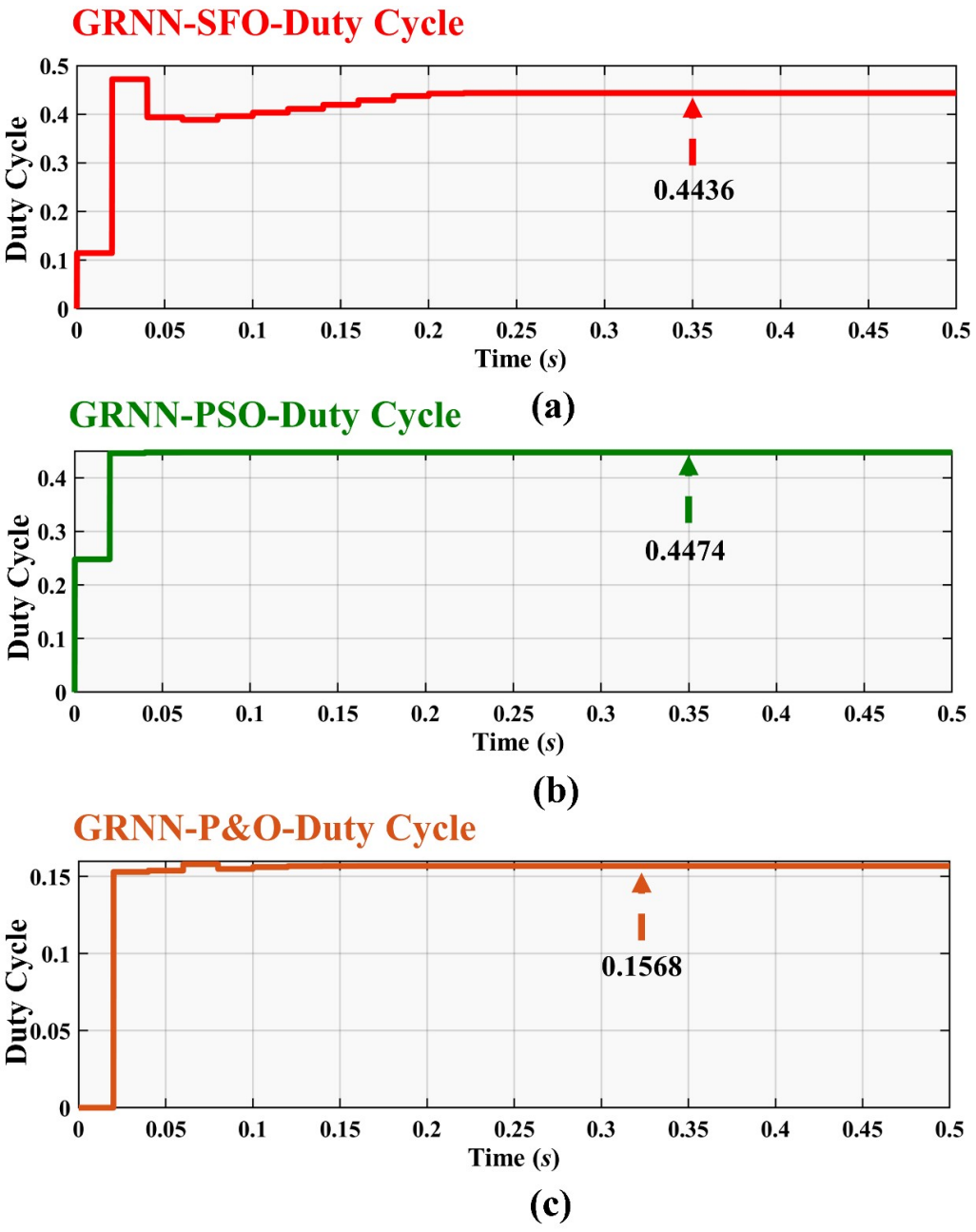

FIGURE 4.16: Duty Cycle variation for PV panels for (a) Sail Fish Optimizer (b) Particle Swarm Optimization (c) Perturb and Observe trained by GRNN(GRNN-SFO, GRNN-PSO, GRNN-P&O) under Partial Shading Condition

4.4.3 Performance Evaluation: Case 2

In case 2, two sets of techniques, that is, GRNN and RBF have been utilized. GRNN-SFO has been compared with P&O and PSO along with RBFN trained with SFO, PSO and P&O. Therefore GRNN-SFO has been compared with five techniques under PSC. The cumulative set of results in terms of tracking time,

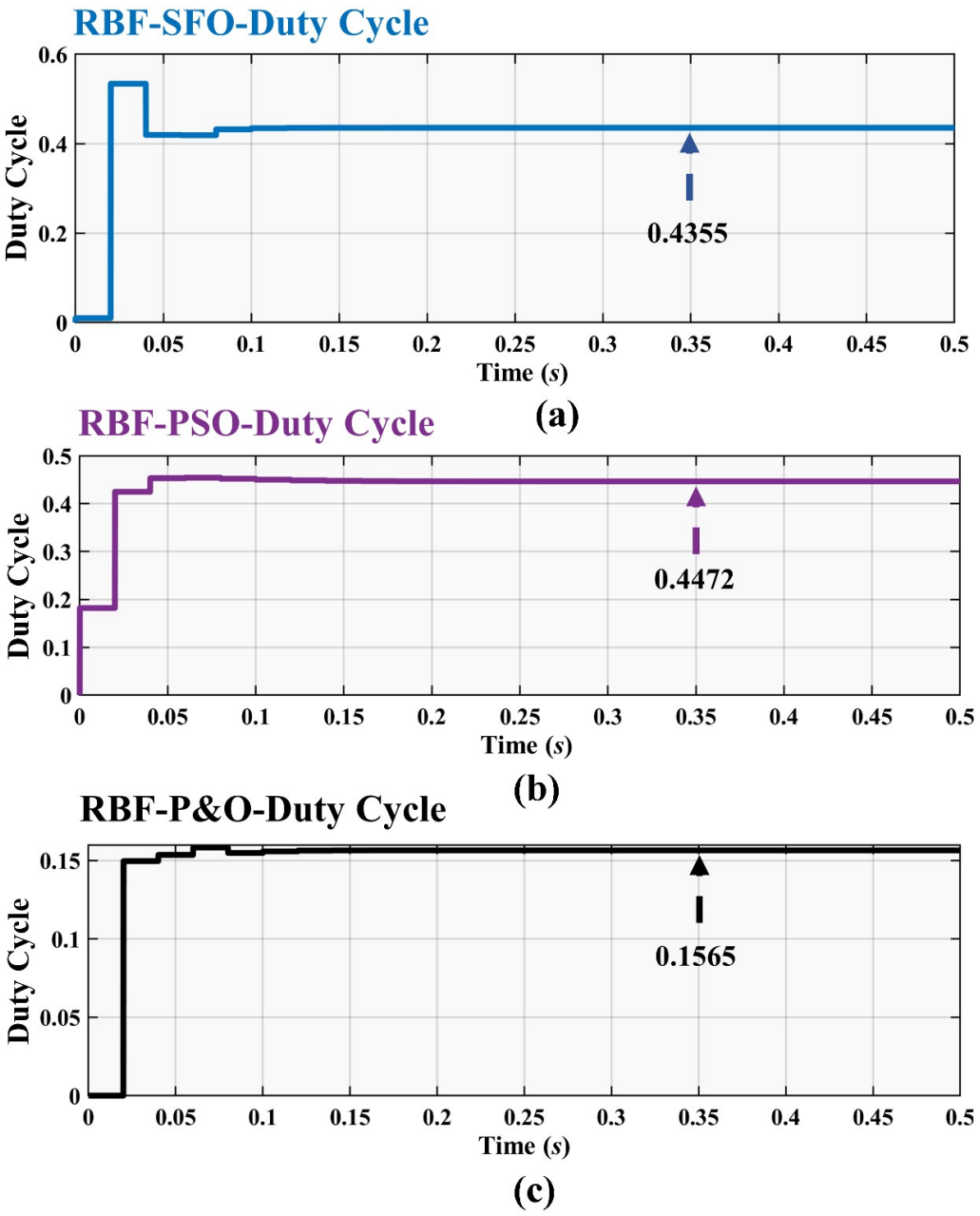

FIGURE 4.17: Duty Cycle variation for PV panels for (a) Sail Fish Optimizer (b) Particle Swarm Optimization (c) Perturb and Observe trained by Radial Basis Function (RBF-SFO, RBF-PSO, RBF-P&O) under Partial Shading Condition

settling time, energy, average power tracked and efficiency has been illustrated in Table 4.5.

GRNN-SFO has the ability to settle at GM with low oscillations. In addition, GRNN-SFO tracks GM in less iteration as compared to other MPPT techniques.

GRNN-SFO tracks GMPP at 604.4 W. As with conventional MPPT techniques like P&O, it gets trapped in LM due to its working behavior which affects the

TABLE 4.5: Combined Performance Analysis for Case 2: Partial Shading Condition

Tech	**Tracking Time(ms)**	**Settling Time (ms)**	**Energy (KJ)**	**Avg. Power Tracked W**	**Efficiency (%)**
GRNN-SFO	89	131	0.2847	604.4	99.99
GRNN-PSO	101	143	0.2825	601.8	99.47
GRNN-P&O	66	100	0.2477	520.6	86.04
RBF-SFO	92	135	0.2839	603.4	99.73
RBF-PSO	105	147	0.2820	601.1	99.35
RBF-P&O	68	102	0.2471	519.8	85.91

training of GRNN and therefore GRNN-P&O also gets stuck in LM during PSC. GRNN-PSO even though with its high efficiency, that is, 99.47% is not up to the mark since the time it takes to track GM and time it takes to settle is 101ms and 143ms respectively. In the similar manner, RBF-SFO outperforms all other techniques except for GRNN-SFO. The highest power is achieved by GRNN-SFO with an efficiency of 99.90%. From the results, it is evident that GRNN-SFO is a powerful technique when it comes to MPPT.

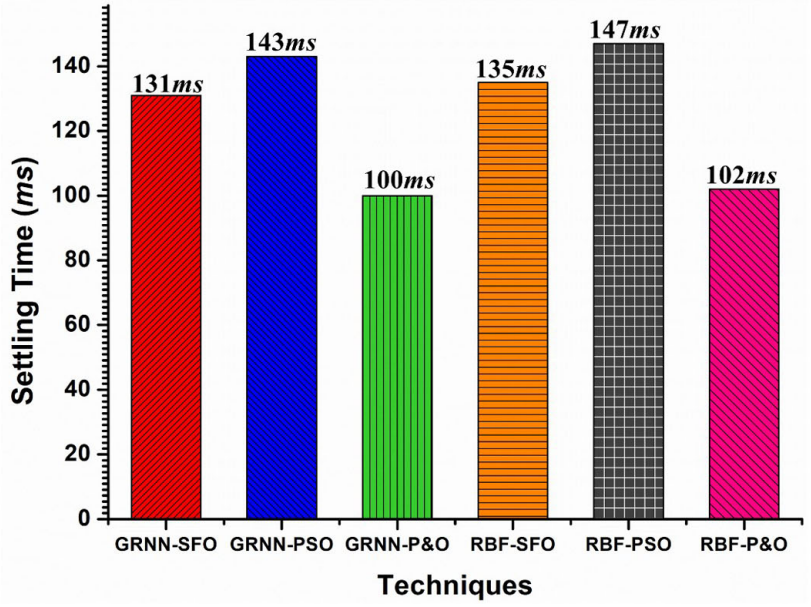

FIGURE 4.18: Settling Time comparative analysis of all techniques for case 2

Figure 4.18 illustrates the settling time of all six techniques.

The results show that GRNN-SFO settles at 131ms, GRNN-PSO settles at 143ms, GRNN-P&O settles at 100ms, RBF-SFO settles at 135ms, RBF-PSO settles at 147ms, and RBF-P&O settles at 102ms.

The second evaluation criterion that is used in this thesis is tracking time. Tracking time corresponds to better efficiency. Figure 4.19 shows the tracking time of all six techniques. The results show that GRNN-SFO tracks power in 89ms, GRNN-PSO in 101ms, GRNN-P&O in 66ms, RBF-SFO in 92ms, RBF-PSO in 105ms, and RBF-P&O in 68ms.

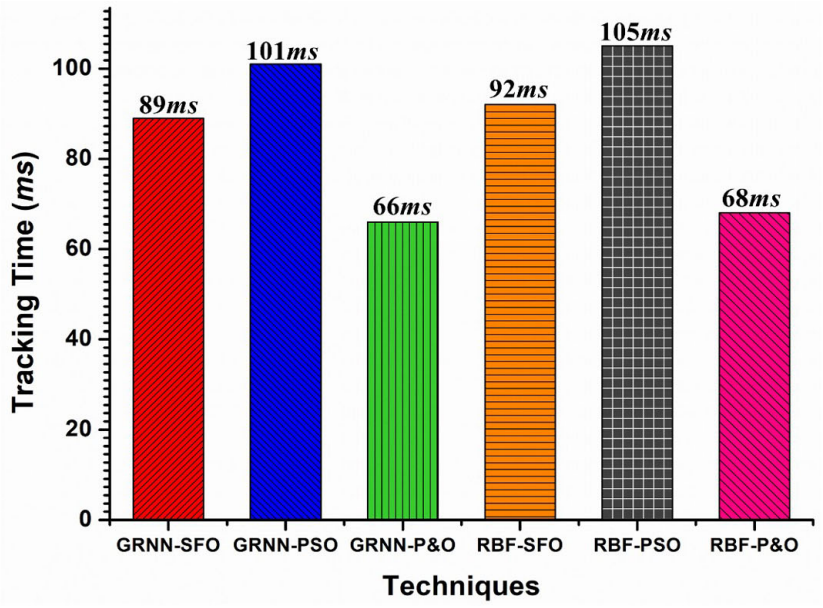

FIGURE 4.19: Tracking Time comparative analysis of all techniques for case 2

The third criterion to test the performance of all techniques is efficiency. Figure 4.18 and 4.19 give an impression some techniques are better than GRNN-SFO. However, efficiency of techniques is based on all of the parameters combined. The objective is to achieve high efficiency. Figure 4.20 shows the comparative analysis of efficiencies achieved by all six techniques which clearly shows the superior performance of GRNN-SFO under PSC.

Figure 4.21 is a comparative graphical illustration of all the techniques that have been presented for tracking MPP under PSC. The graph shows the superior performances of GRNN-SFO in terms of tracking time, power tracked and efficiency.

It can be clearly seen that GRNN-SFO tracks power in 89ms, and RBF-SFO in 92ms with 604.4W and 603.4W power tracked respectively. GRNN-SFO tracks

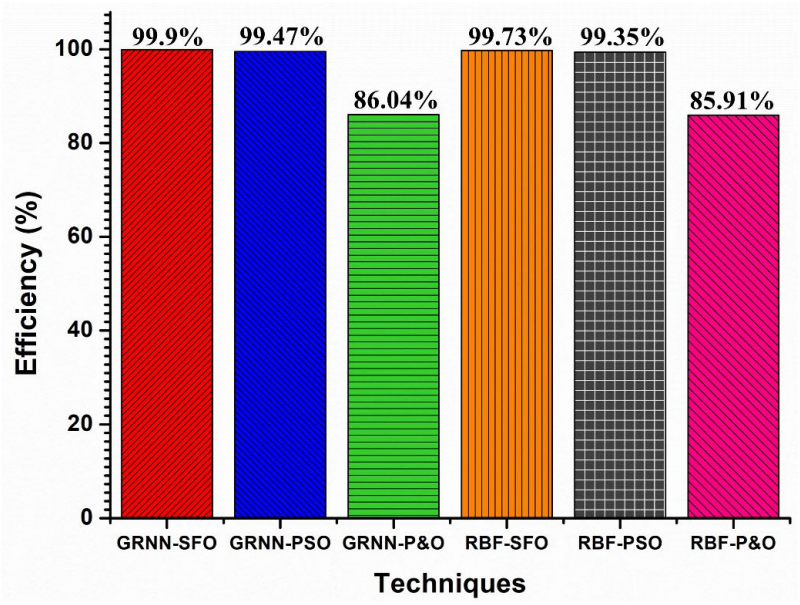

FIGURE 4.20: Efficiency comparison of all techniques for case 2

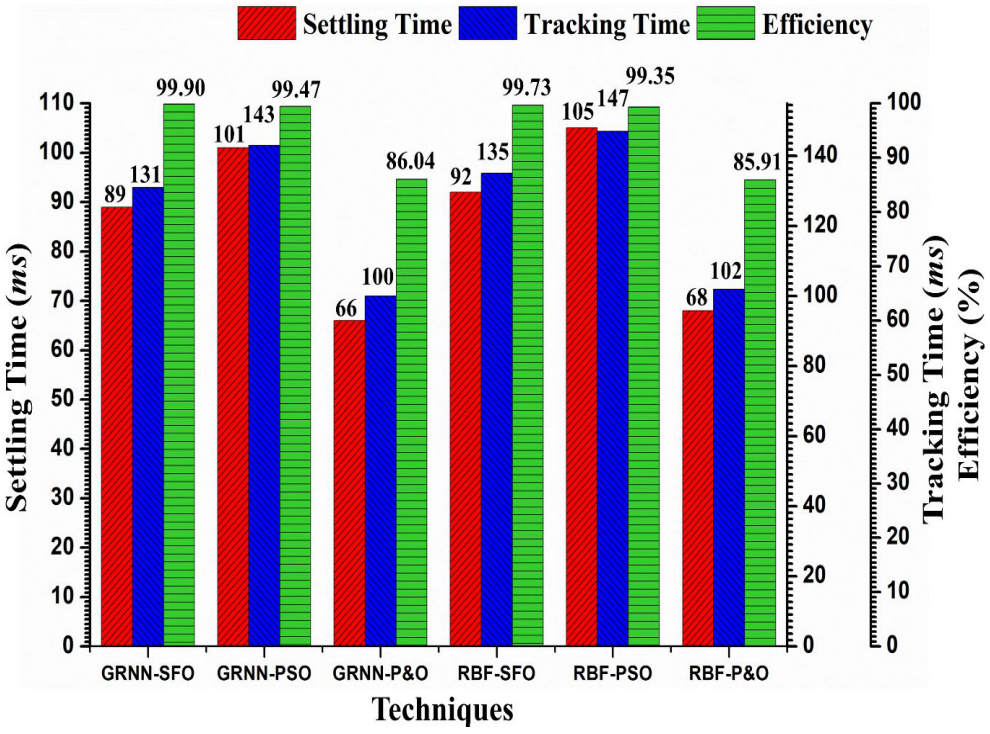

FIGURE 4.21: Comparative analysis of all 6 techniques in terms of settling time, tracking time, and efficiency for case 2: Partial Shading Condition

MPP with 99.90% efficiency whereas RBF-SFO tracks MPP with 99.73% efficiency. The high efficiency of GRNN-SFO with fast tracking time makes it a much better choice in tracking the MPP.

4.5 Case 3: Complex Partial Shading (CPS) Condition

In case 3, complex partial shading is presented with 8 PV modules are connected in series. The irradiance levels for case 3 is presented in Table 4.6. Table 4.6 illustrates the irradiances which all PV panels receive. In this case all PV panels receive varying irradiance creating a condition where LMPP and GMPP are so close that is becomes extremely hard to track the MPP.

4.5.1 Testing: Case 3

Eight PV panels have been used in order to test the performance of the techniques. All PV panels receive changing irradiance which imitates the condition of CPS. Case 3 illustrates a condition where the difference between GMPP and LMPP is very minute. This low difference makes tracking of GMPP extremely hard for MPPT techniques.

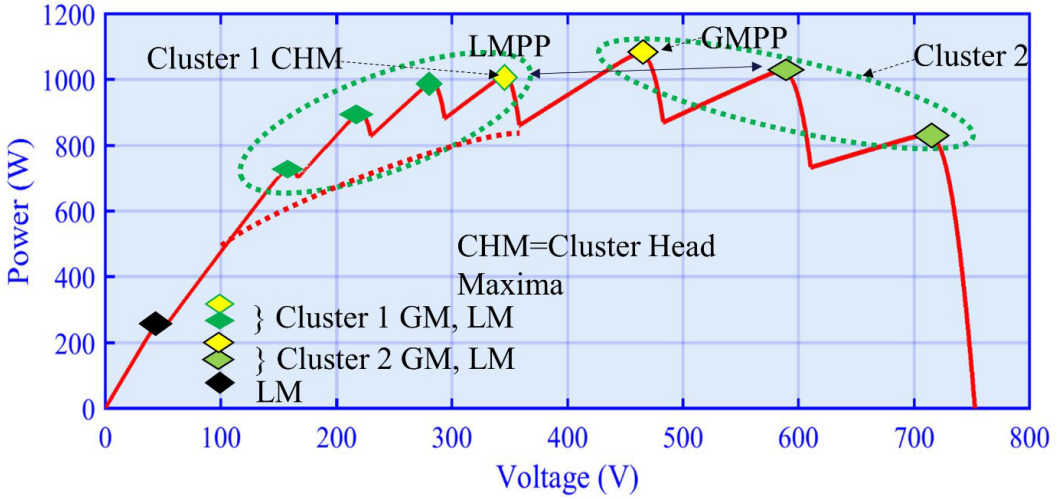

FIGURE 4.22: CPS scheme and cluster formation

PSC arises when the modules of a PV array do not get equal irradiation. The bypass diode effect in series-connected PV modules causes the PV curves to become complicated, with several peaks appearing in the curve. Number of peaks are dependant upon he number of PV panels undergoing shading.

If the number of partially shaded modules is considerable and the shading is widely dispersed, a unique type of PV curve with numerous closely connected maximum points appears on the PV curve, as illustrated in Figure 4.22. The cluster head 1 and LM2 of cluster 2 have relatively comparable values, which is intriguing.

As a result, the method is not activated or initialized, and swarm particles are unable to scan the region between these two sites. Furthermore, near the conclusion of iteration cycles, the velocity vectors are purposely designed to be slowed down for improved convergence and less oscillations at MPP. In this scenario, the outcome is undetected GMPP. It results in a considerable reduction in available power. The CPS is to blame for this loss. Table 4.6 depicts the irradiances recieved by all panels establishing a CPS state.

TABLE 4.6: Complex Partial Shading Condition Pattern for Case 3 consisting of 8 Photo-Voltaic Panels

Cases	**Irradiance S_i ($\frac{KW}{m^2}$)**			
Case 3	PV1	0.46	PV5	0.68
	PV2	0.31	PV6	0.77
	PV3	0.54	PV7	0.85
	PV4	0.40	PV8	0.90

Case 3 deals with a special condition of CPS. This is a special case, where a long array of PV system gets partially shaded. This PS can be caused by the shadows of nearby trees, buildings, mountains, or dust. PV panels are installed with built-in protection diodes known as bypass diodes.

These diodes are installed in order to protect the PV panel from getting hotspots which can be caused by PS. These bypass diodes have a shortcoming as well. At one hand, where they provide protection against hotspots, on the other hand they result in a non-linear power curve which contains multiple power points rather than only one. In this curve, there is only one global power point in between several local power points. These local power points makes it very hard and difficult to track the GMPP. This is where the conventional algorithms fail to perform as desired.

In order to replicate the condition of PSC, eight different irradiances of $0.85\frac{KW}{m^2}$, $0.31\frac{KW}{m^2}$, $0.77\frac{KW}{m^2}$, $0.68\frac{KW}{m^2}$, $0.54\frac{KW}{m^2}$, $0.46\frac{KW}{m^2}$, $0.40\frac{KW}{m^2}$, and $0.90\frac{KW}{m^2}$ have been used. This complex shading results in increased number local minima's as compared to the simple case of PS and it makes it very complex for the MPPT techniques to track the MPP. The probability of tracking the MPP wrong is exceptionally high in this case.

Figure 4.23 illustrates the maximum power that can be extracted under the given irradiance conditions shown in Table 4.6. This means that for the irradiance of $0.85\frac{KW}{m^2}$, $0.31\frac{KW}{m^2}$, $0.77\frac{KW}{m^2}$, $0.68\frac{KW}{m^2}$, $0.54\frac{KW}{m^2}$, $0.46\frac{KW}{m^2}$, $0.40\frac{KW}{m^2}$, and $0.90\frac{KW}{m^2}$ the maximum power that can be extracted is $1077.6\,W$.

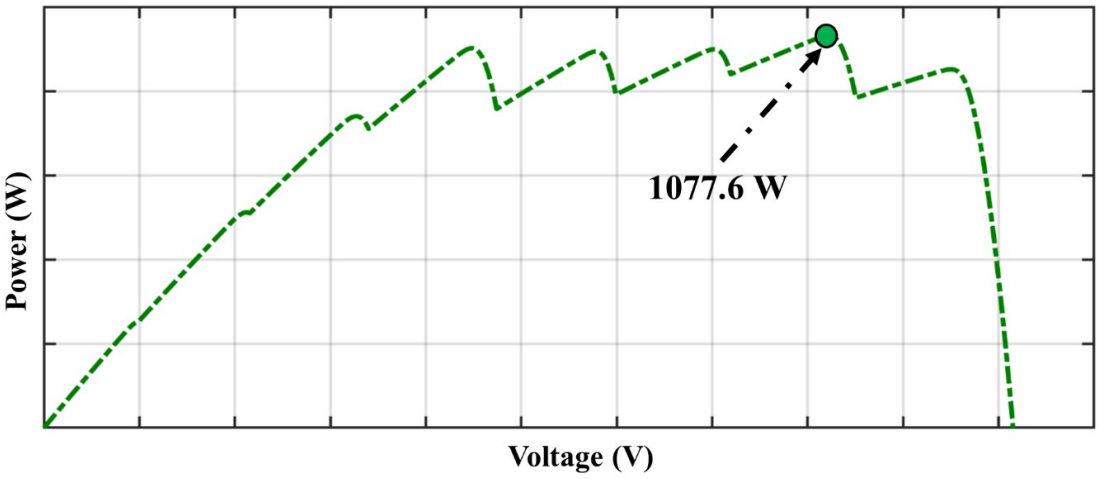

FIGURE 4.23: Maximum Power under partial shading condition for the given irradiances in Table 4.6

4.5.2 Results: Case 3

Figure 4.24 to Figure 4.27 represents the power, and duty cycle tracked by the six techniques under CPS.

The results indicate that CPS results in increased number of local minima's as compared to the simple case of PS making MPPT more difficult. The comparison amongst GRNN-SFO, GRNN-P&O, GRNN-PSO, RBF-SFO, RBF-PSO and RBF-P&O states that the highest performance is achieved by GRNN-SFO.

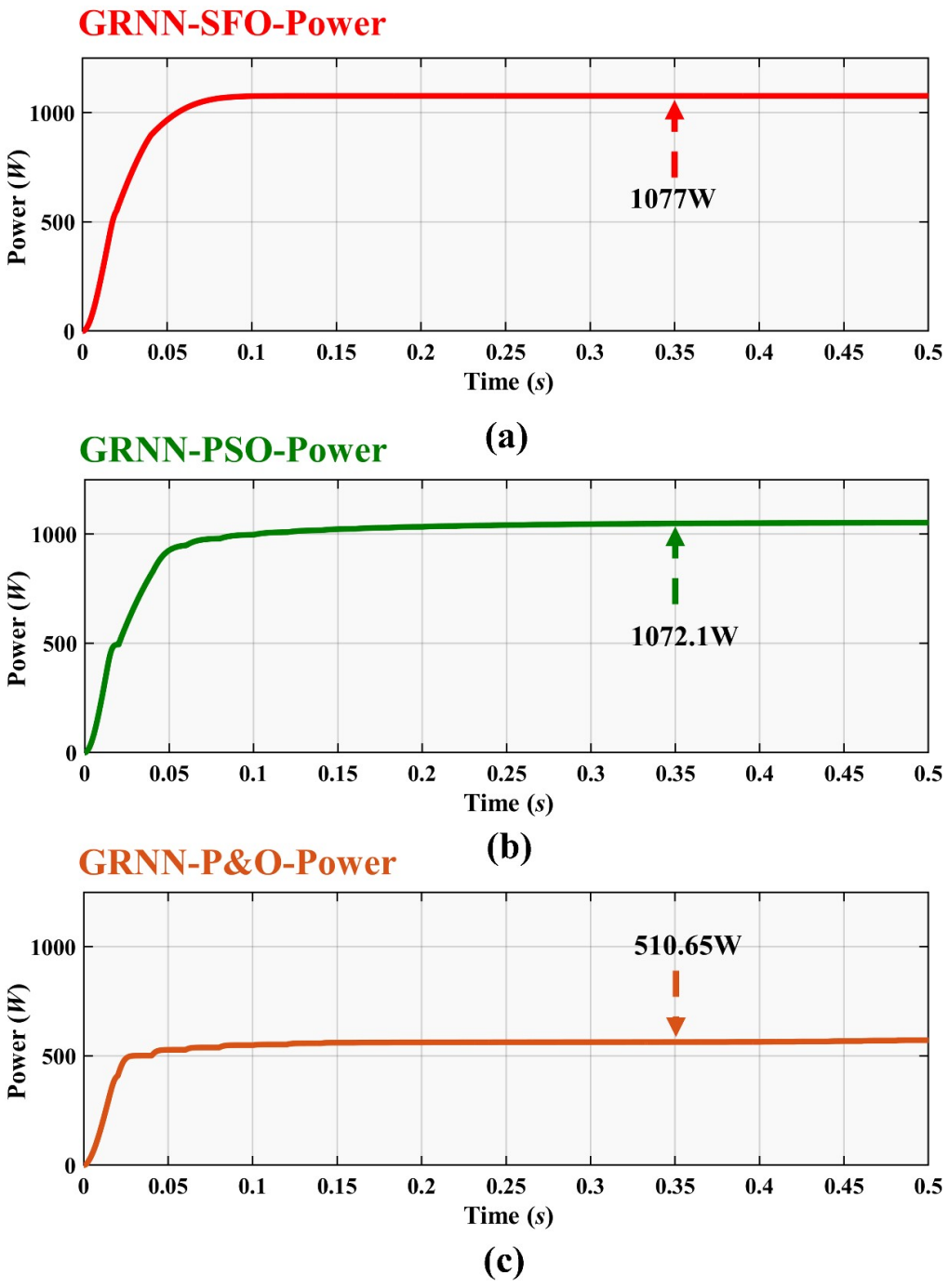

FIGURE 4.24: Power Tracking for PV panels for (a) Sail Fish Optimizer (b) Particle Swarm Optimization (c) Perturb and Observe trained by GRNN(GRNN-SFO, GRNN-PSO, GRNN-P&O) under Complex Partial Shading Condition

Figure.4.24 represents the power tracking curve of GRNN trained using SFO, PSO and P&O (GRNN-SFO, GRNN-PSO, GRNN-P&O) under CPS.

GRNN-SFO's capability to track the power in $89ms$ under CPS as opposed to GRNN-PSO's $101ms$ and GRNN-P&O's $66ms$ makes it a suitable technique for MPP. Training of GRNN with SFO helps to track MPP quickly, that is, it tracks

1077 W power with a high efficiency of 99.94%. The results conclude that GRNN-SFO is quick, robust and suitable in order to track the MPP under rapid changing irradiance levels.

The second set of technique includes the training of conventional and swarm based techniques with RBFN. Figure 4.25 illustrates the power tracking curve for RBFN trained with SFO, PSO and P&O (RBF-SFO, RBF-PSO, RBF-P&O) under PSC.

RBF-SFO tracks the power in fast changing irradiance condition and tracks power in 92ms, RBF-PSO in 10ms, and RBF-P&O in 68ms. RBF-SFO is swiftness in order to track MPP makes it well contended techniques for MPP applications. RBF-SFO tracks 1076.3 W power which is just 0.7 W less than GRNN-SFO.

However, even with high performance of RBF-SFO, results shows that GRRN-SFO outperforms RBF-SFO.

It can be concluded that GRNN-SFO works exceptionally well for the tracking the MPP.

The order of performance of all the techniques is as follows: GRNN-SFO > RBF-SFO > GRNN-PSO > RBF-PSO > GRNN-P&O > RBF-P&O for CPS.

Figure 4.26 represents the duty cycle variation of GRNN trained with SFO, PSO and P&O (GRNN-SFO, GRNN-PSO, GRNN-P&O) under CPS.

The proposed technique has been compared with GRNN trained with SFO, PSO and P&O GRNN-SFO is very quick to adjust the duty cycle to reach the MPP as compared to GRNN-PSO and GRNN-P&O under CPS. Integration of SFO with GRNN makes it very proficient for the MPPT. GRNN-SFO's ability to extract 0.4847KJ energy makes it an excellent choice for tracking the MPP.

Figure 4.27 illustrates the duty cycle variation of RBFN trained with SFO, PSO and P&O (RBF-SFO, RBF-PSO, RBF-P&O) under PSC for the second technique that has been proposed in this thesis.

RBF-SFO adjusts its duty cycle in fast changing irradiance condition whilst harvesting the energy of 0.4839KJ which is more as compared to RBF-PSO and

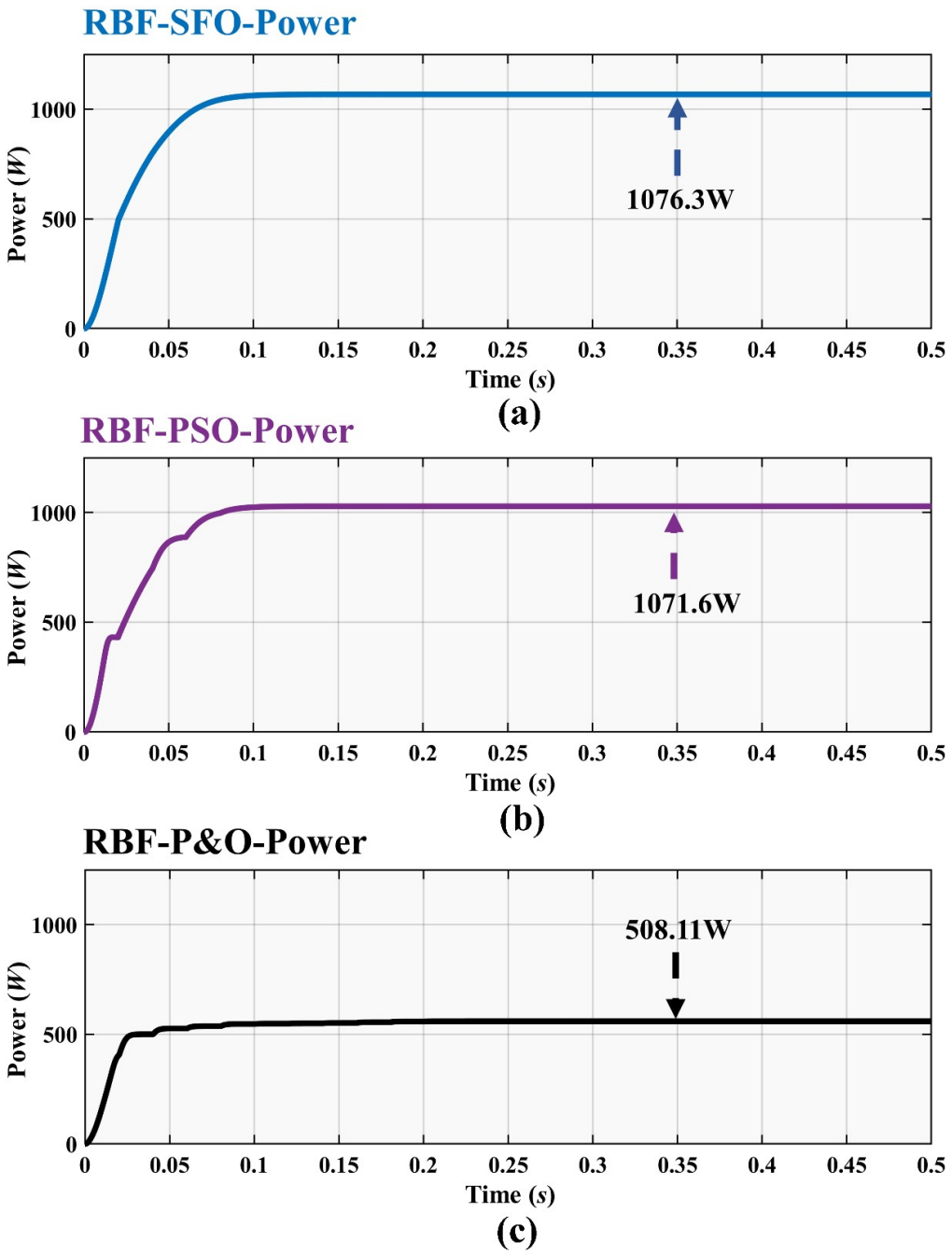

FIGURE 4.25: Power Tracking for PV panels for (a) Sail Fish Optimizer (b) Particle Swarm Optimization (c) Perturb and Observe trained by Radial Basis Function (RBF-SFO, RBF-PSO, RBF-P&O) under Complex Partial Shading Condition

RBF-P&O. GRNN-SFO in terms of Duty cycle in a similar manner to power works better as compared to RBF-SFO illustrating the high functionality of GRNN-SFO. Results denote that for duty cycle the order of performance is such that GRNN-SFO > RBF-SFO > GRNN-PSO > RBF-PSO > GRNN-P&O > RBF-P&O.

The control parameter, that is, duty cycle as shown in Figure 4.26 and Figure

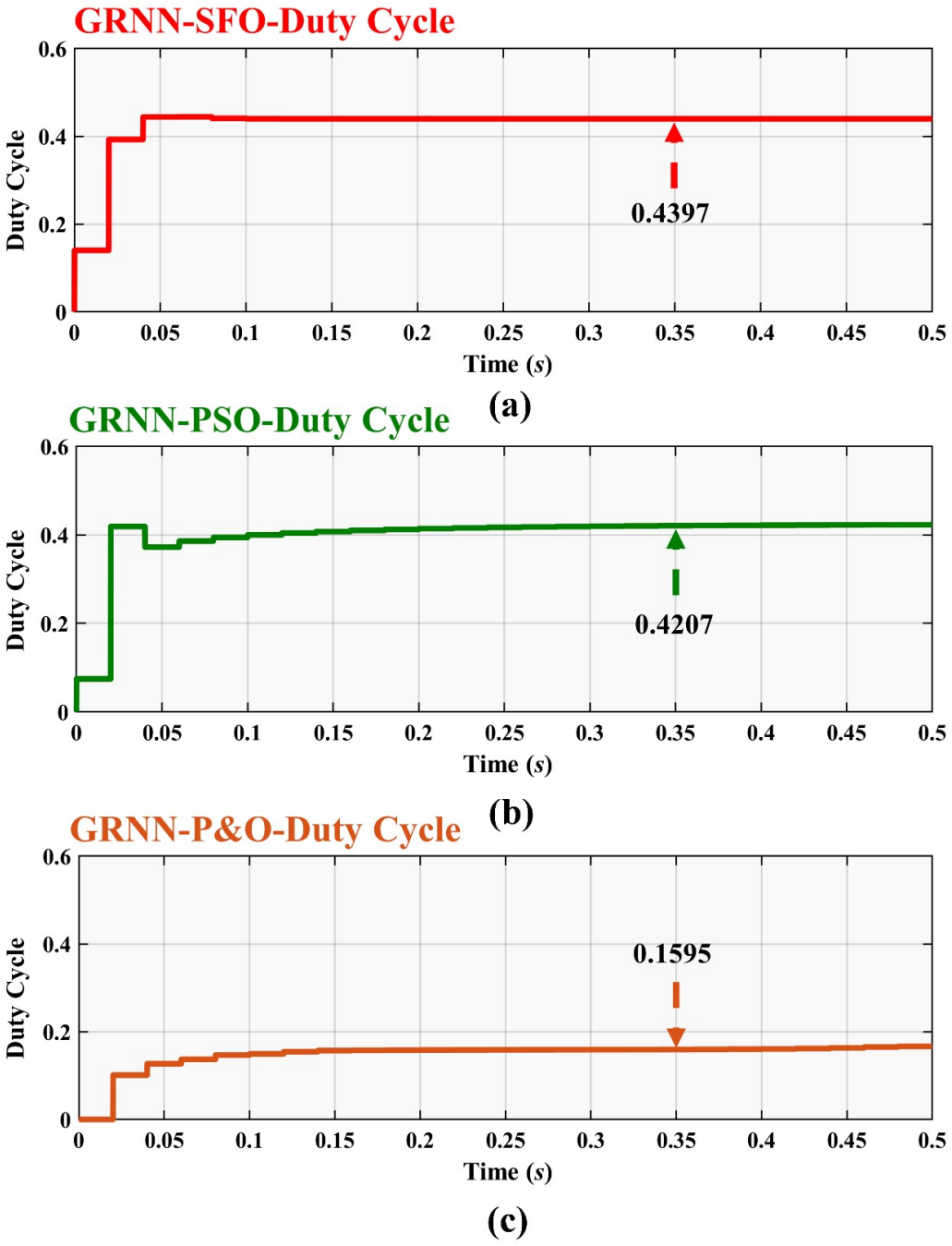

FIGURE 4.26: Duty Cycle variation for PV panels for (a) Sail Fish Optimizer (b) Particle Swarm Optimization (c) Perturb and Observe trained by GRNN(GRNN-SFO, GRNN-PSO, GRNN-P&O) under Complex Partial Shading Condition

4.27 shows that the highest efficiency is achieved by GRNN-SFO. The efficiency of GRNN-SFO, RBF-SFO, GRNN-PSO, RBF-PSO, GRNN-P&O, and RBF-P&O is 99.94%, 99.88%, 99.48%, 99.44%, 47.38%, and 47.15% respectively.

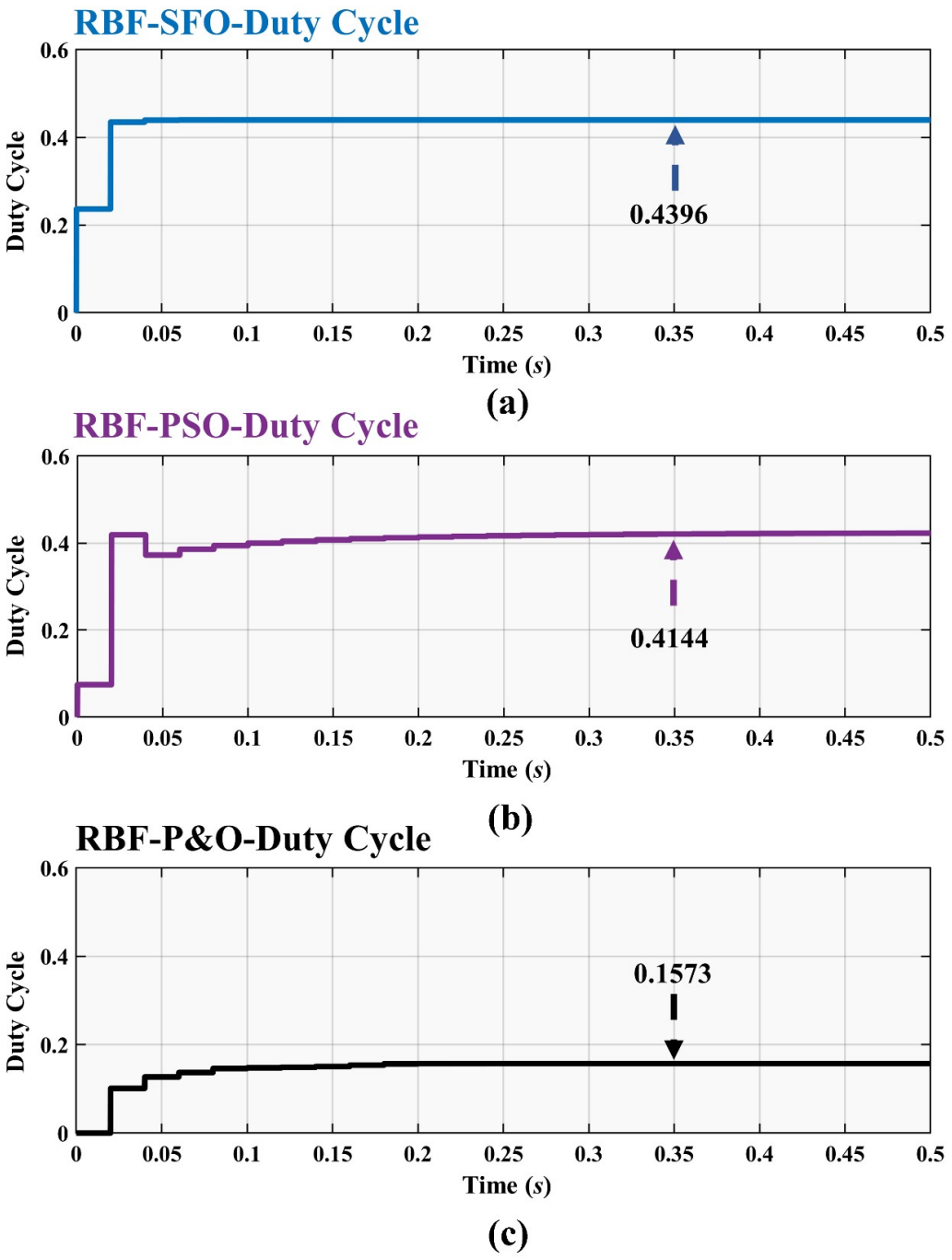

FIGURE 4.27: Duty Cycle variation for PV panels for (a) Sail Fish Optimizer (b) Particle Swarm Optimization (c) Perturb and Observe trained by Radial Basis Function (RBF-SFO, RBF-PSO, RBF-P&O) under Complex Partial Shading Condition

4.5.3 Performance Evaluation: Case 3

The power tracked by GRNN-SFO, GRNN-PSO, GRNN-P&O, RBF-SFO, RBF-PSO and RBF-P&O is 1077 W, 1072.1 W, 510.65 W, 1076.3 W, 1071.6 W and 508.11 W

respectively. RBF-PSO and GRNN-PSO gets stuck in local maxima due to velocity vector which restricts the movement of population. RBF-SFO achieves maxima by breaking the local maxima trap and stabilizing with zero oscillations at GM as shown in Figure 5.21 in less iterations.

GMPP tracking time of GRNN-SFO, GRNN-PSO, GRNN-P&O, RBF-SFO, RBF-PSO and RBF-P&O is $89ms$, $101ms$, $66ms$, $92ms$, $105ms$ and $68ms$ respectively. Performance comparison of these techniques in the form of ranking can be represented as GRNN-SFO > RBF-SFO > GRNN-PSO > RBF-PSO > GRNN-P&O > RBF-P&O.

In case 3, two proposed techniques, that is, GRNN and RBFN trained with SFO has been compared with PSO and P&O which have also been trained by GRNN an RBF under CPS. The cumulative set of results in terms of tracking time, settling time, energy, average power tracked an efficiency has been illustrate in the Table 4.7. From the table it is evident that GRNN-SFO bypass all other techniques in terms of performance for MPPT.

TABLE 4.7: Combined Performance Analysis for Case 3: Complex Partial Shading Condition

Tech	**Tracking Time(ms)**	**Settling Time (ms)**	**Energy (KJ)**	**Avg. Power Tracked W**	**Efficiency (%)**
GRNN-SFO	89	131	0.4847	1077	99.94
GRNN-PSO	101	143	0.4825	1072.1	99.48
GRNN-P&O	66	100	0.4477	510.5	47.38
RBF-SFO	92	135	0.4839	1076.3	99.88
RBF-PSO	105	147	0.4820	1071.6	99.44
RBF-P&O	68	102	0.4471	508.11	47.15

The results show that GRNN-SFO settles at $131ms$, GRNN-PSO settles at $143ms$, GRNN-P&O settles at $100ms$, RBF-SFO settles at $135ms$, RBF-PSO settles at $147ms$, and RBF-P&O settles at $102ms$. Figure 4.28 illustrates the settling of all six techniques.

The second evaluation criterion that is used in this thesis is tracking time. Tracking time corresponds to better efficiency.

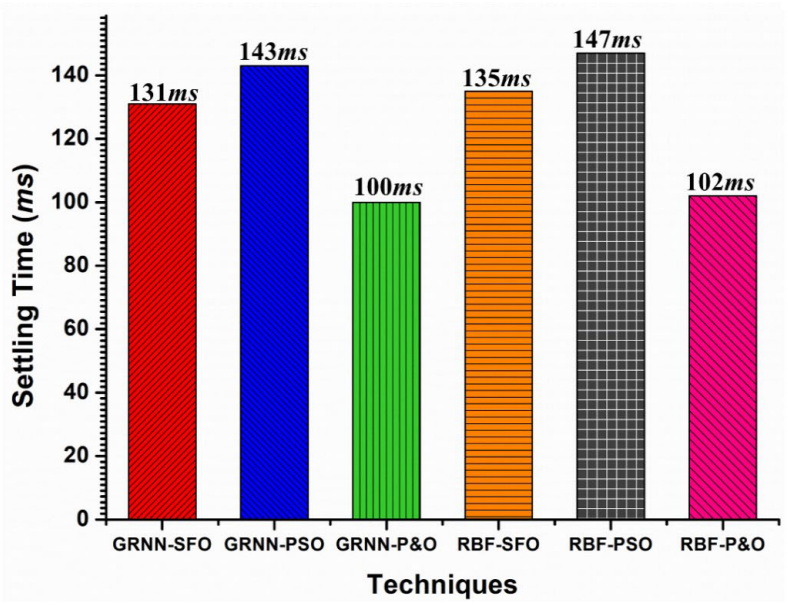

FIGURE 4.28: Settling Time comparative analysis of all techniques for Case 3

Figure 4.29 shows the tracking time of all six techniques. The results show that GRNN-SFO tracks power in 89ms, GRNN-PSO in 101ms, GRNN-P&O in 66ms, RBF-SFO in 92ms, RBF-PSO in 105ms, and RBF-P&O in 68ms.

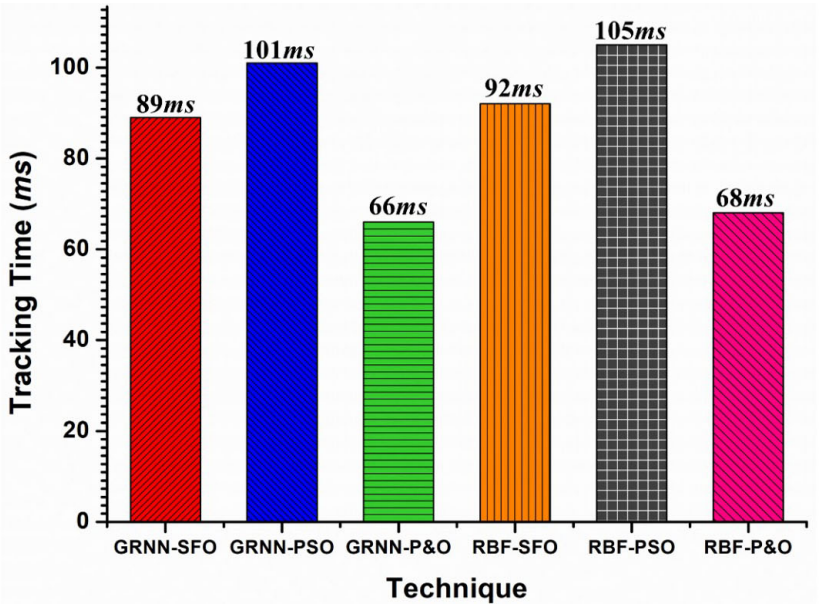

FIGURE 4.29: Tracking Time comparative analysis of all techniques for Case 3

Figure 4.30 shows the efficiency comparison of all 6 techniques.

Figure 4.31 is a comparative graphical illustration of all the techniques that has been presented for tracking MPP under PSC.

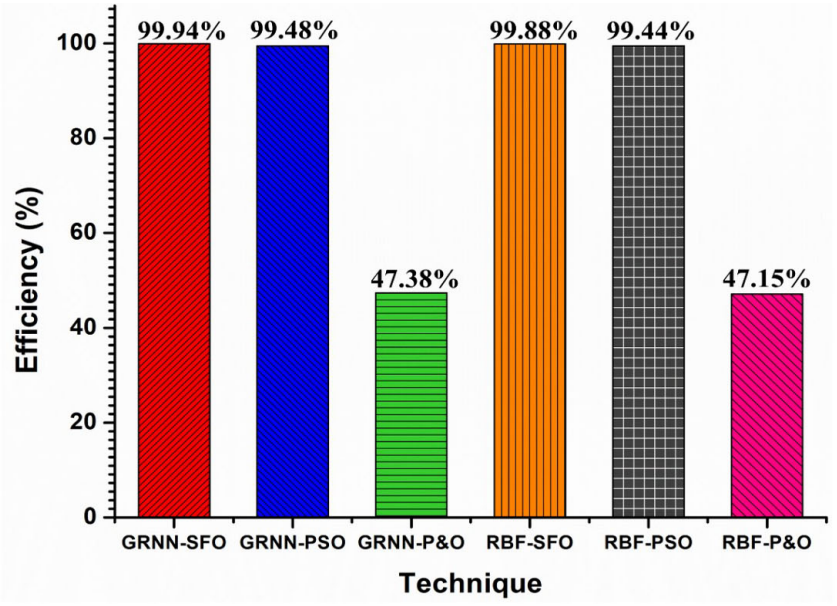

FIGURE 4.30: Efficiency comparison of all techniques for case 3

The graph shows the superior performances of GRNN-SFO and RBF-SFO in terms of tracking time, power tracked and efficiency.

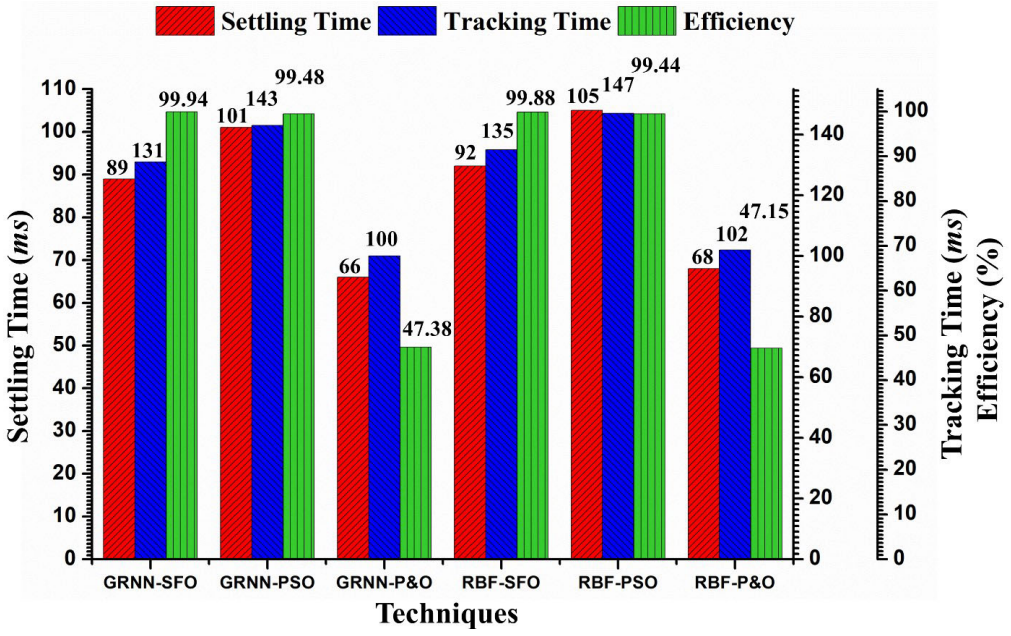

FIGURE 4.31: Comparative analysis of all 6 techniques in terms of settling time, tracking time, and efficiency for case 3: Complex Partial Shading Condition

It can be clearly seen that GRNN-SFO tracks power in 89ms, and RBF-SFO in 92ms with 1077W and 1076.3W power tracked respectively. GRNN-SFO tracks the MPP with 99.94% efficiency whereas RBF-SFO tracks MPP with 99.88% efficiency. The high efficiency of GRNN-SFO and RBF-SFO with fast tracking time

makes them a much better choice, particularly GRNN-SFO in tracking the MPP since GRNN-SFO offers better results more so than RBF-SFO. Case 3 deals with CPS condition on PV panels. On the basis of these results, it is concluded that GRNN-SFO > RBF-SFO > GRNN-PSO > RBF-PSO > GRNN-P&O > RBF-P&O. One of the major area of problems in tracking the MPPT under CPS is that the techniques either tend to get stuck in local minimums or they take significantly longer time to get to the GMPP and track it since it is easier to get stuck in LMPP. Both of these major issues are dealt with GRNN-SFO and RBF-SFO

4.6 Efficiency and Performance Evaluation

The performance evaluation of GRNN-SFO and RBF-SFO with other competing techniques helps to understand common characteristics. We know that conventional P&O is a comparatively faster and a simple to implement technique because of gradient based control, however significant power loss due to oscillations under varying irradiances and trapping of LM makes P&O a non-desirable technique.

On the other hand another technique, under PS, PSO has high efficiency in locating GMPP but it offers a low power efficiency. As seen in case 3, GRNN-P&O causes large fluctuations, which are not very desirable.

One of the best approaches to grasp the overlapping features of GRNN-SFO with other MPPT techniques is to do a performance evaluation. Case 2 states that GRNN-PSO gives rise to immense fluctuations which are not very desirable.

On the other hand, GRNN-SFO provides a solution to these issues with its high efficiency of 99.9% under all operating conditions. In comparison to other techniques, it is safe to say that GRNN-SFO clearly shows an upper hand performance. Moreover, GRNN-SFO has an ability to track GM at a fast rate which is evident from case I, which shows that GRNN-SFO performs better in the transient phase. The ability of other techniques in comparison to power convergence as stated in case 2 is lower whereas the GM is located successfully and rapidly by GRNN-SFO. Figure 4.32 shows the statistical analysis comparison of all 6 techniques.

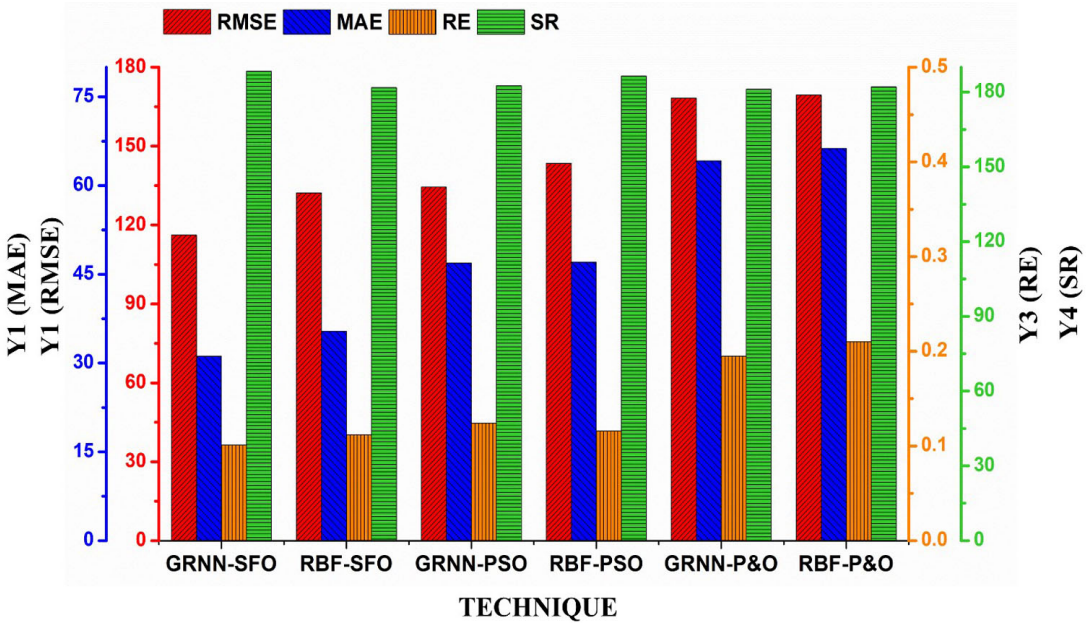

FIGURE 4.32: Statistical Analysis Comparison of Competing Techniques

Results conclude that:

- GRNN-SFO has an outstanding tracking ability, as demonstrated by case 1,2 and 3 where it outperforms all other techniques.
- Case 2 and 3 shows that GRNN-SFO can tackle CPS better. The performance of RBF-SFO and other comparative techniques are hampered by the use of random initialization even after they have located the GMPP.
- Robustness and sensitivity of all techniques inspected by mean, standard deviation (SD), relative error (RE) by Equation 4.1, mean absolute error (MAE) by Equation 4.2 and root means square error (RMSE) by Equation 4.3.

$$Error_{RE} = \frac{(P_{PVI} - P_{PV})}{P_{PV}} \times 100 \tag{4.1}$$

$$Error_{MAE} = \frac{\sum_{i=1}^{n} (P_{PVI} - P_{PV})}{n} \tag{4.2}$$

$$Error_{RMSE} = \sqrt{\frac{\sum_{i=1}^{n} \left(P_{PVI} - P_{PV}\right)^2}{n}} \tag{4.3}$$

Where P_{pvi} represents the power at STC, n represent the number of samples. Figure 4.32 presents RMSE, MAE, RE, and SR.

4.7 Chapter Summary

In this chapter, the proposed MPPT technique is tested on different scenarios which include fast varying irradiance, PSC and CPS. The comparison of GRNN-SFO is made against GRNN-PSO, GRNN-P&O, RBFNN-SFO, RBFNN-PSO and RBFNN-P&O. The proposed technique is also analyzed using the statistical analysis. The proposed technique shows better results as compared to other competing techniques.

Chapter 5

Conclusion and Future Work

5.1 Conclusion

The author concluded the following research work in this thesis in following manners:

1. The importance of renewable energy is established and its significance is highlighted. The effects of Partial Shading (PS) are conceptualized for a better understanding of large-scale PV system power generation. The work is presented in chapters 1 and 2. Complex partial shading (CPS) is also introduced and conceptualized.

2. In chapter 3, the author proposed a hybrid meta heuristic and machine learning based MPPT technique which uses Sailfish Optimizer to train the GRNN(GRNN-SFO). The outcome verifies that the proposed technique is superior to other compared techniques in terms of GMPP tracking and reduced oscillations around GMPP. Tracking efficiency of up to 99.9% and negligible oscillations are notable contributions in this field.

3. Proposed work is tested on Fast Varying Irradiance, PSC and CPS. Also, the statistical analysis is presented to check the superior performance of proposed technique.

5.2 Future Work

Using a unique hybrid intelligence-based method, this thesis made a significant contribution in the field of MPPT of PV systems under PS and CPS circumstances. The knowledge and experience gained through study in this sector has shown a number of limitations and benefits in the field of PV system MPPT control. Field investigations, CPS, and hardware components, in particular, need a significant amount of effort. A uniform environment, stronger counter-measures, and thorough models of such systems are all needed.

In future a scaled up the model of upto 1 MW will be implemented inorder to study the performance of proposed technique. Also integration of the thermoelectric generator with the PV system for producing energy from waste heat recovery will be inspected. The performance of the proposed MPPT technique will be tested on the hybrid PV-TEG models. Morever, complex partial shading will be investigated further in order for PV systems to operate perfectly when integrated with DC microgrids.

Bibliography

[1] S. Mirjalili, A. H. Gandomi, S. Z. Mirjalili, S. Saremi, H. Faris, and S. M. Mirjalili, "Salp swarm algorithm: A bio-inspired optimizer for engineering design problems," *Advances in Engineering Software*, vol. 114, pp. 163–191, 2017.

[2] H. E. Murdock, D. Gibb, T. André, J. L. Sawin, A. Brown, F. Appavou, G. Ellis, B. Epp, F. Guerra, F. Joubert *et al.*, "Renewables 2020-global status report," 2020.

[3] H. Mamur and Y. Coban, "Detailed modeling of a thermoelectric generator for maximum power point tracking," *Turkish Journal of Electrical Engineering & Computer Sciences*, vol. 28, no. 1, pp. 124–139, 2020.

[4] H. Karbaschi, N. Nouri, M. Rezaei, and G. Rashedi, "Thermoelectric power generation efficiency of zigzag monolayer nanoribbon of bismuth," *Nanotechnology*, vol. 31, no. 37, p. 375403, 2020.

[5] X. Wen, J. Ji, Z. Song, Z. Li, H. Xie, and J. Wang, "Comparison analysis of two different concentrated photovoltaic/thermal-teg hybrid systems," *Energy Conversion and Management*, vol. 234, p. 113940, 2021.

[6] Y. Cai, W.-W. Wang, C.-W. Liu, W.-T. Ding, D. Liu, and F.-Y. Zhao, "Performance evaluation of a thermoelectric ventilation system driven by the concentrated photovoltaic thermoelectric generators for green building operations," *Renewable Energy*, vol. 147, pp. 1565–1583, 2020.

[7] A. Q. Al-Shetwi, M. Hannan, K. P. Jern, M. Mansur, and T. Mahlia, "Grid-connected renewable energy sources: Review of the recent integration requirements and control methods," *Journal of Cleaner Production*, vol. 253, p. 119831, 2020.

[8] M. Roslan, M. Hannan, P. J. Ker, and M. Uddin, "Microgrid control methods toward achieving sustainable energy management," *Applied Energy*, vol. 240, pp. 583–607, 2019.

[9] M. Salihmuhsin and B. A. Aldwihi, "Modeling of photovoltaic panels using matlab/simulink," *Kahramanmaraş Sütçü İmam Üniversitesi Mühendislik Bilimleri Dergisi*, vol. 22, no. 2, pp. 78–87, 2019.

[10] S. Motahhir, A. El Ghzizal, S. Sebti, and A. Derouich, "Modeling of photovoltaic system with modified incremental conductance algorithm for fast changes of irradiance," *International Journal of Photoenergy*, vol. 2018, 2018.

[11] T. Ma, H. Yang, and L. Lu, "Solar photovoltaic system modeling and performance prediction," *Renewable and Sustainable Energy Reviews*, vol. 36, pp. 304–315, 2014.

[12] M. RASHEED, S. SHIHAB, and T. RASHID, "Estimation of single-diode model parameters of pv cell," *Journal of Al-Qadisiyah for Computer Science and Mathematics*, vol. 13, no. 1, pp. Page–139, 2021.

[13] M. S. Rasheed and S. Shihab, "Modelling and parameter extraction of pv cell using single-diode model," *Advanced Energy Conversion Materials*, pp. 96–104, 2020.

[14] H. K. Mehta, H. Warke, K. Kukadiya, and A. K. Panchal, "Accurate expressions for single-diode-model solar cell parameterization," *IEEE Journal of Photovoltaics*, vol. 9, no. 3, pp. 803–810, 2019.

[15] N. Anani and H. Ibrahim, "Adjusting the single-diode model parameters of a photovoltaic module with irradiance and temperature," *Energies*, vol. 13, no. 12, p. 3226, 2020.

[16] M. Aourir, A. Abouloifa, I. Lachkar, C. Aouadi, F. Giri, and J. M. Guerrero, "Nonlinear control and stability analysis of single stage grid-connected photovoltaic systems," *International Journal of Electrical Power & Energy Systems*, vol. 115, p. 105439, 2020.

[17] B. Yang, M. Zhang, X. Zhang, J. Wang, H. Shu, S. Li, T. He, L. Yang, and T. Yu, "Fast atom search optimization based mppt design of centralized thermoelectric generation system under heterogeneous temperature difference," *Journal of Cleaner Production*, vol. 248, p. 119301, 2020.

[18] S. Kumar, H. S. Sahu, and S. K. Nayak, "Estimation of mpp of a double diode model pv module from explicit i–v characteristic," *IEEE Transactions on Industrial Electronics*, vol. 66, no. 9, pp. 7032–7042, 2018.

[19] B. G. Pardhu and V. R. Kota, "Radial movement optimization based parameter extraction of double diode model of solar photovoltaic cell," *Solar Energy*, vol. 213, pp. 312–327, 2021.

[20] L. M. P. Archila, J. D. B. Rodríguez, and R. Correa, "Implicit modelling of series-parallel photovoltaic arrays using double-diode model and its solution," *Solar Energy*, vol. 214, pp. 131–137, 2021.

[21] M. Abdel-Basset, R. Mohamed, A. El-Fergany, M. Abouhawwash, and S. Askar, "Parameters identification of pv triple-diode model using improved generalized normal distribution algorithm," *Mathematics*, vol. 9, no. 9, p. 995, 2021.

[22] M. A. Soliman, H. M. Hasanien, and A. Alkuhayli, "Marine predators algorithm for parameters identification of triple-diode photovoltaic models," *IEEE Access*, vol. 8, pp. 155 832–155 842, 2020.

[23] H. Nunes, J. Pombo, S. Mariano, and M. Calado, "Suitable mathematical model for the electrical characterization of different photovoltaic technologies: Experimental validation," *Energy Conversion and Management*, vol. 231, p. 113820, 2021.

[24] A. El Hammoumi, S. Motahhir, A. Chalh, A. El Ghzizal, and A. Derouich, "Real-time virtual instrumentation of arduino and labview based pv panel characteristics," in *IOP Conference Series: Earth and Environmental Science*, vol. 161, no. 1. IOP Publishing, 2018, p. 012019.

[25] V. Kumar, S. Ghosh, N. S. Naidu, S. Kamal, R. Saket, and S. Nagar, "Load voltage-based mppt technique for standalone pv systems using adaptive step," *International Journal of Electrical Power & Energy Systems*, vol. 128, p. 106732, 2021.

[26] J. Lin, T. Liao, and B. Lin, "Performance analysis and load matching of a photovoltaic–thermoelectric hybrid system," *Energy Conversion and Management*, vol. 105, pp. 891–899, 2015.

[27] M. C. Cavalcanti, F. Bradaschia, A. J. do Nascimento, G. M. Azevedo, and E. J. Barbosa, "Hybrid maximum power point tracking technique for pv modules based on a double-diode model," *IEEE Transactions on Industrial Electronics*, vol. 68, no. 9, pp. 8169–8181, 2020.

[28] E. M. Vicente, P. S. Vicente, R. L. Moreno, and E. R. Ribeiro, "High-efficiency mppt method based on irradiance and temperature measurements," *IET Renewable Power Generation*, vol. 14, no. 6, pp. 986–995, 2020.

[29] H. Goverde, D. Goossens, J. Govaerts, V. Dubey, F. Catthoor, K. Baert, J. Poortmans, and J. Driesen, "Spatial and temporal analysis of wind effects on pv module temperature and performance," *Sustainable Energy Technologies and Assessments*, vol. 11, pp. 36–41, 2015.

[30] F. A. Touati, M. A. Al-Hitmi, and H. J. Bouchech, "Study of the effects of dust, relative humidity, and temperature on solar pv performance in doha: comparison between monocrystalline and amorphous pvs," *International journal of green energy*, vol. 10, no. 7, pp. 680–689, 2013.

[31] M. Mansoor, A. F. Mirza, Q. Ling, and M. Y. Javed, "Novel grass hopper optimization based mppt of pv systems for complex partial shading conditions," *Solar Energy*, vol. 198, pp. 499–518, 2020.

[32] A. Darwish, "Bio-inspired computing: Algorithms review, deep analysis, and the scope of applications," *Future Computing and Informatics Journal*, vol. 3, no. 2, pp. 231–246, 2018.

[33] J. Teo, R. H. Tan, V. Mok, V. K. Ramachandaramurthy, and C. Tan, "Impact of bypass diode forward voltage on maximum power of a photovoltaic system under partial shading conditions," *Energy*, vol. 191, p. 116491, 2020.

[34] M. Dhimish and G. Badran, "Current limiter circuit to avoid photovoltaic mismatch conditions including hot-spots and shading," *Renewable Energy*, vol. 145, pp. 2201–2216, 2020.

[35] H. S. Moreira, J. L. de Souza Silva, M. V. G. dos Reis, D. de Bastos Mesquita, B. H. K. de Paula, and M. G. Villalva, "Experimental comparative study of photovoltaic models for uniform and partially shading conditions," *Renewable Energy*, vol. 164, pp. 58–73, 2021.

[36] D. Atsu, I. Seres, M. Aghaei, and I. Farkas, "Analysis of long-term performance and reliability of pv modules under tropical climatic conditions in sub-saharan," *Renewable Energy*, vol. 162, pp. 285–295, 2020.

[37] V. F. Onyshchenko, L. Karachevtseva *et al.*, "Photoconductivity relaxation time in macroporous silicon," *Emerging Science Journal*, vol. 4, no. 3, pp. 192–204, 2020.

[38] S. Bhattacharya and S. John, "Beyond 30% conversion efficiency in silicon solar cells: a numerical demonstration," *Scientific reports*, vol. 9, no. 1, pp. 1–15, 2019.

[39] B. Zaidi, I. Saouane, and C. Shekhar, "Simulation of single-diode equivalent model of polycrystalline silicon solar cells," *International Journal of Materials Science and Applications*, vol. 7, no. 8, 2018.

[40] C. Strümpel, M. McCann, G. Beaucarne, V. Arkhipov, A. Slaoui, V. Švrček, C. Del Cañizo, and I. Tobias, "Modifying the solar spectrum to enhance silicon solar cell efficiency—an overview of available materials," *Solar energy materials and solar cells*, vol. 91, no. 4, pp. 238–249, 2007.

[41] H. Bakir and A. A. Kulaksiz, "Modelling and voltage control of the solar-wind hybrid micro-grid with optimized statcom using ga and bfa," *Engineering Science and Technology, an International Journal*, vol. 23, no. 3, pp. 576–584, 2020.

[42] D. Hao, T. Zhang, L. Guo, Y. Feng, Z. Zhang, and Y. Yuan, "A high-efficiency, portable solar energy-harvesting system based on a foldable-wings mechanism for self-powered applications in railways," *Energy Technology*, vol. 9, no. 4, p. 2000794, 2021.

[43] Z. Huang, T. Mendis, and S. Xu, "Urban solar utilization potential mapping via deep learning technology: A case study of wuhan, china," *Applied Energy*, vol. 250, pp. 283–291, 2019.

[44] K. Lappalainen and J. Kleissl, "Analysis of the cloud enhancement phenomenon and its effects on photovoltaic generators based on cloud speed sensor measurements," *Journal of Renewable and Sustainable Energy*, vol. 12, no. 4, p. 043502, 2020.

[45] X. Chen, Y. Du, E. Lim, H. Wen, K. Yan, and J. Kirtley, "Power ramp-rates of utility-scale pv systems under passing clouds: Module-level emulation with cloud shadow modeling," *Applied Energy*, vol. 268, p. 114980, 2020.

[46] V. Fung, J. Bosch, S. Roberts, and J. Kleissl, "Cloud shadow speed sensor," *Atmospheric Measurement Techniques*, vol. 7, no. 6, pp. 1693–1700, 2014.

[47] K. Lappalainen and S. Valkealahti, "Number of maximum power points in photovoltaic arrays during partial shading events by clouds," *Renewable Energy*, vol. 152, pp. 812–822, 2020.

[48] M. Parvez, A. T. Pereira, N. Ertugrul, N. H. Weste, D. Abbott, and S. F. Al-Sarawi, "Wide bandgap dc–dc converter topologies for power applications," *Proceedings of the IEEE*, vol. 109, no. 7, pp. 1253–1275, 2021.

[49] S. Shadravan, H. R. Naji, and V. K. Bardsiri, "The sailfish optimizer: A novel nature-inspired metaheuristic algorithm for solving constrained engineering

optimization problems," *Engineering Applications of Artificial Intelligence*, vol. 80, pp. 20–34, 2019.

[50] J. Jana, H. Samanta, K. D. Bhattacharya, and H. Saha, "A four stage battery charge controller working on a novel maximum power point tracking based algorithm for solar pv system," in *2016 21st Century Energy Needs-Materials, Systems and Applications (ICTFCEN)*. IEEE, 2016, pp. 1–4.

[51] J. Kim, J. Hong, and H. Park, "Prospects of deep learning for medical imaging," *Precision and Future Medicine*, vol. 2, no. 2, pp. 37–52, 2018.

[52] F. K. Abo-Elyousr, A. M. Abdelshafy, and A. Y. Abdelaziz, "Mppt-based particle swarm and cuckoo search algorithms for pv systems," in *Modern Maximum Power Point Tracking techniques for photovoltaic energy systems*. Springer, 2020, pp. 379–400.

[53] G.-G. Wang, "Moth search algorithm: a bio-inspired metaheuristic algorithm for global optimization problems," *Memetic Computing*, vol. 10, no. 2, pp. 151–164, 2018.

[54] M. Alshinwan, L. Abualigah, M. Shehab, M. A. Elaziz, A. M. Khasawneh, H. Alabool, and H. A. Hamad, "Dragonfly algorithm: a comprehensive survey of its results, variants, and applications," *Multimedia Tools and Applications*, vol. 80, no. 10, pp. 14 979–15 016, 2021.

[55] M. H. Zafar, T. Al-shahrani, N. M. Khan, A. Feroz Mirza, M. Mansoor, M. U. Qadir, M. I. Khan, and R. A. Naqvi, "Group teaching optimization algorithm based mppt control of pv systems under partial shading and complex partial shading," *Electronics*, vol. 9, no. 11, p. 1962, 2020.

[56] Q. Askari and I. Younas, "Improved political optimizer for complex landscapes and engineering optimization problems," *Expert Systems with Applications*, vol. 182, p. 115178, 2021.

[57] T. A. Khan and S. H. Ling, "A novel hybrid gravitational search particle swarm optimization algorithm," *Engineering Applications of Artificial Intelligence*, vol. 102, p. 104263, 2021.

[58] O. P. Bharti, K. Sarita, A. S. S. Vardhan, A. S. S. Vardhan, and R. K. Saket, "Controller design for dfig-based wt using gravitational search algorithm for wind power generation," *IET Renewable Power Generation*, vol. 15, no. 9, pp. 1956–1967, 2021.

[59] C. Charin, D. Ishak, M. A. A. M. Zainuri, B. Ismail, and M. K. M. Jamil, "A hybrid of bio-inspired algorithm based on levy flight and particle swarm optimizations for photovoltaic system under partial shading conditions," *Solar Energy*, vol. 217, pp. 1–14, 2021.

[60] B. Guan, J. Zhang, W. A. Sethares, R. Kijowski, and F. Liu, "Spectral domain convolutional neural network," in *ICASSP 2021-2021 IEEE International Conference on Acoustics, Speech and Signal Processing (ICASSP)*. IEEE, 2021, pp. 2795–2799.

[61] H. Bahri and A. Harrag, "Ingenious golden section search mppt algorithm for pem fuel cell power system," *Neural Computing and Applications*, vol. 33, no. 14, pp. 8275–8298, 2021.

[62] A. Nadeem, H. A. Sher, A. F. Murtaza, and N. Ahmed, "Online current-sensorless estimator for pv open circuit voltage and short circuit current," *Solar Energy*, vol. 213, pp. 198–210, 2021.

[63] Z. M. Ali, N. V. Quynh, S. Dadfar, and H. Nakamura, "Variable step size perturb and observe mppt controller by applying θ-modified krill herd algorithm-sliding mode controller under partially shaded conditions," *Journal of Cleaner Production*, vol. 271, p. 122243, 2020.

[64] H. H. Ammar, A. T. Azar, R. Shalaby, and M. I. Mahmoud, "Metaheuristic optimization of fractional order incremental conductance (fo-inc) maximum power point tracking (mppt)," *Complexity*, vol. 2019, 2019.

[65] A. M. Silveira and R. E. Araújo, "A new approach for the diagnosis of different types of faults in dc–dc power converters based on inversion method," *Electric Power Systems Research*, vol. 180, p. 106103, 2020.

[66] A. M. Eltamaly, "Performance of mppt techniques of photovoltaic systems under normal and partial shading conditions," in *Advances in renewable energies and power technologies*. Elsevier, 2018, pp. 115–161.

[67] H. Jafari Siahroodi, H. Mojallali, and S. S. Mohtavipour, "A new optimization framework for harmonic compensation considering plug-in electric vehicle penetration using adaptive particularly tunable fuzzy chaotic particle swarm optimization," *Energy Technology*, vol. 9, no. 4, p. 2000564, 2021.

[68] Y. Wang, D. Wang, and Y. Tang, "Clustered hybrid wind power prediction model based on arma, pso-svm, and clustering methods," *IEEE Access*, vol. 8, pp. 17 071–17 079, 2020.

[69] Y.-Y. Hong and P. M. P. Buay, "Robust design of type-2 fuzzy logic-based maximum power point tracking for photovoltaics," *Sustainable Energy Technologies and Assessments*, vol. 38, p. 100669, 2020.

[70] A. Abazari, M. Babaei, S. Muyeen, and I. Kamwa, "Learning adaptive fuzzy droop of pv contribution to frequency excursion of hybrid micro-grid during parameters uncertainties," *International Journal of Electrical Power & Energy Systems*, vol. 123, p. 106305, 2020.

[71] A. Harrag and S. Messalti, "Ic-based variable step size neuro-fuzzy mppt improving pv system performances," *Energy Procedia*, vol. 157, pp. 362–374, 2019.

[72] H. Doubabi, I. Salhi, M. Chennani, and N. Essounbouli, "High performance mppt based on ts fuzzy–integral backstepping control for pv system under rapid varying irradiance—experimental validation," *ISA transactions*, vol. 118, pp. 247–259, 2021.

[73] X. Li, H. Wen, Y. Hu, and L. Jiang, "A novel beta parameter based fuzzy-logic controller for photovoltaic mppt application," *Renewable energy*, vol. 130, pp. 416–427, 2019.

[74] P. K. Atri, P. Modi, and N. S. Gujar, "Comparison of different mppt control strategies for solar charge controller," in *2020 International Conference on*

Power Electronics & IoT Applications in Renewable Energy and its Control (PARC). IEEE, 2020, pp. 65–69.

[75] M. K. Behera and L. C. Saikia, "An intelligent hybrid gmppt integrating with accurate psc detection scheme for pv system using essa optimized awfopi controller," *Sustainable Energy Technologies and Assessments*, vol. 46, p. 101233, 2021.

[76] U. Yilmaz, O. Turksoy, and A. Teke, "Improved mppt method to increase accuracy and speed in photovoltaic systems under variable atmospheric conditions," *International Journal of Electrical Power & Energy Systems*, vol. 113, pp. 634–651, 2019.

[77] A. Feroz Mirza, M. Mansoor, Q. Ling, M. I. Khan, and O. M. Aldossary, "Advanced variable step size incremental conductance mppt for a standalone pv system utilizing a ga-tuned pid controller," *Energies*, vol. 13, no. 16, p. 4153, 2020.

[78] R. B. Bollipo, S. Mikkili, and P. K. Bonthagorla, "Critical review on pv mppt techniques: classical, intelligent and optimisation," *IET Renewable Power Generation*, vol. 14, no. 9, pp. 1433–1452, 2020.

[79] M. Mao, L. Cui, Q. Zhang, K. Guo, L. Zhou, and H. Huang, "Classification and summarization of solar photovoltaic mppt techniques: A review based on traditional and intelligent control strategies," *Energy Reports*, vol. 6, pp. 1312–1327, 2020.

[80] K. Y. Yap, C. R. Sarimuthu, and J. M.-Y. Lim, "Artificial intelligence based mppt techniques for solar power system: A review," *Journal of Modern Power Systems and Clean Energy*, vol. 8, no. 6, pp. 1043–1059, 2020.

[81] L. Avila, M. De Paula, M. Trimboli, and I. Carlucho, "Deep reinforcement learning approach for mppt control of partially shaded pv systems in smart grids," *Applied Soft Computing*, vol. 97, p. 106711, 2020.

[82] E. Almeshaiei, A. Al-Habaibeh, and B. Shakmak, "Rapid evaluation of micro-scale photovoltaic solar energy systems using empirical methods combined

with deep learning neural networks to support systems' manufacturers," *Journal of Cleaner Production*, vol. 244, p. 118788, 2020.

[83] A. Zameer, J. Arshad, A. Khan, and M. A. Z. Raja, "Intelligent and robust prediction of short term wind power using genetic programming based ensemble of neural networks," *Energy conversion and management*, vol. 134, pp. 361–372, 2017.

[84] A. M. Kassem, "Mppt control design and performance improvements of a pv generator powered dc motor-pump system based on artificial neural networks," *International Journal of Electrical Power & Energy Systems*, vol. 43, no. 1, pp. 90–98, 2012.

[85] A. Ali, K. Almutairi, M. Z. Malik, K. Irshad, V. Tirth, S. Algarni, M. Zahir, S. Islam, M. Shafiullah, N. K. Shukla *et al.*, "Review of online and soft computing maximum power point tracking techniques under non-uniform solar irradiation conditions," *Energies*, vol. 13, no. 12, p. 3256, 2020.

[86] W. Hayder, E. Ogliari, A. Dolara, A. Abid, M. Ben Hamed, and L. Sbita, "Improved pso: a comparative study in mppt algorithm for pv system control under partial shading conditions," *Energies*, vol. 13, no. 8, p. 2035, 2020.

[87] S. Motahhir, A. El Hammoumi, and A. El Ghzizal, "The most used mppt algorithms: Review and the suitable low-cost embedded board for each algorithm," *Journal of cleaner production*, vol. 246, p. 118983, 2020.

[88] Z. Zhen, S. Pang, F. Wang, K. Li, Z. Li, H. Ren, M. Shafie-khah, and J. P. Catalão, "Pattern classification and pso optimal weights based sky images cloud motion speed calculation method for solar pv power forecasting," *IEEE Transactions on Industry Applications*, vol. 55, no. 4, pp. 3331–3342, 2019.

[89] L. Xu, R. Cheng, Z. Xia, and Z. Shen, "Improved particle swarm optimization (pso)-based mppt method for pv string under partially shading and uniform irradiance condition," in *2020 Asia Energy and Electrical Engineering Symposium (AEEES)*. IEEE, 2020, pp. 771–775.

[90] K. Osmani, A. Haddad, T. Lemenand, B. Castanier, and M. Ramadan, "An investigation on maximum power extraction algorithms from pv systems with corresponding dc-dc converters," *Energy*, vol. 224, p. 120092, 2021.

[91] R. Ayop and C. W. Tan, "Design of boost converter based on maximum power point resistance for photovoltaic applications," *Solar Energy*, vol. 160, pp. 322–335, 2018.

[92] S. Vavilapalli, S. Umashankar, P. Sanjeevikumar, V. K. Ramachandaramurthy, L. Mihet-Popa, and V. Fedák, "Three-stage control architecture for cascaded h-bridge inverters in large-scale pv systems–real time simulation validation," *Applied Energy*, vol. 229, pp. 1111–1127, 2018.

[93] S. M. Fatemi, M. S. Shadlu, and A. Talebkhah, "Comparison of three-point p&o and hill climbing methods for maximum power point tracking in pv systems," in *2019 10th International Power Electronics, Drive Systems and Technologies Conference (PEDSTC)*. IEEE, 2019, pp. 764–768.

[94] K. K. Ghosh, S. Ahmed, P. K. Singh, Z. W. Geem, and R. Sarkar, "Improved binary sailfish optimizer based on adaptive β-hill climbing for feature selection," *IEEE Access*, vol. 8, pp. 83 548–83 560, 2020.

[95] N. M. Khan, U. A. Khan, and M. H. Zafar, "Maximum power point tracking of pv system under uniform irradiance and partial shading conditions using machine learning algorithm trained by sailfish optimizer," in *2021 4th International Conference on Energy Conservation and Efficiency (ICECE)*. IEEE, 2021, pp. 1–6.